

Acknowledgements

I owe my deepest gratitude to my parents for giving me the opportunity to not only write this thesis but also enabling me to do my study and for their unlimited support during that time.

Probably the most important person to thank is my supervisor Prof. Klaus Richter for guiding me through the work, constantly supplying me with ideas for different reasonable approaches to the topic and for discussing my results to ultimately create a consistent overall concept of the system. Then I want to thank Prof. Herbert Ipser and the Institute of Inorganic Chemistry/Material Chemistry welcoming me in their workgroup and for the permission to commence my thesis there as well as to use all the department devices.

I also want to express my gratitude to Dr. Christian Leinenbach and the EMPA for inviting me to Zurich and giving me the opportunity to enhance my work with diffusion brazing experiments and Dr. Liliana Duarte for supervising me there and introducing me to this and other methods.

I appreciate Alfred Amon and Jürgen Kolos work investigating specific problems of this work in course of their Bachelor thesis. I am bound to Dr. Stephan Puchegger for spending a lot of time introducing me to SEM measurement and troubleshooting the device. Finally I want to thank all my colleges providing me with frequent hints and a convenient atmosphere at the university and especially Mag. Martin Marker for patiently instructing me to a lot of methods crucial for my thesis.

Table of contents

1. Introduction	1
2. Literature	3
2.1. Binary phase diagrams	3
2.1.1. Aluminium – Germanium	3
2.1.2. Aluminium – Titanium	6
2.1.3. Germanium – Titanium.....	9
2.2. Ternary phase diagram Aluminium – Germanium - Titanium.....	11
3. Theoretical Background	12
3.1. Phase diagrams [29]	12
3.2. Methods	16
3.2.1. Scanning Electron Microscopy (SEM) [30]	16
3.2.2. X-ray Diffractometry (XRD) [31]	20
3.2.3. Differential Thermal Analysis (DTA) [32], [33]	24
4. Experimental section	26
4.1. Sample compositions.....	26
4.2. Sample preparation.....	30
4.2.1. Basic metals and weighing.....	30
4.2.2. Arc furnace.....	31
4.2.3. Equilibration	32
4.2.4. Problems	33
4.3. Measurements.....	34
4.3.1. SEM, EPMA	34
4.3.2. X-ray powder diffractometry (XRD).....	35
4.3.3. Differential thermal analysis (DTA).....	36

5. Results and discussion.....	38
5.1. Partial isothermal sections	38
5.1.1. 400°C.....	38
5.1.2. 520°C.....	41
5.1.3. 1000°C.....	48
5.2. Structure of new compounds	53
5.2.1. The α -phase	53
5.2.2. The β -phase	54
5.2.3. The γ -phase.....	55
5.2.4. The δ -phase.....	59
5.3. Reaction scheme, isopleths and liquidus projection	61
5.4. Discussion of the binary Ge-Ti system.....	72
6. Diffusion brazing and wetting.....	76
6.1. Theoretical background [7].....	76
6.2. Experimental section.....	77
6.3. Results and discussion	78
7. Appendices	83
7.1. List of figures	83
7.2. List of tables.....	85
8. References	87
9. Curriculum Vitae	90
10. Abstract	91
11. Zusammenfassung.....	92

1. Introduction

Aluminium-titanium alloys, especially AlTi (CuAu-type, [1]) and AlTi₃ (Ni₃Sn-type, [2]) are of technical interest, because of their high melting point in combination with low density, good corrosion resistance and terrific mechanical properties [3]. Therefore, they are commonly used in the aircraft industry for example for turbine blades. Though, one major drawback is the energy consumption during production and processing of this material leading also to high costs [4]. Also, joining of two work pieces is a problem. Formed oxides during welding may inhibit diffusion at the interface. Therefore, it is most commonly done under vacuum or inert gas [5]. For diffusion bonding the pieces are pressed together with a high pressure for a long time. It is therefore a time and energy consuming and thus a costly method while also stressing the material [6]. For an economical use it is crucial to decrease the overall cost of using such alloys by finding a proper method to repair damages as well as by finding an efficient joining technique.

Diffusion brazing may be the answer to both tasks. Under good conditions it yields joints with the same physicochemical properties as the bulk material without the necessity of high temperatures during the process. Thereby, a low melting solder is used in between two pieces, which is molten, solidified and distributed over the whole piece by diffusion in order to obtain no contribution of the solder material to the properties of the joint. Therefore, this is not only the application of physical force as high pressure or temperature to the work piece but the beneficial properties of different material is used in the process. As a consequence the chemical background has to be investigated in form of the phase diagram of the relevant elements. It is crucial to understand which phase may be formed during the process and to optimize the parameters of the method, such as the composition of the solder or the used temperature program, to avoid the formation of disadvantageous phases. [7]

The principal decision of which elements to be use for the possible solder was in favour of aluminium, titanium and germanium. Aluminium and titanium were obvious choices since they are also present in the bulk material and therefore reduce the necessary time for diffusion until the joint shares the composition with the bulk. Another element was necessary as melting point depressant. Germanium was chosen because it forms a low

melting eutectic with aluminium [8] which may contribute to a beneficial overall composition providing a low enough melting point as well as a similar composition to the bulk.

Because of the mentioned reasons, the focus of this research lies on the phase diagram. For this task three partial isothermal sections were investigated. In the titanium poor part 400°C were investigated since samples above this temperature would have been partially liquid. But in other, higher melting, regions 400°C would have been too low to reach thermodynamic equilibrium. Therefore 520°C and 1000°C were used in other parts of the phase diagram. Since the goal was to propose a solder mainly for AlTi, the phase diagram was just investigated up to approximately 50 at.% titanium. The produced data were used to construct a liquidus projection and a reaction scheme. After all, also preliminary wetting and brazing tests for the final application were done.

2. Literature

2.1. Binary phase diagrams

2.1.1. Aluminium – Germanium

McAlister and Murray [9] presented 1984 the first assessment (Figure 1) combining the work of Kroll [10], Stohr and Klemm [11], Clark and Pistorius [12], Glazov et al [13], Wilder [14], Eslami et al [15], [16] and others. They combined literature data with their own thermodynamic calculations.

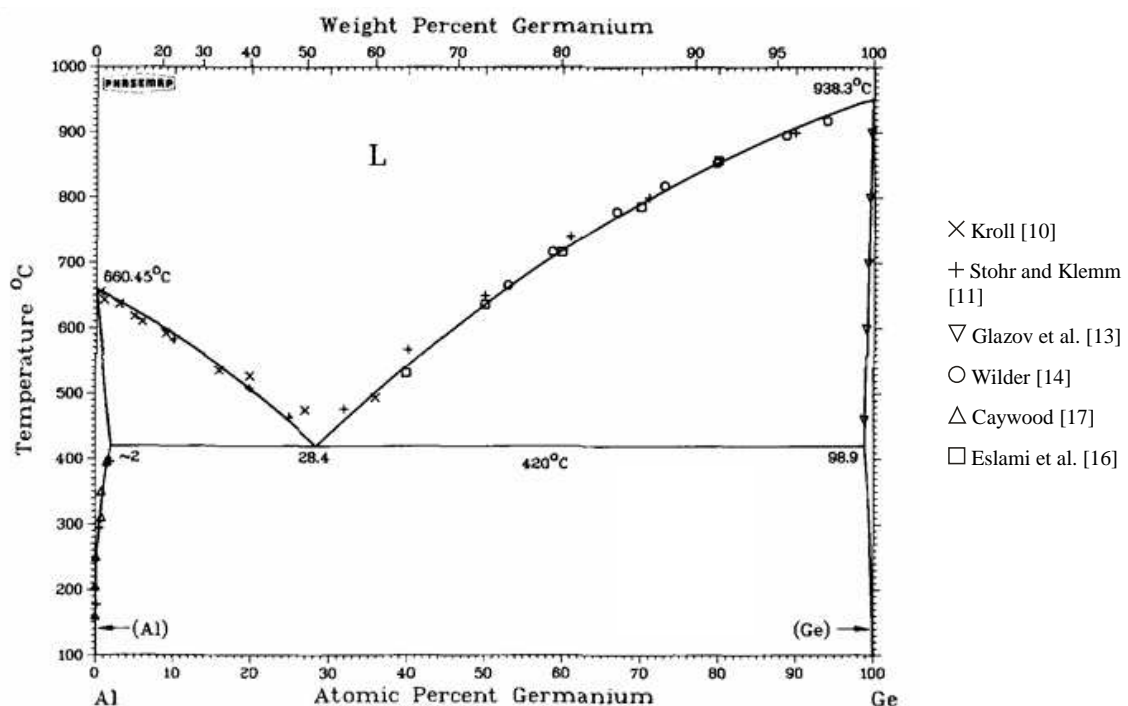


Figure 1: Calculated Al-Ge phase diagram by McAlister and Murray [9] and experimental data by different authors; the legend was adopted to fit to this work

The phase diagram shows a simple eutectic system with the three phases aluminium solid solution (fcc), germanium solid solution (diamond) and liquid with the eutectic point at 28.4 at.% germanium.

However, the eutectic temperature could not be determined reliably. It varies from 424°C [11] to 415±1°C [12] in different works. Electrochemical cell data yield values of 417±3°C [15], [16] and thermodynamic calculations result in 420°C. They also

calculated a solubility of 2 at.% germanium in (Al) and 1.1 at.% aluminium in (Ge). At the time of this assessment the solvus of (Ge)/(Al)+(Ge) and the solidus on the aluminium-rich side wasn't investigated yet.

More recently Minaminon et al [18] did electron probe micro analysis in order to obtain information about the solidus in the aluminium-rich part and to determine the solubility of Ge in (Al), both of which show a significant divergence to the phase diagram proposed by McAlister and Murray [9]. Therefore Srikanth et al [8] used those new data by Minaminon et al. [18] in addition to SGTE data for the phase stabilities of pure elements as well as the data used by McAlister and Murray [9] in their work to recalculate the phase diagram (Figure 2).

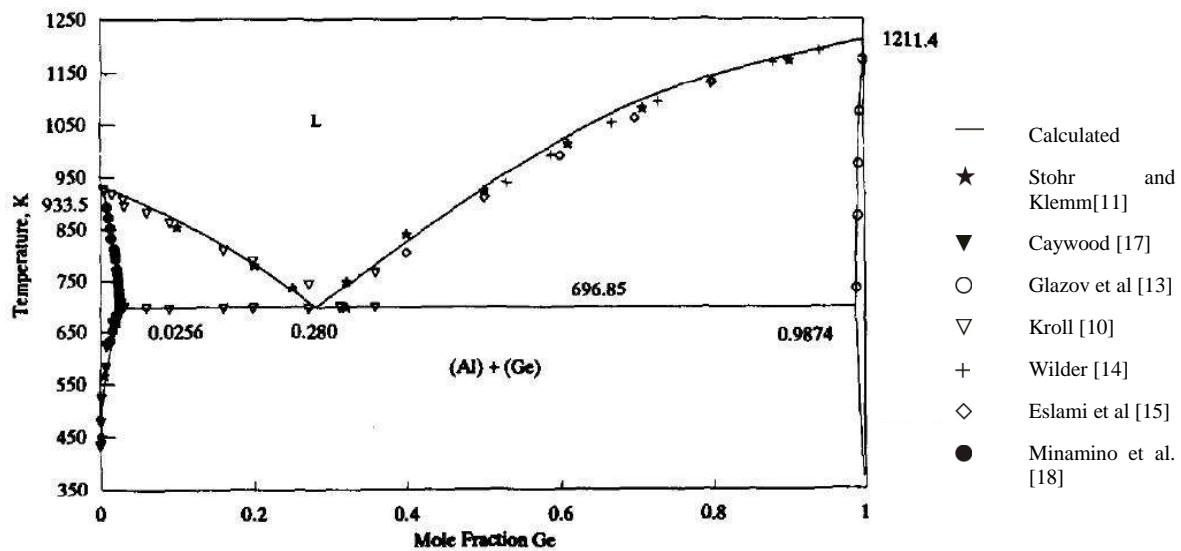


Figure 2: Calculated Al-Ge phase diagram by Srikanth et al [10] and experimental data by different authors; the legend was adopted to fit to this work

The main difference of the new calculation is the slightly higher eutectic temperature of 423.7°C as well as the solubility of up to 2.56 at.% Ge in (Al). Binary reactions and structural information about present phases are listed in the following tables (Table 1 and Table 2).

Phase	Pearson symbol	Space group	Strukturbericht designation	Prototype
(Al)	cF4	$Fm\bar{3}m$	A1	Cu
(Ge)	cF8	$Fd\bar{3}m$	A4	C(diamond)

Table 1: Crystal structure for the binary Al-Ge phase diagram [11], [10]

Reaction	Composition, at.% Ge	Temperature °C	Reaction Type
$L \leftrightarrow (Al) + (Ge)$	28 2.56 98.7	423.7	Eutectic
$L \leftrightarrow Al$	0	660.35	Melting
$L \leftrightarrow Ge$	100	938.25	Melting

Table 2: Phase equilibria for the binary Al-Ge phase diagram [11], [10]

2.1.2. Aluminium – Titanium

Since this system is of high technical interest, it was investigated several times with varying results. For a long time the assessed phase diagram by J.L. Murray [19] (Figure 3) was considered to be valid.

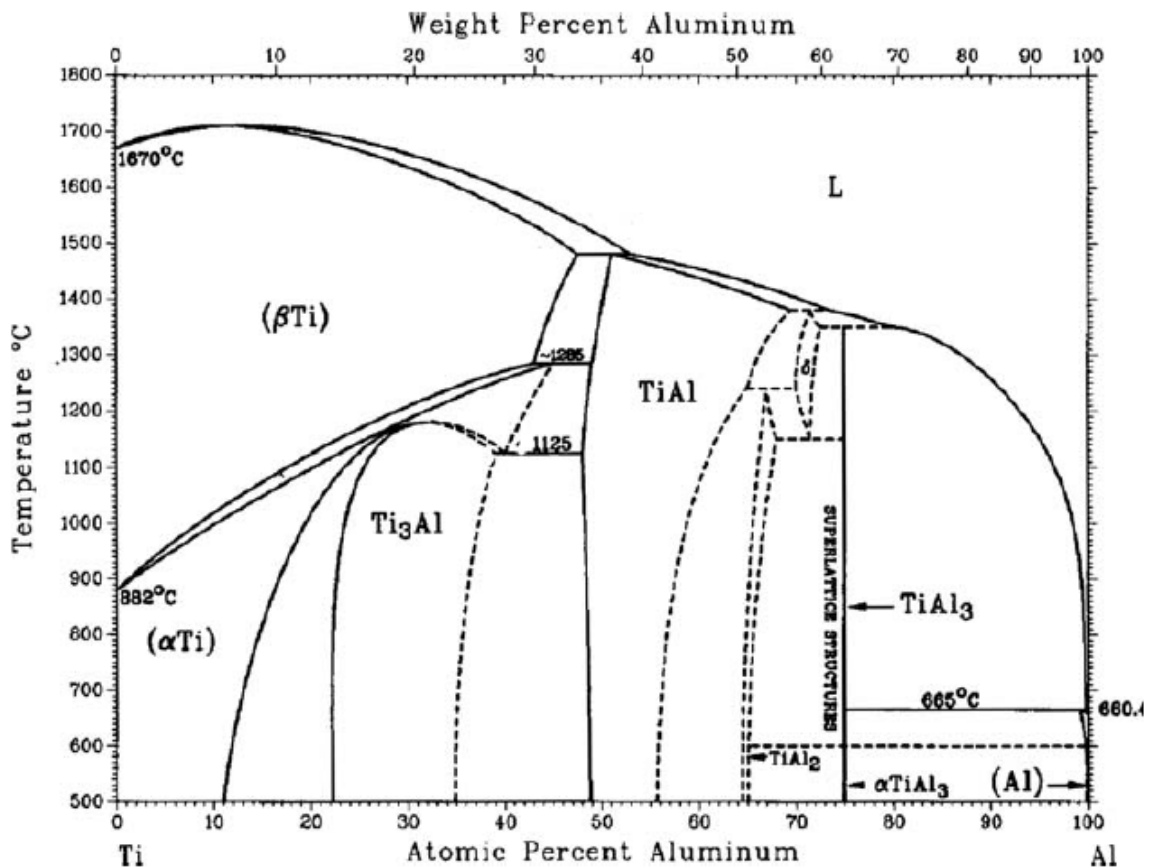


Figure 3: Al-Ti phase diagram by Murray [19]

Okamoto [20], [21] did two updates (Figure 4) on it. In the first he claimed, based on Kattner et al [22], that α Ti is formed peritectic out of β Ti and liquid instead of peritectoid out of β Ti and AlTi. As a result the two phase field between β Ti and AlTi disappeared. In the second update he introduced a two phase field between β Ti and Ti₃Al based on the work of Kainuma et al [23]. In both updates it was not mentioned why the melting point maximum of β Ti is neglected.

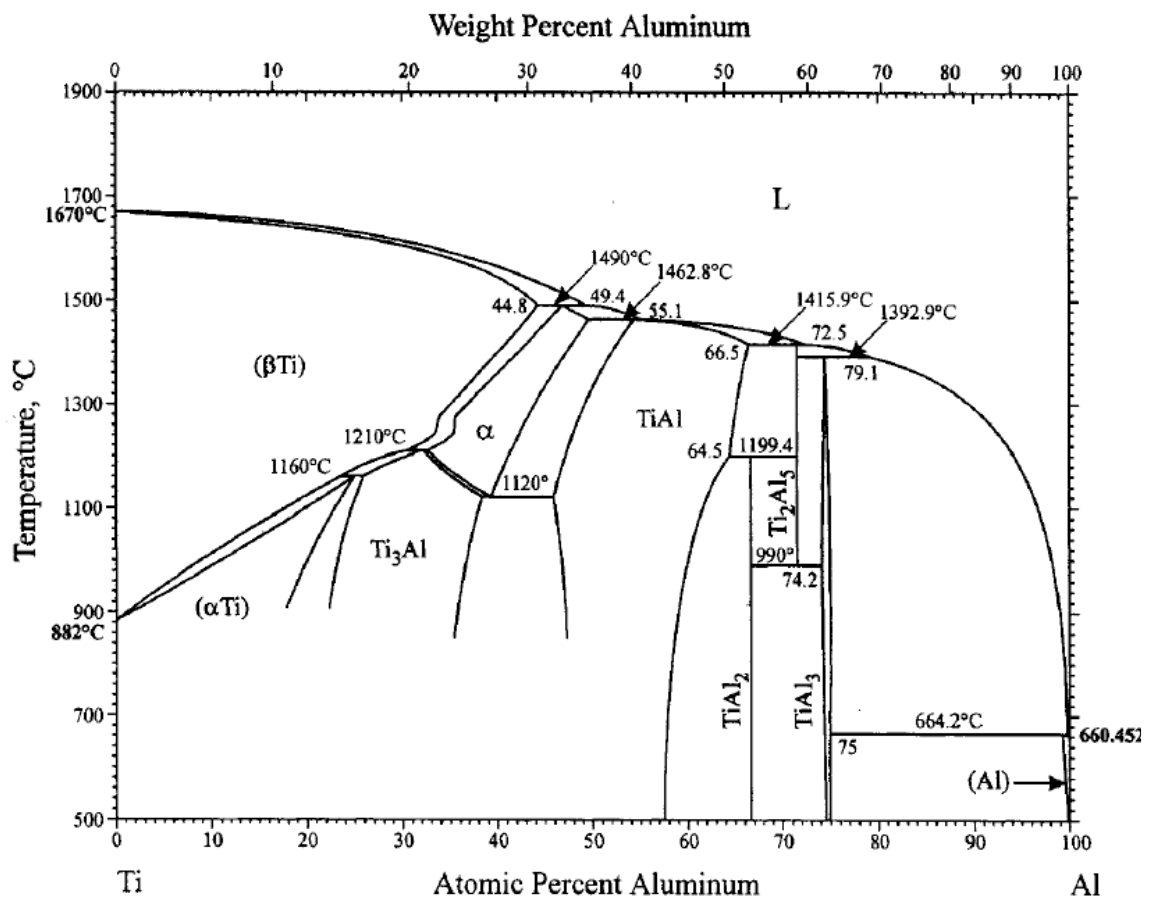


Figure 4: Al-Ti phase diagram after second update by Okamoto [12], [13]

Schuster and Palm [24] did a very thorough assessment of this system in 2005 (Figure 5) discussing in detail all relevant data available and combining them to the most probable phase diagram. Beside some temperature shifts and different shapes for the phase boundaries, the main differences between Okamoto's [20], [21] and Schuster's [24] phase diagram are on the aluminium rich side. On one hand the Al₃Ti phase is separated into a high- and a low-temperature modification. On the other hand Schuster [24] states that it still remains uncertain whether the phase 1d-APS, which is named Al₅Ti₂ in Okamoto's phase diagram [20], [21], forms in a second order transition out of the single phase field of AlTi or if a two-phase field in between exists or if 1d-APS is a metastable phase formed during quenching out of AlTi, which may be unstable at room temperature, while the formation of stable phases at room temperature are kinetically inhibited.

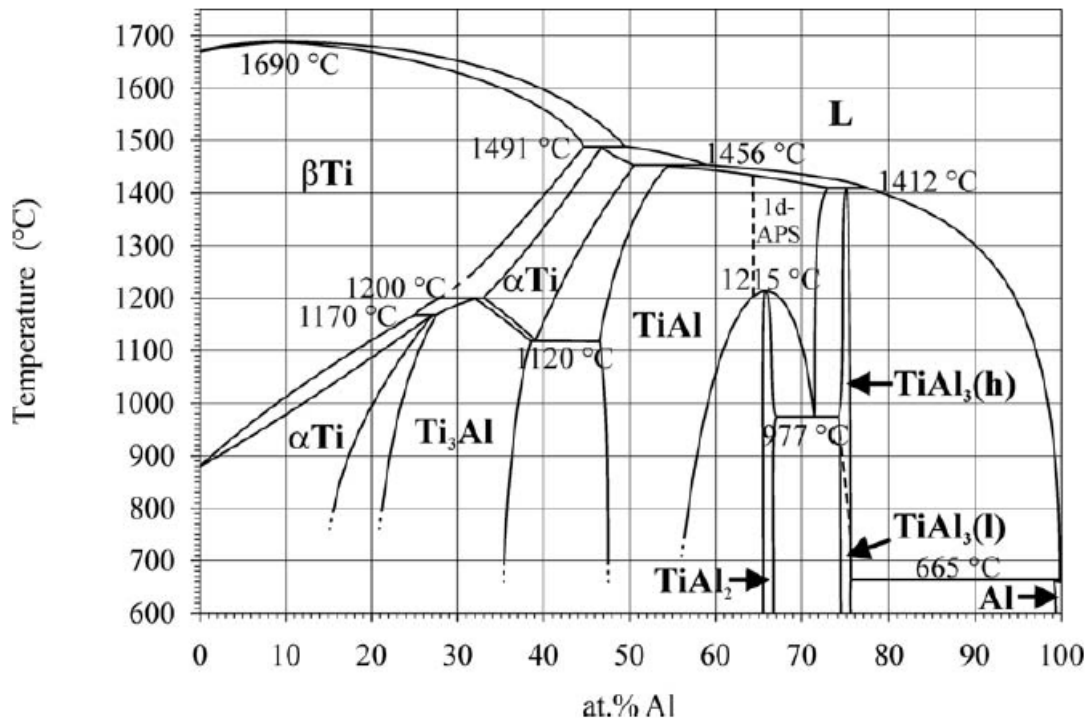


Figure 5: Assessed phase diagram by Schuster et al [24]

Binary reactions and structural information about present phases are listed in the following tables (Table 3 and Table 4).

Phase	Pearson symbol	Space group	Strukturbericht designation	Prototype
Al	cF4	Fm $\bar{3}$ m	A1	Cu
β Ti	cI2	Im $\bar{3}$ m	A2	W
α Ti	hP2	P6 ₃ /mmc	A3	Mg
AlTi ₃	hP8	P6 ₃ /mmc	D0 ₁₉	Ni ₃ Sn
AlTi	tP4	P4/mmm	L1 ₀	AuCu
Al ₂ Ti	tI24	I4 ₁ /amd		HfGa ₂
Al ₃ Ti(h)	tI8	I4/mmm	D0 ₂₂	Al ₃ Ti(h)
Al ₃ Ti(l)	tI32	I4/mmm		Al ₃ Ti(l)

Table 3: binary Al-Ti phases [24]

Reaction	Composition, at.% Al	Temperature °C	Reaction Type
$L \leftrightarrow Al$	100	660	Melting
$L + Al_3Ti(l) \leftrightarrow (Al)$	99.92 75.5 99.2	665	Peritectic
$L + 1d-APS \leftrightarrow Al_3Ti(h)$	~77.5 ~73 75	1412	Peritectic
$AlTi/1d-APS \leftrightarrow Al_2Ti$	65.7	1215	Congruent
$AlTi/1d-APS \leftrightarrow Al_2Ti + Al_3Ti(h)$	71.5 67.0 74.2	~975-980	Eutectoid
$Al_3Ti(h) \leftrightarrow Al_3Ti(l)$			
$(\beta Ti) + AlTi_3 \leftrightarrow (\alpha Ti)$	25 ~27.5 27	1170±10	Peritectoid
$(\alpha Ti) \leftrightarrow AlTi_3 + AlTi$	39 38.5 46.5	1120 ± 10	Eutectoid
$(\beta Ti) + (\alpha Ti) \leftrightarrow AlTi_3$	~28 33 32	1200 ± 10	Peritectoid
$L + (\alpha Ti) \leftrightarrow AlTi$	59 50.5 54.5	1456	Peritectic
$L + (\beta Ti) \leftrightarrow \alpha Ti$	49.5 44.6 46.7	1491	Peritectic
$L \leftrightarrow (\beta Ti)$	8.5 ± 3.5	1690 ± 10	Congruent
$L \leftrightarrow \beta Ti$	0	1668	Melting

Table 4: binary Al-Ti reactions [24]

2.1.3. Germanium – Titanium

In contrast to the Al-Ti system, little is known about the Ge-Ti phase diagram. Rudometkina et al [25] did an investigation of this system in the course of a ternary phase diagram study in 1989 using only DTA to investigate this system concluding with the phase diagram shown in Figure 6. Some obvious weaknesses of this phase diagram are, that solubilities of the single phases aren't investigated and reaction temperatures have either non or a rather high error bar. Also, the amount of the investigated samples is rather low.

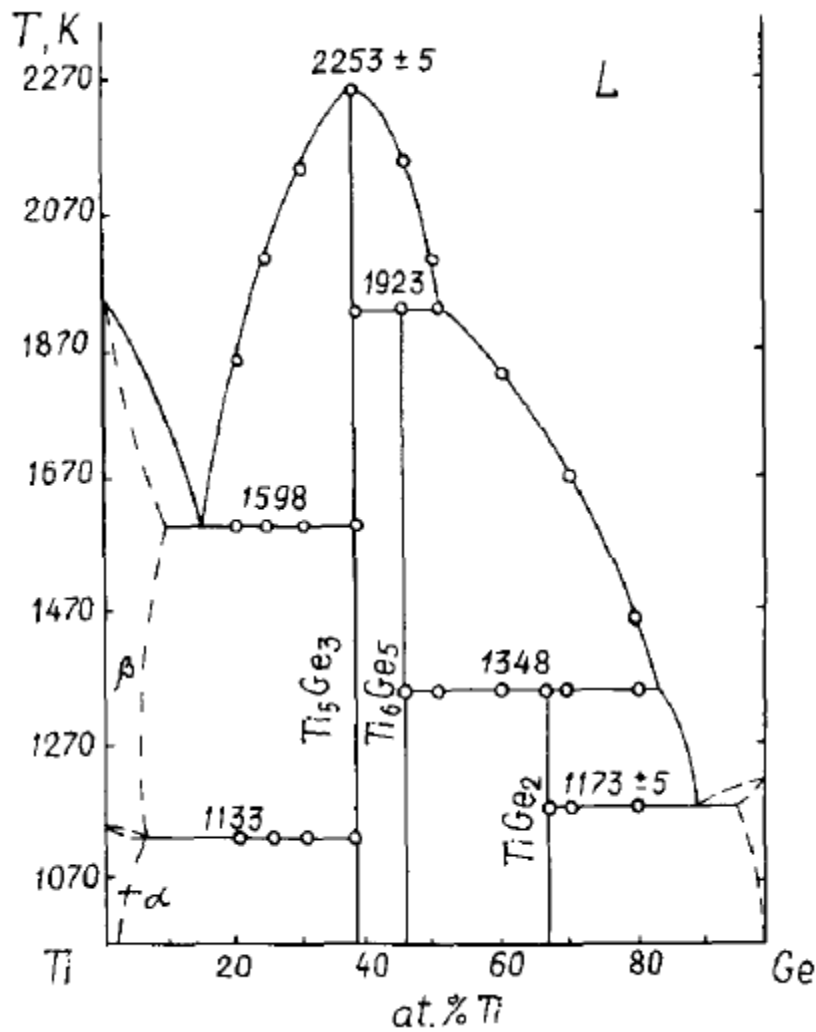


Figure 6: Ge-Ti phase diagram by Rudometkina et al [17]

Wirringa et al [26] performed chemical vapour transport experiments in the Ge-Ti system. They were not able to transport Ti_6Ge_5 and found Ti_5Ge_3 in equilibrium with $TiGe_2$, so they conclude in their work that Ti_6Ge_5 is not thermodynamic stable at 700 and 800°C.

There are also some disagreements between the current work and the phase diagram by Rudometkina et al [25], which will be discussed in 5.4. Therefore further experiments are desirable to clarify the real relations in this system.

Binary reactions and structural information about present phases are listed in Table 5 and Table 6.

Phase	Pearson symbol	Space group	Strukturbericht designation	Prototype
β Ti	cI2	$Im\bar{3}m$	A2	W
α Ti	hP2	$P6_3mmc$	A3	Mg
Ti ₅ Ge ₃	hP16	$P6_3/mcm$	D8 ₃	Mn ₅ Si ₃
Ti ₆ Ge ₅	oI44	Immm		Nb ₆ Sn ₅
TiGe ₂	oF24	Fddd	C54	TiSi ₂
Ge	cF8	$Fm\bar{3}m$	A4	C(diamond)

Table 5: binary Ge-Ti phases [19]

Reaction	Composition, at.% Ge	Temperature °C	Reaction Type
$L \leftrightarrow \beta$ Ti	0	1670	Melting
β Ti \leftrightarrow α Ti	0	882	Allotropic
$(\beta$ Ti) \leftrightarrow (α Ti) + Ti ₅ Ge ₃	? ? 37.5	860	Eutectic
$L \leftrightarrow (\beta$ Ti) + Ti ₅ Ge ₃	15 ? 37.5	1325	Eutectic
$L \leftrightarrow$ Ti ₅ Ge ₃	37.5	1980	Congruent
$L +$ Ti ₅ Ge ₃ \leftrightarrow Ti ₆ Ge ₅	? 37.5 45.5	1650	Peritectic
$L +$ Ti ₆ Ge ₅ \leftrightarrow TiGe ₂	? 45.5 66.7	1075	Peritectic
$L \leftrightarrow$ TiGe ₂ + (Ge)	89 66.7 ~100	900	Eutectic
$L \leftrightarrow$ Ge	100	938.3	Melting

Table 6: binary Ge-Ti reactions [19]

2.2. Ternary phase diagram Aluminium – Germanium - Titanium

Literature data about the ternary phase diagram only exists for the titanium rich corner of the phase diagram. Hayes [27] did a review primary based on the work of Nartova and Mogutova [28]. They investigated four isothermal sections at 600, 800, 1000 and 1100°C using DTA, XRD and microstructure analysis.

No literature data for the titanium poor side below 50 at.%, which is the main target for this investigation, exist yet.

3. Theoretical Background

3.1. Phase diagrams [29]

Phase diagrams describe the thermodynamic stable phases in a single- or a multi-component system as a function of composition, temperature and pressure. A phase thereby is a region where all physical properties are uniform, such as the chemical composition or, in case of solid matter, the crystal structure. The three different states of matter are solid, liquid and gaseous.

Phase diagrams are crucial to understand solidification processes and other reactions in order to predict the properties of materials and to improve beneficial properties of existing materials systematically.

Since a phase diagram has a dependency of several variables and therefore is multidimensional, it is almost impossible to illustrate the whole diagram. Thus, there are several common ways to project two dimensional illustrations out of the phase diagram. The overall pressure dependency is often minor in solid phases, so it is very common in material chemistry to print phase diagrams with a certain constant pressure value. In a ternary system, the composition dependency is divided into two independent variables. Only the concentrations of these two elements can be freely chosen while the last one adds up to 100 at.%, providing none of them is negative. Three degrees of freedom are therefore left. These are the temperature and the other two are the composition. For a clearly represented two dimensional projection it is necessary to keep one additional degree of freedom constant.

In case of isothermal sections in ternary systems the temperature is kept constant in addition to the pressure. Hence, it is a diagram printing the two degrees of freedom of the composition against each other. Isopleths on the other hand show the temperature dependency while varying one degree of freedom of the composition. In this case the pressure and the other degree of freedom are constant. For both of these possibilities there is an example in Figure 7. In other systems different ways of illustration may be more practical but in this work only these two presented ways will be used.

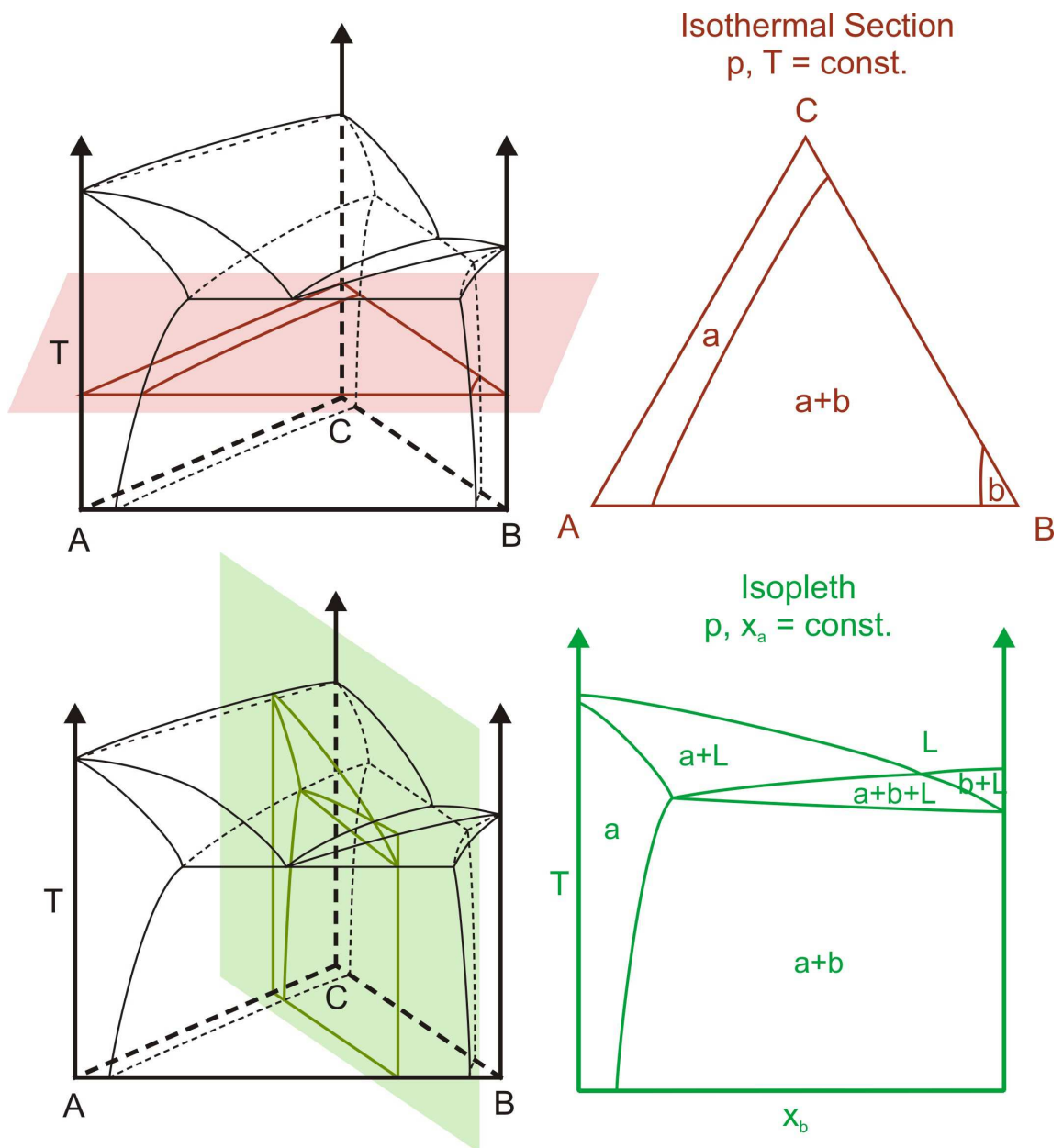


Figure 7: Examples for: isothermal section: red; isopleth: green; ternary phase diagram at constant pressure: black

Lines drawn in such diagrams are borders for regions of different phase fields, in which a certain number of phases can coexist. Under single phase field conditions the whole sample has the same crystal structure and composition all over. However, in phase fields with a higher number of phases in equilibrium, there is a mixture of different phases, each with a different composition, depending on overall composition of the sample, temperature and pressure. A binary example is given in Figure 8. All rules valid

in binary systems can also be adapted to ternary systems. In this example a sample with the composition x_1 is heated to the temperature T_1 . Since it is located in a two-phase-field, it consists out of a mixture of the bordering phases a and b. The composition of a and b is highlighted by the red dots at T_1 , while the ratio of a and b is defined by the overall composition of the sample.

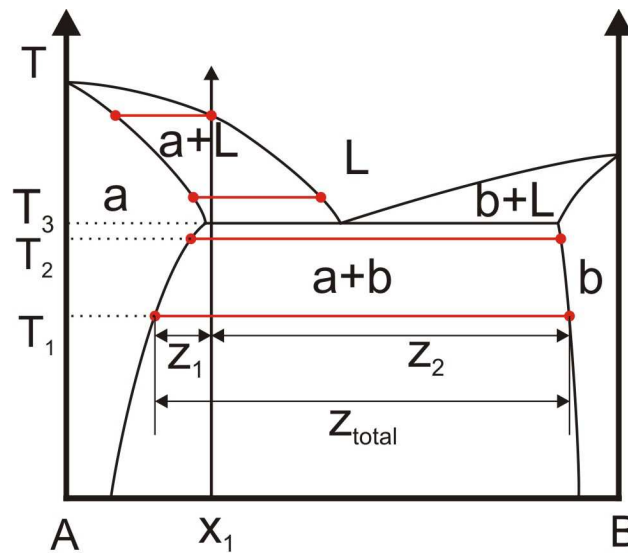


Figure 8: Binary example phase diagram for lever rule and invariant and non-invariant reactions

The ratio can be calculated by the lever rule, which says that the amount of b is given by

$$x_b = \frac{z_1}{z_{total}}, \text{ while } x_a = \frac{z_2}{z_{total}}.$$

During heating to T_2 the amount of b decreases continuously, while the amount of a increases, according to the lever rule. This is therefore a non-invariant reaction temperature-wise where b reacts to a. Finally by reaching T_3 b stops to be stable at the chosen composition. All of it has to decompose therefore at T_3 before higher temperatures can be reached, assuming ideal behaviour. The whole system keeps the same temperature until b reacts with a to form liquid. This is consequently called an invariant reaction. Since reactions in phase diagrams are always reversible, there is the convention to write them from the point of view of cooling, which leads to the reaction $L \leftrightarrow a + b$. Further heating instantaneous leads to another non-invariant reaction decreasing the amount of a and forming liquid until no a is left anymore since $z_1 = z_{total}$ and the whole sample is molten.

The central rule for phase diagrams is the Gibb's phase rule. It connects the number of phases in equilibrium in a sample with the degrees of freedom within a phase field. The rule says $P + F = C + 2$ with P standing for the number of phases in equilibrium, F for the degrees of Freedom and C for the order of the system. Considering one degree of freedom is already used due to the constant pressure it can be written as $P + F' = C + 1$. Using this equation

for a binary phase diagram ($C=2$) this yields $F'=2$ for a single-phase-field ($P=1$), $F'=1$ for a two-phase-field ($P=2$), and $F'=0$ for a three-phase-field ($P=3$). In Figure 9 one can see at the very left a sample with a certain temperature and certain composition in a single-phase-field represented by a blue spot. The Gibb's rule now says that there are two degrees of freedom in a single-phase-field. So here the composition of the phase or the temperature can change without the necessity to change the other variable as well. In a two-phase-field there is just one degree of freedom. By changing the temperature from T_1 to T_2 the compositions of phase a and phase b also change accordingly represented by the red spots and cannot be freely chosen. The other way around: After choosing a composition for phase a it is necessary to heat to a certain temperature in order to obtain this composition and the composition of phase b will also be defined. So the other two variables cannot be freely chosen. The last possibility in a binary phase diagram is a three-phase-field represented by the green spots. There are no degrees of freedom left. Therefore neither the temperature nor the composition of any phase can be changed without leaving the three-phase-equilibrium.

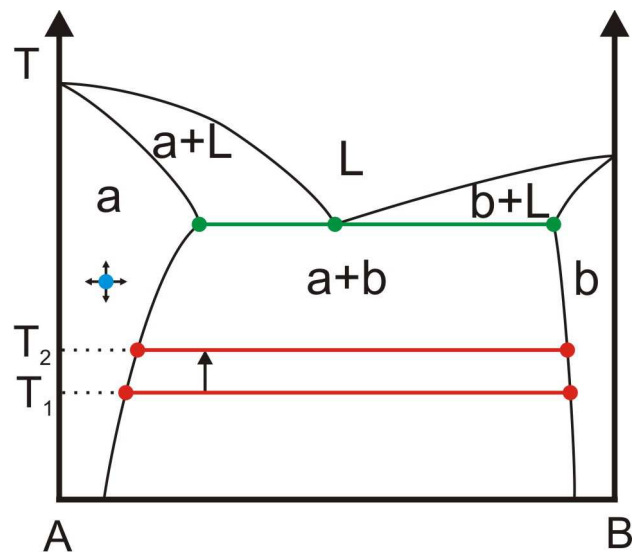


Figure 9: Binary examples for Gibb's (phase rule

A simple but crucial rule for constructing phase diagrams is the Landau and Palatnik rule. It describes the dimension of the borders between different phase fields and says $r_1 = r - d^- - d^+$ with r_1 as the dimension of the border, r as the dimension of the phase diagram, d^- as the number of phases lost during the transition from one phase field to another and d^+ as the number of phases added. Some examples are given

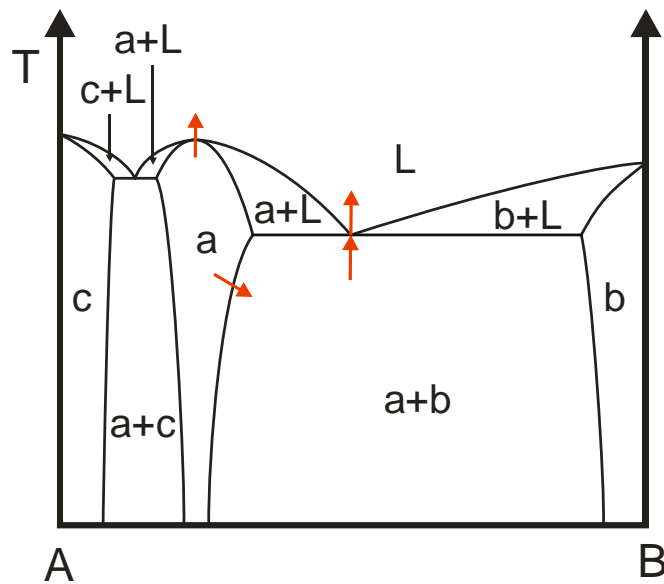


Figure 10: Binary example for Landau and Palatnik rule

in Figure 10 with red arrows. The first example at the very left is a transition from a single-phase-field to another. It is a two dimensional phase diagram and one phase is lost, one phase is added, so the result of this equation is zero. Thus the border for this transition is just a single point. The next example is the transition from the a phase field to the a+b phase field. One phase is added, none is lost, so r_1 equals one in this case, which leads to a line as phase boundary. The last example is a little bit more complicated. Since there is the three-phase-field a+b+L between the single-phase-field L and the two-phase-field a+b, the transition from L to a+b has to be split in two separate transitions considering the three-phase-field. The first transition is from a+b to a+b+L and is according to the rule a one-dimensional line, while the second a+b+L to L is just a point again. Not considering the three-phase-field would lead to incorrect results.

3.2. Methods

3.2.1. Scanning Electron Microscopy (SEM) [30]

SEM measurements in backscattered (BSE) or secondary electrons (SE) mode are used for imaging with high magnification and resolution of a surface. Different phases are thereby distinguishable from each other because by different grey scales in BSE mode.

In SE mode contrast is produced by the topography of the sample. The energy dispersive X-ray spectroscopy (EDX) mode is used to measure the element distribution of the different present phases.

The measurement is done with an electron beam. It is produced by a heated tungsten filament or CaB_6 tip. It is accelerated towards the polished surface of the sample and focused by several electromagnetic lenses in order to obtain a good shape and small diameter for the beam as well as for the excitation of the sample. This is crucial for a good resolution and precise measurements. The electron beam then triggers a cascade of different effects in the sample as you can see in Figure 11. This is just a schematically figure, which should give an idea about the present effects. The shape and depth where these effects take place is dependent on several settings like the energy of the electron beam or the chemical composition of the target and is therefore not true to scale. Also the single regions for those effects are also not sharply separated.

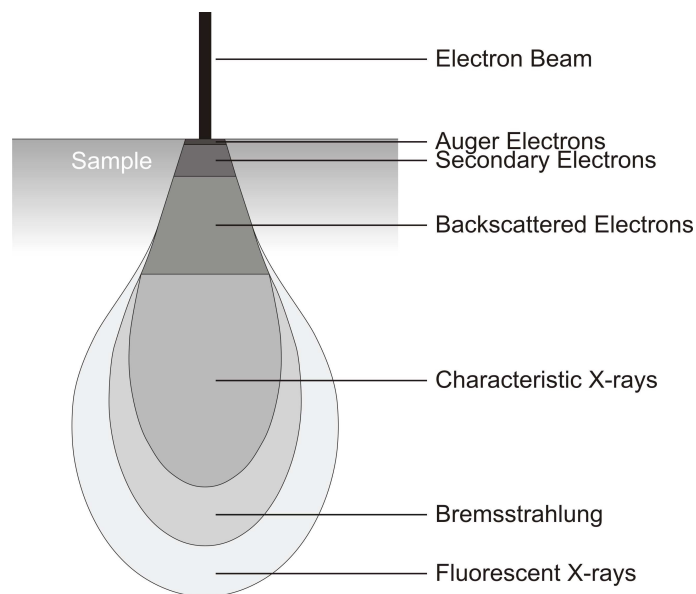


Figure 11: Interactions between electron beam and solid matter

The first important effect is backscattered electrons. Electrons of the primary beam interact with the high electron density around an atom which leads to elastic and inelastic scattering, changing the flight direction of the primary electron. Multiple collisions can cause the electron to leave the sample again. Larger atoms have a greater cross sectional area and it is therefore more likely for an incoming electron to hit and

interact with a larger atom. Thus, the intensity of the backscattered electrons is the higher, the greater the mean atomic number in the measured area is. After scanning over an area it is possible to plot the intensity representing the mean atomic number as different grey scales in a picture. Since single phases have a homogeneous composition they also have a homogeneous mean atomic number which leads to a single grey scale for each phase in a measurement. By adjusting brightness and contrast it is therefore possible to distinguish different phases unless they have the same mean atomic number which can of course occur randomly.

The next important mode for SEM measurements is based on secondary electrons. Secondary electrons are produced by inelastic collisions of electrons in the primary beam with weakly bound electrons in the outer shells. The electron in the atom thereby absorbs rather little energy in most cases but still enough to leave the atom. Because of the low energy these electrons barely can penetrate matter, so this is almost purely a surface effect. Thus, if the primary beam, and therefore the currently investigated area, targets a sloping area, the beam can interact with more atoms within the very limited distance to the surface. Such zones yield a higher intensity of detected secondary electrons. Often the detector is mounted on one side of the primary beam, which leads to another effect. Secondary electrons emitted on surfaces averted to the detector are partially reabsorbed. So the intensity there is lower than on a surface facing the detector. Also other circumstances like increasing roughness in a microscopic way or higher atomic number increases the final intensity at a certain point. The charge of the area also has an influence. Negatively charged regions emit more electrons than positively charged. After allocating grey scales to intensities it is possible to plot a picture based mainly on the topography of the sample. Secondary electrons can be distinguished from backscattered electrons by their kinetic energy. While the energy of backscattered electrons is dependent of the acceleration voltage which is in the range of several kV, secondary electrons have below 50eV.

In EDX mode the characteristic X-rays provide the information content. The electron beam removes electrons from inner shells in atoms by collisions which lead to reoccupation by other electrons in energetically more unfavourable shells. The energy difference is then released in form of characteristic X-rays. Since the energy difference between two shells is dependent on the constitution of the excited element, as well as on the participating shells (Figure 12), every element produces a unique spectrum,

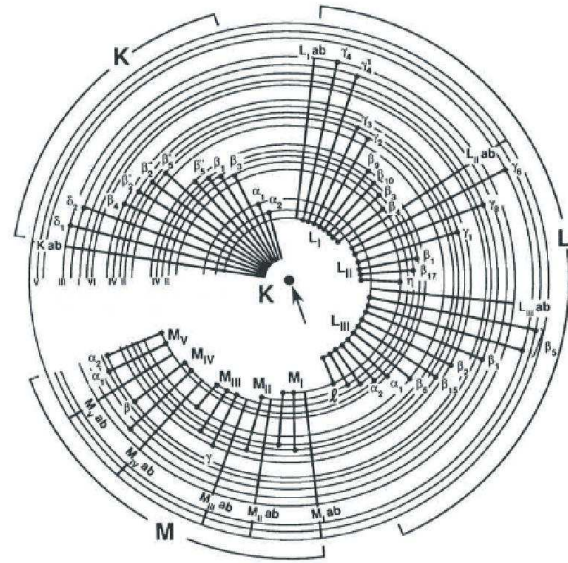


Figure 12: Possible transitions for the K, L and M shell [23]

which consists of the combination of all possible transitions weighted with their probability. Hence, a measured spectrum can be decomposed into the spectra of the pure elements, each weighted with the amount of the element present. With this method the composition of a very small spot, limited by the beam size, can be measured very accurately.

Whenever an electron undergoes a deceleration within the field of an atom, the lost energy is transformed into a photon which may also be in the X-ray range. Any amount of energy up to the total energy of the electron can be lost in a single event. Therefore a continuous radiation up to the total energy of the electron is produced forming the background of the measurement. This kind of radiation is called Bremsstrahlung based on the German words "bremsen" and "Strahlung" which mean deceleration and radiation.

X-ray fluorescent occurs by excitation of atoms not by the electron beam but by other X-rays. Excitation by Bremsstrahlung or characteristic X-rays is both possible. Like in visible fluorescence the exciting X-rays have to have a higher energy than the emitted ones. Therefore a shift to longer wavelengths takes place and the volume of the measured space further increases.

Auger Electrons are produced in a similar way as characteristic X-rays. But after ionization by removing an inner shell electron, the energy difference of the occurring transition of an outer shell electron to the energetic more desirable state is used to emit another outer shell electron. This emitted electron has now a kinetic energy reflecting the transition. Therefore auger electrons yield similar information to characteristic X-rays but with a different depth profile in the sample.

3.2.2. X-ray Diffractometry (XRD) [31]

XRD is used to identify the present phases via their known structure as well as to identify the structure of unknown phases. The idea behind this method is that waves diffract at a grid. The grids, or rather the distances between the single lattice planes, thereby are formed by the electron densities of atoms in the crystal. Since the positions of the atoms are depended on the crystal structure, different planes can be put into each crystal structure, each with a characteristic distance to its proximate parallel plane defined by the lattice parameter. Thus, the geometry induces an ensemble of the different lattice distances. Since the angle of the diffraction is amongst others dependent on those distances, every angle can be brought in correlation with such a distance. Hence, by measuring the angle, conclusions can be drawn about the crystal structure producing such an observed ensemble of distances

The question is now under which conditions the sample diffracts a ray under a certain angle. This is just possible if constructive interference occurs. An illustration for such a situation is given in Figure 13.

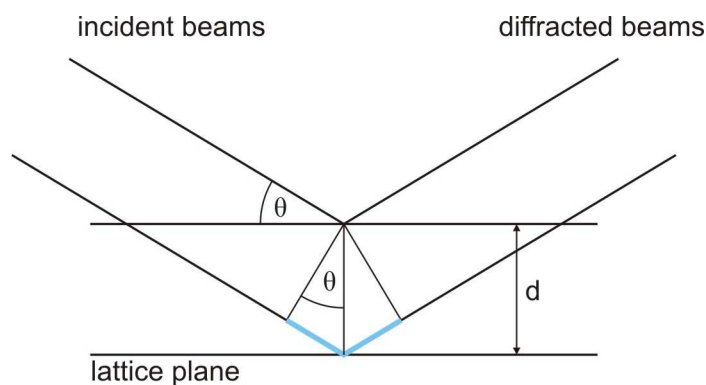


Figure 13: Diffraction of X-rays, Bragg Equation

The two different beams in this example have a different distance to cover. The distance for the second beam is increased by the blue section in comparison to the first one. If the blue section now is a multiple of the wavelength of the X-ray, then the first and the second beam are in-phase after the diffraction, provided they have been in-phase before. This leads to constructive interference and to a detectable signal. In every other case the beams will erase each other and just the background will be detected. The distance of the blue section is dependent on the angle and on the distance between two lattice planes, while of course the wavelength defines the possible lengths for constructive interference. This is combined by the Bragg equation, which says $2d \sin \theta = n\lambda$. It can be used to evaluate the distances between single planes if the wavelength is known and the angle is measured. The different plane distances in a crystal are dependent on the crystal structure as well as on the lattice parameters of the cell, while the intensities of the single peaks are depended on the electron density distribution forming those planes. But it is not possible to distinguish the sources of the electron densities. For example positions with atoms with higher electron densities but vacancies may yield the same diffractogram as positions fully occupied with atoms with lower electron density or even with a mixture of atoms with high and low electron density.

As diffraction works best with photons having their wavelength in the same order as the grid spacing, which is in the low Angstrom range, X-ray radiation (e.g. Cu $K\alpha = 1.541\text{\AA}$) is used. For the generation of such radiation, high voltage is applied to a heated tungsten filament. The filament emits electrons which are accelerated towards a target consisting of an appropriate material. The electrons interact with the material in the same way as discussed in chapter 3.2.1. But in this case just Bremsstrahlung and characteristic X-rays of the target are of interest. Since the diffraction angles should be brought into correlation with the crystal structure, every other angle dependency in this device should be avoided. But as the diffraction angles are also dependent on the wavelength of the electromagnetic wave, monochromatic waves are preferable. The possibilities to filter everything except one specific wavelength are, however, very limited and therefore often abandoned. Then it is necessary to take the more complicated spectrum into account during the evaluation.

For the detection of X-rays in principal every observable interaction between matter and the radiation can be used. Very common is a detector based on a NaI crystal doped with

thallium. X-rays produce light flashes when interacting with the crystal, which then can be detected with a photomultiplier. Such a detector is called scintillation counter. Another method is based on semiconductors. The radiation thereby produces electron and hole pairs in the semiconductor changing its conductivity. A fast and efficient detector can be obtained by arranging many small such semiconductor stripes, out of silicon for example, close to each other.

Since there is no material known yet capable to work as a lens for X-rays, just the geometry and slits can be used in order to obtain a working device. The goal thereby is to construct an arrangement able to scan over all angles to detect whether the sample diffracts with a certain angle or not. Such can be achieved by placing the X-ray tube, the sample and the detector on a common focusing-circle. This will also cause a focusing effect, as you can see in Figure 14.

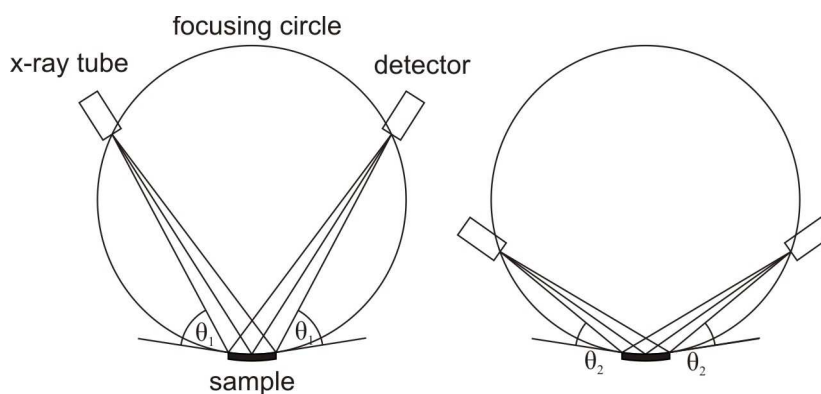


Figure 14: Focusing circle

With this arrangement every ray emitted by the X-ray tube and hitting the detector is diffracted under the same angle by the sample independent of the location for this interaction. The sample thereby has to cover the surface of the circle and should be therefore concave. It works for every angle adjusted as long all three are moved on the same circle. But this arrangement is impractical. The movement of the detector and the X-ray tube has to be done simultaneously about their own axis as well as about the centre of the circle in a very accurate way. Since small deviations already corrupt the results, this put great demands to the mechanic. One way to circumvent this problem is to arrange everything according to the Bragg-Brentano pseudo focusing circle. A scheme can be found in Figure 15.

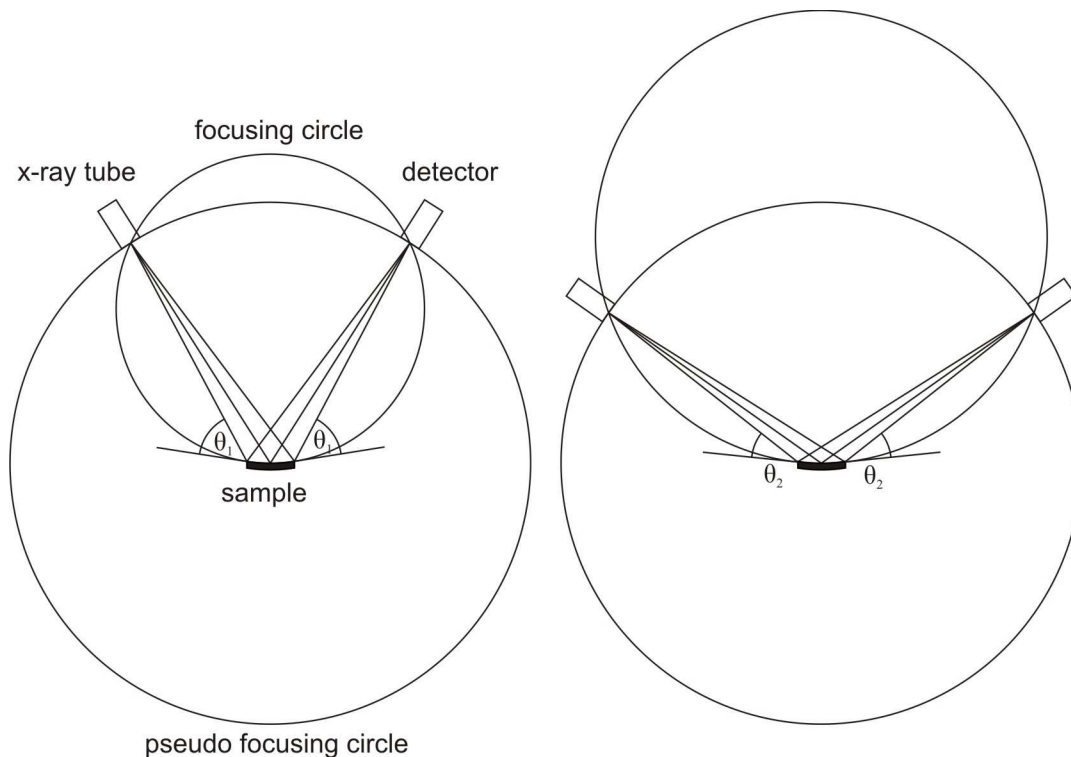


Figure 15: Bragg-Brentano pseudo focusing circle

Thereby no longer the radius of the focusing circle is kept constant but the distances between sample and detector as well as between sample and X-ray tube. A changing angle leads to a changing focusing circle but the principal effect stays the same. In this arrangement the detector and the tube can just be mounted on an arm rotating them about the centre of the pseudo focusing circle which is by far easier to accomplish. To further lighten the requirements for the mechanic it is common to keep one of those three parts fixed and just move the other two accordingly. In some cases, most often dictated by the sample, it is necessary to keep the sample holder fixed and move X-ray tube and detector each by the angle θ , as shown in the figures. Such an arrangement is therefore called θ/θ . The easier way is to keep the heavy X-ray tube fixed and turn sample holder and detector. The detector has to be rotated twice as fast as the sample holder in this case to maintain the geometry. It is therefore called $\theta/2\theta$ arrangement. As the focusing circle changes, in this case the curvature of the sample holder also has to change. Since very often silicon single crystals are used cut in a certain angle to deny diffractions of the sample holder itself, it is technically almost impossible to achieve such a changing sample holder. Usually a flat sample holder is used instead.

For the evaluation it is possible to calculate a theoretical diffractogram just out of fundamental parameters and a set of initial variables, like the lattice parameters of the cell, atom position within the cell but also displacement of the sample in relation to the ideal sample position and several more. This can then be compared with the measured one. By refining the variables to minimize the square error, so called R-value, the calculated diffractogram can be trimmed to fit to the measured one by an iteration of several such refining steps. In the end the parameters of the calculated diffractogram can be used for further evaluation. This method is named Rietveld-refinement after his inventor Hugo Rietveld.

3.2.3. Differential Thermal Analysis (DTA) [32], [33]

DTA is one of main tools to construct the temperature dependency of a phase diagram out of samples which obviously can only be tempered at one temperature.

Each phase transition goes hand in hand with a heat exchange of the sample and surrounding. This occurs because during a rearrangement, energy is necessary to break existing interactions between atoms, while the formation of new interactions releases energy. Those two energies do compensate each other up to a certain degree. In case of DTA these phase transitions are induced by heating or cooling the sample.

Hence, in a DTA device a temperature program is applied to the sample. During this, the actual temperature of the sample and of a second reference material is measured with sensitive thermocouples. The difference between the non-reacting reference material and the sample is then plotted against the reference temperature. Each deviation indicates a reaction in the sample and after evaluating the exact temperatures they can be plotted in the phase diagram.

Invariant and non-invariant reactions yield different shapes of signals in the DTA. To show this, an example for a theoretical DTA signal with the according phase diagram is given in Figure 16. A sample with the composition x_1 is heated. Due to the change of composition with the temperature, the amount of a increases while the amount of b decreases in a non-invariant reaction while heating from T_0 to T_1 . Since this reaction is

rather slow due to the fact that the progress of the reaction is temperature dependent and the sample is slowly heated, it yields a flat and broad signal.

At T_1 an invariant reaction takes place. The whole transformation energy is consumed at the constant temperature T_1 . Such reactions yield steep and sharp peaks with characteristic linear peak onset. After this reaction another non-invariant reaction starts during heating from T_1 to T_2 again with a broad and flat peak shape. At T_2 the reaction with the corresponding heat consumption stops and exponential cooling to the baseline begins. Because of the different shape of the

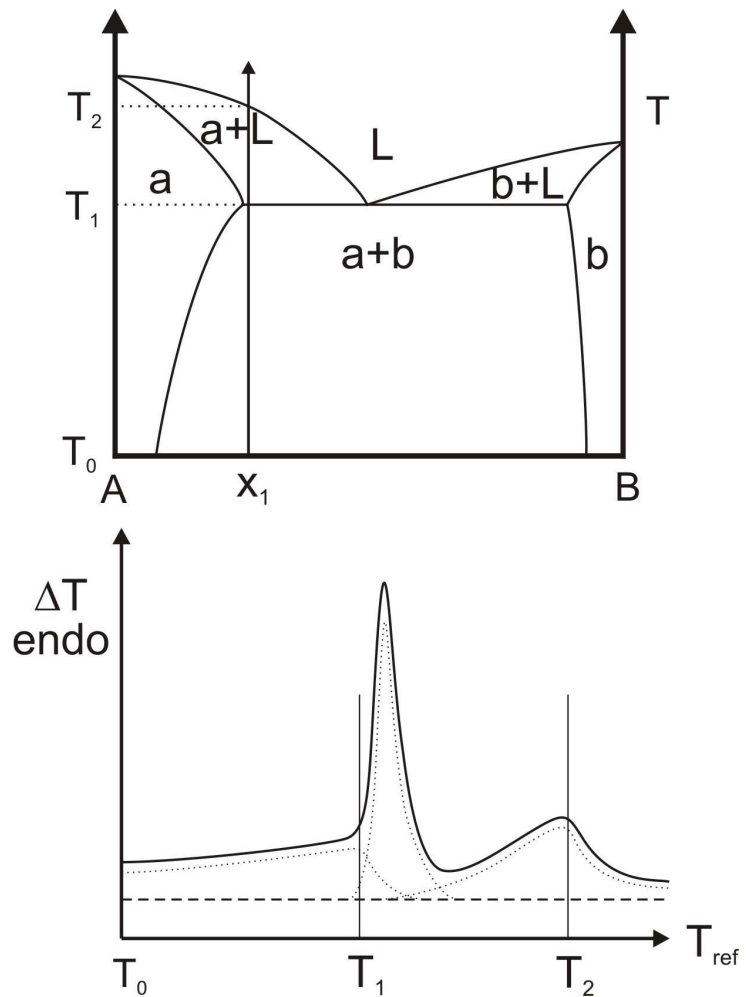


Figure 16: Example for DTA signal

signals different points have to be evaluated. In case of invariant reactions the onset is of interest, since the reaction starts only if the sample reaches the right temperature. On the other hand for non-invariant reactions the start of exponential cooling is important because at this point no more heat is exchanged and therefore the temperature equals the corresponding phase border in the phase diagram.

4. Experimental section

4.1. Sample compositions

Sample compositions were selected to assume to have at least one sample in each three phase field for partial isothermal sections and to get DTA data for several isopleths to be able to propose a possible reaction scheme for higher temperatures. Almost no knowledge of the phase diagram is necessary to prepare samples on an isopleth but for samples in three phase fields a rough concept of possible equilibria is required.

Therefore at the very beginning two isopleths were investigated. The first one was a section at 10% Ti. The second was with constant 1:1 Al:Ti ratio and various Ge content. Since the phase AlTi was of special interest, the solubility of Ge in this phase also was investigated with several samples. Afterwards some important samples which were not in equilibrium after the initial treatment were prepared once again. Also some phase pure ternary compounds, which were found in other samples, were prepared for identification of their structure. Another intersection between the eutectic mixture of Aluminium and Germanium and AlTi was investigated since one main goal of this study was to find a low melting brazing material for AlTi which would very likely be part of this intersection. Also interesting for the brazing was the solubility of Germanium in Al₃Ti and it was therefore studied. Those samples already clarified some three phase fields but others needed additional samples to verify them. Also, a certain composition was selected and prepared to do some brazing experiments. Since some results contradicted the binary phase diagram, also some investigations were done in the binary Ti-Ge. All prepared samples are drawn in Figure 17 and listed in Table 6 with the used temperature program. All samples which were found to be in thermal equilibrium are bold in this table. Samples not in equilibrium showed more than three phases or remaining titanium pieces. Further details about the samples can be found in chapter 5.

Sample	desired Atom%			real Atom%			Temperature program and comments
	Al	Ge	Ti	Al	Ge	Ti	
1	80	10	10	80.07	9.97	9.96	400°C, 3 Weeks
2	70	20	10	69.96	20.01	10.03	400°C, 3 Weeks
3	60	30	10	59.93	30.00	10.06	400°C, 3 Weeks
4	50	40	10	50.07	39.92	10.01	400°C, 3 Weeks
5	40	50	10	39.96	50.01	10.03	400°C, 3 Weeks
6	30	60	10	30.03	60.01	9.96	400°C, 3 Weeks
7	20	70	10	20.01	69.98	10.01	400°C, 3 Weeks
8	10	80	10	10.06	79.91	10.03	400°C, 3 Weeks
9	47.5	5	47.5	47.56	5.00	47.44	1000°C, 2 Weeks
10	45	10	45	44.97	10.02	45.01	1000°C, 2 Weeks
11	42.5	15	42.5	42.59	14.99	42.43	1000°C, 2 Weeks
12	40	20	40	40.04	19.95	40.01	1000°C, 2 Weeks
13	35	30	35	34.93	30.00	35.07	1000°C, 2 Weeks
14	30	40	30	30.00	40.02	29.97	1000°C, 2 Weeks
15	37	8	55	36.96	8.02	55.02	1000°C, 2 Weeks
16	44	8	48	44.02	7.99	47.99	1000°C, 2 Weeks
17	51	8	41	50.96	7.98	41.06	1000°C, 2 Weeks
18	58	8	34	58.00	8.00	34.00	1000°C, 2 Weeks
19	80	10	10	80.02	10.02	9.96	590 → 400°C, 96 Hours
20	70	20	10	70.07	19.97	9.96	powdered, 400°C, 3 Weeks
21	60	30	10	60.04	30.01	9.95	powdered, 400°C, 3 Weeks
22	50	40	10	50.06	39.92	10.01	powdered, 400°C, 3 Weeks
23	40	50	10	39.91	50.01	10.08	powdered, 400°C, 3 Weeks
24	30	60	10	30.05	59.94	10.01	powdered, 400°C, 3 Weeks
25	20	70	10	20.09	69.90	10.00	powdered, 400°C, 3 Weeks
26	10	80	10	9.90	80.07	10.02	powdered, 400°C, 3 Weeks
27	70	26	4	70.01	26.01	3.98	550°C → 400°C, 75 Hours
28	67	29	4	66.97	29.01	4.01	550°C → 400°C, 75 Hours
29	58	22	20	57.98	22.00	20.02	550°C → 400°C, 75 Hours; 400°C, 1 Week
30	52	34	14	52.00	34.01	13.99	550°C → 400°C, 75 Hours; 400°C, 1 Week
31	20	70	10	20.10	69.93	9.98	550°C → 400°C, 75 Hours
32	69.5	24.5	6	69.48	24.49	6.03	560°C → 400°C, 48 Hours; 400°C, 5 Days

4. Experimental section

Sample	desired Atom%			real Atom%			Temperature program and comments
	Al	Ge	Ti	Al	Ge	Ti	
33	68	23	9	67.98	22.98	9.04	560°C → 400°C, 48 Hours; 400°C, 5 Days
34	66.5	21	12.5	66.51	20.98	12.51	560°C → 400°C, 48 Hours; 400°C, 5 Days
35	65	19	16	65.03	18.99	15.98	560°C → 400°C, 48 Hours; 400°C, 5 Days
36	61	14	25	61.03	14.00	24.96	900°C → 520°C, 48 Hours; 520°C, 5 Days
37	56	8	36	56.03	7.99	35.98	900°C → 520°C, 48 Hours; 520°C, 5 Days
38	55	20	25	55.01	20.04	24.95	900°C → 520°C, 48 Hours; 520°C, 5 Days
39	50	25	25	50.01	24.99	25.00	900°C → 520°C, 48 Hours; 520°C, 5 Days
40	2.5	95	2.5	2.47	95.06	2.47	900°C → 520°C, 48 Hours; 520°C, 5 Days
41	5	90	5	4.99	90.02	4.99	900°C → 520°C, 48 Hours; 520°C, 5 Days
42	7.5	85	7.5	7.50	85.04	7.46	900°C → 520°C, 48 Hours; 520°C, 5 Days
43	15	70	15	15.05	69.93	15.02	900°C → 520°C, 48 Hours; 520°C, 5 Days
44	20	60	20	19.90	60.09	20.01	900°C → 520°C, 48 Hours; 520°C, 5 Days
45	25	50	25	25.05	49.97	24.98	900°C → 520°C, 48 Hours; 520°C, 5 Days
46	65	15	20	65.01	14.99	20.00	560°C → 400°C, 48 Hours; 400°C, 4 Weeks
47	71	9	20	70.99	8.98	20.03	560°C → 400°C, 48 Hours; 400°C, 4 Weeks
48	6	61	33	6.08	60.95	32.98	900°C, 1 Week; 900°C → 520°C, 48 Hours; 520°C, 3 Weeks
49	13	54	33	12.96	54.04	33.00	520°C, 4 Weeks
50	19	47	34	19.00	46.99	34.01	520°C, 4 Weeks
51	35	30	35	35.01	29.98	35.00	520°C, 4 Weeks
52	30	40	30	29.95	39.99	30.06	520°C, 4 Weeks
53	8	65	27	8.06	64.95	26.99	900°C, 1 Week; 900°C → 520°C, 48 Hours; 520°C, 3 Weeks
54	2	44	54	1.95	44.01	54.04	1000°C, 4 Weeks
55	5	41	54	4.90	41.04	54.05	1000°C, 4 Weeks
56	8	38	54	8.03	38.02	53.95	1000°C, 4 Weeks

Sample	desired Atom%			real Atom%			Temperature program and comments
	Al	Ge	Ti	Al	Ge	Ti	
57	11	35	54	11.01	34.98	54.02	1000°C, 4 Weeks
58	24	41	35	24.02	41.03	34.95	520°C, 4 Weeks
59	69.5	24.5	6	69.49	24.47	6.03	560°C → 400°C, 48 Hours; 400°C, 4 Weeks
60	70.18	27.82	2	70.18	27.83	1.99	Arc furnace only
61	73	12.5	14.5	73.01	12.48	14.51	560°C → 450°C, 48 Hours; 450°C, 4 Weeks
62	67	15.5	17.5	67.02	15.50	17.47	560°C → 450°C, 48 Hours; 450°C, 4 Weeks
63	4	44	52	4.07	43.98	51.95	1000°C, 4 Weeks
64	4	38	58	4.06	37.96	57.98	1000°C, 4 Weeks
65	51.5	34.2	14.3	51.48	34.20	14.32	800°C → 550°C, 48 Hours; 550°C, 4 Weeks
66	0	51	49	0.00	51.00	49.00	1000°C, 4 Weeks
67	0	42	58	0.00	42.00	58.00	1000°C, 4 Weeks
68	0	32	68	0.00	31.97	68.03	1000°C, 4 Weeks
69	5	68	27	4.93	68.10	26.97	1000°C, 1 Weeks; 1000°C → 520°C, 48 Hours; 520°C, 3 Weeks
70	20	32	48	20.09	32.00	47.91	1000°C, 4 Weeks
71	6	56	38	6.00	56.01	37.99	520°C, 4 Weeks
72	4	58	38	4.02	57.97	38.02	520°C, 4 Weeks
73	73	11	16	73.02	10.99	15.99	400°C, 4 Weeks
74	35	30	35	35.00	30.00	35.00	520°C, 4 Weeks
75	50	25	25	50.01	25.01	24.98	520°C, 4 Weeks
76	51.5	34.2	14.3	51.48	34.20	14.32	800°C, 4 Weeks
77	51.5	34.2	14.3	51.48	34.20	14.32	540°C, 4 Weeks
78	0	90	10	0.00	90.00	10.00	Arc furnace only
79	0	42.5	57.5	0.00	42.47	57.53	1000°C, 23 Days

Table 7: Composition and temperature program of all prepared samples.
Equilibrium samples: bold

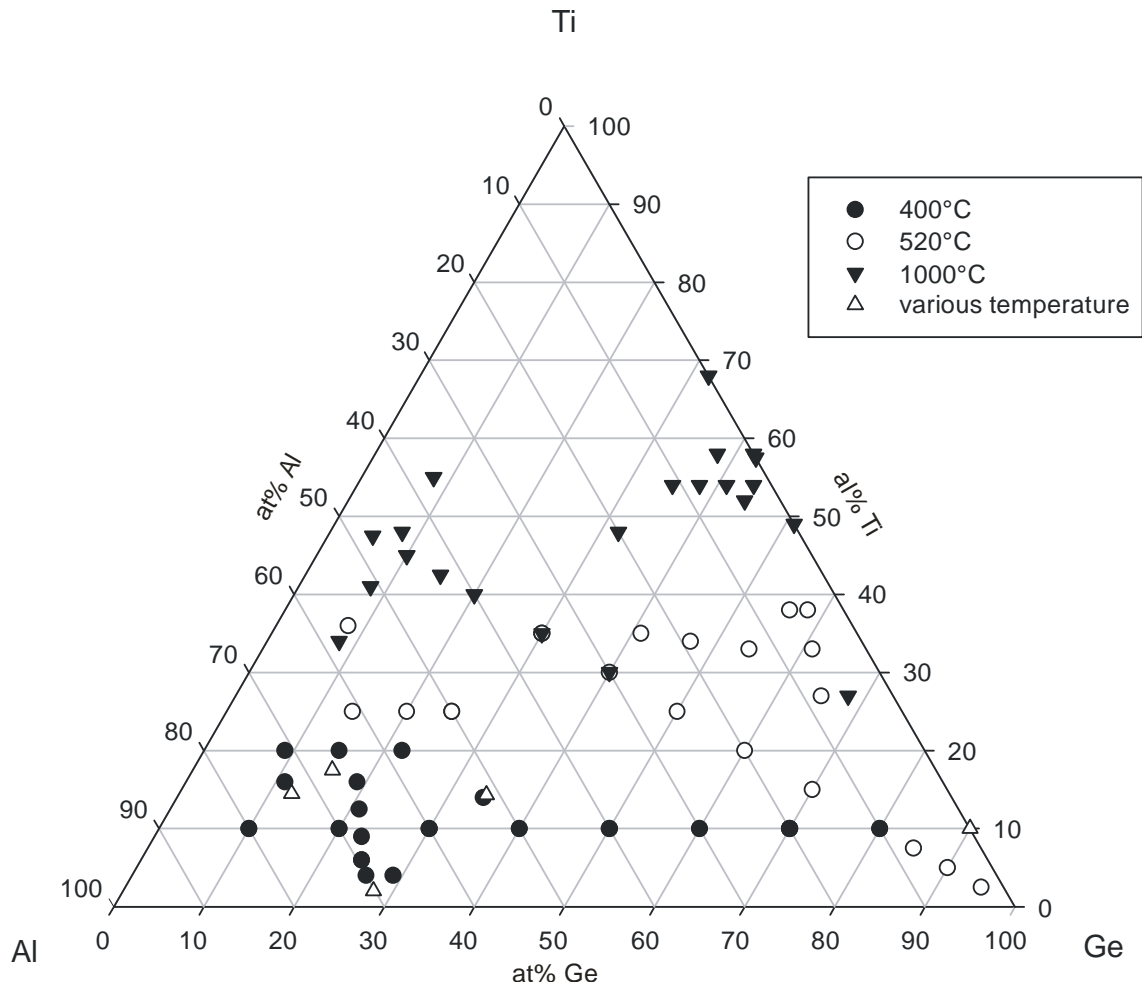


Figure 17: Prepared samples

4.2. Sample preparation

4.2.1. Basic metals and weighing

The following metals basis were used for this investigation:

Aluminium: Aluminium slug, 3.175mm diameter x 6.35mm length, Puratronic 99.999%, Alfa Aesar

Germanium: Germanium pieces, 3-9mm, 99.999%, Alfa Aesar

Titanium: Titanium rod, 6.4mm diameter, 25cm length, 99.99%, Alfa Aesar

The Samples were weighted with a Satorius microbalance R200D with an accuracy of about ± 0.05 mg. Since the total mass of the prepared samples were between 600 and

1000 mg this leads to a weight error of less than 0.01at% for the single elements in the sample.

4.2.2. Arc furnace

Afterwards the samples were molten in an arc furnace MAM 1 by the company Johanna Otto GmbH.

The core of this device is a chamber which two electrodes inside. The first one is a tip on the upper side which is made of tungsten because of the high melting point of this metal. It is possible to move this tip with an arm on top of the chamber. The second electrode is a copper plate with several cavities. Copper is used because of the high thermal conductivity which allows an efficient cooling while the cavities are necessary to bring the different pieces of a sample properly in contact and melt them together. Both electrodes are cooled with water. A vacuum pump as well as an argon gas cylinder (argon 5.0, >99.999%) is connected to the chamber which is crucial to remove oxygen and replace it with an inert atmosphere.

For the melting process the chamber is evacuated and purged with argon several times. Afterwards high voltage is applied to the electrodes and they are being short-circuited by touching the copper plate with the tungsten tip. This creates an arc with about 3000°C. Afterwards a zirconium piece is molten to remove remaining oxygen in the chamber. Due to the high affinity of those two elements they react with each other and form solid zirconium oxides. Every sample is molten three times and turned upside-down in between to obtain a homogeneous distribution of the different elements.



Figure 18: Arc furnace MAM1 Johanna Otto [34]

4.2.3. Equilibration

After melting the sample to a pellet, it was put into an alumina crucible to avoid direct contact between quartz glass and the sample since they would react at higher temperatures. The crucible was placed inside a quartz glass tube which already was closed on one side. After evacuating and purging with argon several times, the tube got evacuated once again to reach a vacuum below $4 \cdot 10^{-3}$ mBar. At this pressure the tube with the sample inside was sealed on the other end using a H₂/O₂ welding equipment. The sealed sample was put into a muffle furnace at temperatures between 400°C and 1000°C for one to four weeks depending on the planned temperature program for the sample.

Most of the samples were sealed directly after the arc furnace but some were powdered with a tungsten carbide mortar, sieved with a mesh of 0.18mm and pressed with an hydraulic press with 15kN for 3 minutes to powder pellets of 5mm diameter. They were sealed for the heat treatment as a pressed pill in an alumina crucible in quartz glass. Since this procedure was not very effective it was just used for one set of samples.

After annealing the samples were quenched in cold water to maintain the thermodynamic conditions at the annealing temperatures. The samples were crushed in a tungsten carbide mortar to get several pieces for different investigations. One part were powdered and sieved with 0.18mm mesh for a X-ray diffraction measurement, another part was used for DTA (differential thermal analysis) measurement and one part was embedded for SEM (scanning electron microscope) or EPMA (electron probe micro analysis).

For embedding one surface of the samples was ground by hand to improve the grinding time in the machine afterwards significantly. Then the prepared piece was placed in a LaboPress by Struers together with phenolic hot mounting resin with carbon filler (Struers PolyFast). The carbon filler is necessary to obtain a sufficient electric conductivity for the following SEM and EPMA measurements. The resin was heated to 180°C for 6 minutes and afterwards cooled with water for 3 minutes. To obtain a flat surface the cylindrical bloc was ground in a MetaServ 2000 grinding and polishing machine with silicon carbide sandpapers with decreasing roughness in the range of 120 to 1200. Then the sample was then polished with an alumina powder with a particle size

of about 1 μm (Buehler, Micropolish II). The surface of the sample was then checked in an optical microscope in the dark-field mode regarding remaining scratches.

4.2.4. Problems

Almost half of the samples did not reach equilibrium. The arc furnace and the annealing program in the muffle furnace caused most of these problems.

One main reason for this was the high difference between the melting points of the metals, which leads to problems during arc melting. A rather low melting liquid is formed by the eutectic mixture of aluminium and germanium and therefore the appearance indicates a homogenous distribution. However, there may still be some pure high melting titanium pieces left. In this case it is impossible to reach equilibrium with reasonable annealing times in the muffle furnace with such samples because of the long diffusion distances. To avoid such problems each sample was melted three times in the arc furnace as well as it was heated for a couple more seconds after it becomes evidently liquid to improve the homogeneity.

Too long heating with the arc leads to another problem. The vapour pressure of aluminium and germanium is not negligible. Therefore, long heating leads to mass loss and the accurate composition of the sample is not longer known. Heating for about 10 to 15 seconds after the initial melting turned out to be an acceptable compromise.

Another problem during the arc furnace melting is the high affinity of titanium and aluminium to oxygen. Therefore, a thorough purging of the chamber with argon is crucial as well as melting a zirconium getter in order to bind remaining oxygen. It is also recommended to check the surface of the zirconium getter after melting it but before treating the sample for obvious changes in colour. The shiny silver surface becomes greyish, blackish and dim with oxygen. It's also important to observe the mass change during the different melting steps. Since mass loss due to evaporation and mass gain due to oxygen can compensate each other, a rather constant mass cannot ensure a neat condition of the sample but a big deviation indicates some kind of problems.

During sealing the glass tube with the sample inside, it is important to ensure that no glass is in contact with the sample because of possible reaction at higher temperatures.

The formation of gaseous species SiO can transport oxygen out of the glass into the sample. So the glass was cleaned properly at the very beginning and only few big pieces of the sample were used.

Since the annealing time is solely based on experience and shorter annealing times are obviously desirable, it happened several times that rather small pieces of a non equilibrium phase were still present within a shell of another phase, while other samples with the same annealing program were in equilibrium. Longer annealing durations increase the chance of getting equilibrium conditions but at the cost of precious time.

4.3. Measurements

4.3.1. SEM, EPMA

The annealed and embedded samples were measured either with a Zeiss Supra 55 VP scanning electron microscope (SEM) or in few cases with a Cameca SX Electron Probe 100 electron probe micro analyzer (EPMA) for the quantitative investigation of the composition of the different phases and to determine solid solubilities and phase equilibria.

For the SEM measurements an acceleration voltage of 20kV was used as well as a 120 μ m aperture. The calibration of the energy dispersive detector was made with cobalt. A backscattered electrons or secondary electrons detector was used for imaging of the sample. The EPMA measurements were done with an acceleration voltage of 15kV and a beam current of 10nA using a wavelength dispersive detector. Imaging was done using a backscattered electrons detector. In each case at least three measurements of each phase were made to obtain reliable mean values. The calibration was done with the pure elements. The used



Figure 19: Scanning electron microscope Zeiss Supra 55 VP [35]

lines and crystals for the evaluation of the content of the different elements can be found in Table 8.

Element	Used X-ray Line	Analyzing crystal
Al	K α	TAP (thallium acid phthalate)
Ge	K α	LLIF (large lithium fluoride)
Ti	K α	PET (pentaerythritol)

Table 8: EPMA setup

4.3.2. X-ray powder diffractometry (XRD)

For these measurements a Bruker D8 Discover Series 2 was used to identify and crosscheck the present phases observed with SEM and to obtain structural parameters.

The device uses a Bragg-Brentano pseudo focusing geometry and a $\theta/2\theta$ arrangement. For the X-ray generation 40kV acceleration voltage and a current of 40mA was set with copper as anode material. A variable aperture was used to maintain a constant amount of X-ray radiation interfering with the sample independent of the current angle. The desired width of the area is 12 mm. The detector (LynxEye) used was based on silicon stripes

for simultaneous measurement of $\sim 3^\circ$ to improve the measuring time without losses in the signal/noise ratio. For the measurement the sample was powdered with a tungsten carbide mortar and afterwards sieved with a 0.18mm mesh. It was applied using grease dissolved in glycerine to a silicon single crystal sample holder. Every sample was measured for approximately one hour.

The evaluation of the data was done with the program TOPAS by Bruker in terms of Rietveld refinement. Structural information about the phases was taken from Pearson's handbook of crystallographic data for intermetallic phases, if available.



Figure 20: X-ray powder diffractometer Bruker D8 Discover Series 2 [36]

4.3.3. Differential thermal analysis (DTA)

Only samples which were found to be in equilibrium by SEM and XRD were measured with DTA to avoid wrong and misleading results. A Setaram SETSYS Evolution TGA & DTA 2400 was used in order to obtain the temperatures of phase transitions and construct a reaction scheme from that.

The thermocouple consists of platinum and platinum90%/rhodium10% (type-S), which works up to 1600°C. For calibration, the melting points of gold, nickel and tin were measured. A sample mass of 20 to 50 mg was used in an open alumina crucible under constant argon flow of 20ml/min with pure titanium foil as reference

material. A scheme of the arrangement can be found in Figure 22. To avoid reactions with oxygen, the system was evacuated three times and purged with argon afterwards. As shown in Figure 23, two cycles were performed for each sample with a heating rate

of 5 K/min starting at room temperature and ending at a temperature slightly above the estimated melting point. Afterwards the samples were weighted back but no significant mass change was observed.

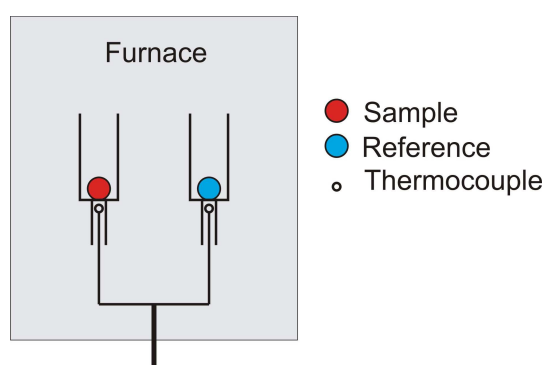


Figure 22: Schematic DTA setup



Figure 21: differential thermal analyzer Setaram SETSYS Evolution TGA & DTA 2400 [37]

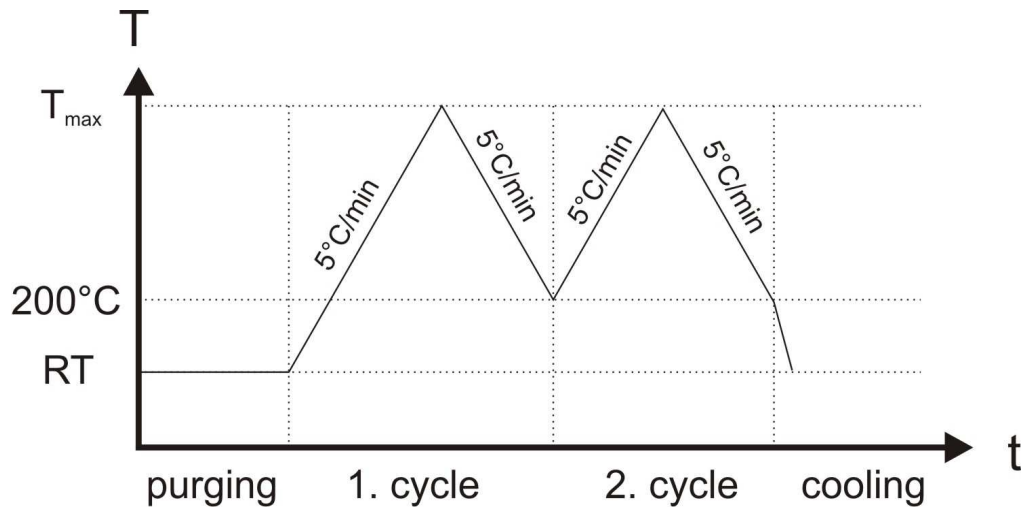


Figure 23: DTA heating program

Only the first heating/cooling sequence was used for the evaluation of effects because during this step the sample definitely was in equilibrium, which wasn't certain in the second sequence. For the determination of liquidus and solidus temperatures both cycles were used.

5. Results and discussion

5.1. Partial isothermal sections

5.1.1. 400°C

The composition of all prepared samples annealed at 400°C is drawn in Figure 24, together with the resulting phase fields. The results of those samples which were found to be in equilibrium are presented in Table 9.

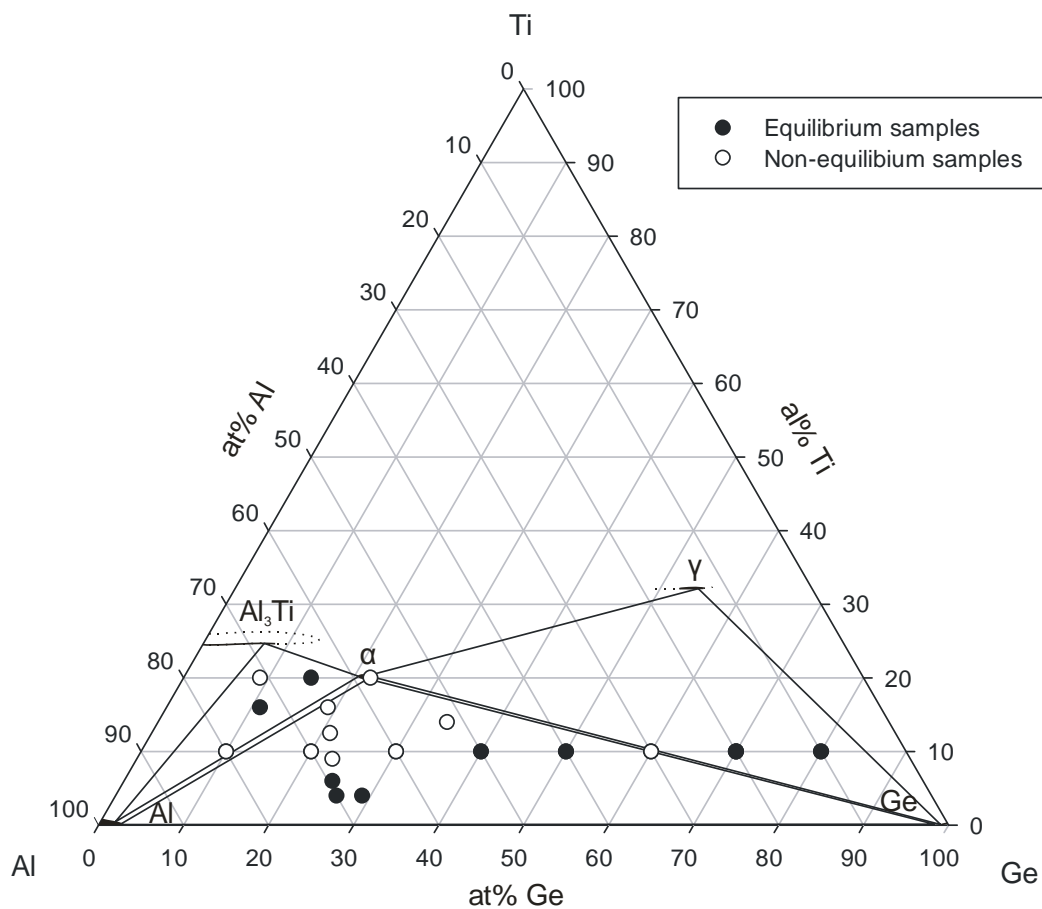


Figure 24: partial isothermal section at 400°C and prepared samples

Equilibrium samples in three-phase-field Al-Ge- α					
Sample	XRD		SEM (at%)		
Composition	Phase	Lattice parameter (\AA)	Al	Ge	Ti
Sample 4 $\text{Al}_{50}\text{Ge}_{40}\text{Ti}_{10}$	Al	a= 4.0523(2)	97.56	2.35	0.09
	Ge	a= 5.66207(3)	2.07	97.80	0.13
	α	*	58.60	21.60	19.80
Sample 5 $\text{Al}_{40}\text{Ge}_{50}\text{Ti}_{10}$	Al	a= 4.0532(3)	97.35	2.57	0.08
	Ge	a= 5.66219(2)	1.21	98.70	0.10
	α	*	58.24	21.86	19.89
Sample 27 $\text{Al}_{70}\text{Ge}_{26}\text{Ti}_4$	Al	a= 4.05054(4)	97.51	2.49	0.00
	Ge	a= 5.66033(2)	0.97	99.04	0.00
	α	*	56.32	23.40	20.28
Sample 28 $\text{Al}_{67}\text{Ge}_{29}\text{Ti}_4$	Al	a= 4.05049(3)	97.33	2.67	0.00
	Ge	a= 5.65929(2)	0.00	100.00	0.00
	α	*	56.50	23.09	20.42
Sample 32 $\text{Al}_{69.5}\text{Ge}_{24.5}\text{Ti}_6$	Al	a= 4.05011(3)	96.50	2.51	0.99
	Ge	a= 5.66017(2)	2.96	97.04	0.00
	α	*	55.99	24.93	19.09
Equilibrium samples in three-phase-field Ge- γ - α					
Sample	XRD		SEM (at%)		
Composition	Phase	Lattice parameter (\AA)	Al	Ge	Ti
Sample 7 $\text{Al}_{20}\text{Ge}_{70}\text{Ti}_{10}$	Ge	a= 5.66074(1)	1.06	98.88	0.06
	γ	a= 3.6852(1) c= 28.297(2)	12.17	56.47	31.37
	α	*	58.18	21.71	20.12
Sample 8 $\text{Al}_{10}\text{Ge}_{80}\text{Ti}_{10}$	Ge	a= 5.66163(2)	0.77	99.17	0.07
	γ	a= 3.6906(1) c= 28.183(2)	14.53	52.55	32.92
	α	*	58.20	21.31	20.49
Sample 31 $\text{Al}_{20}\text{Ge}_{70}\text{Ti}_{10}$	Ge	a= 5.66156(2)	0.00	100.00	0.00
	γ	a= 3.69482(9) c= 28.078(2)	15.29	51.37	33.34
	α	*	55.44	23.72	20.84

Equilibrium samples in three-phase-field Al-Al ₃ Ti- α					
Sample	XRD		SEM (at%)		
Composition	Phase	Lattice parameter (Å)	Al	Ge	Ti
Sample 46 Al ₆₅ Ge ₁₅ Ti ₂₀	Al	a= 4.0486(1)	95.09	2.89	2.02
	Al ₃ Ti	a= 3.8251(1) c= 8.6436(5)	67.51	7.64	24.84
	α	*	59.49	20.59	19.93
Sample 73 Al ₇₃ Ge ₁₁ Ti ₁₆	Al	a= 4.05259(5)	97.84	0.42	1.74
	Al ₃ Ti	a= 3.8351(1) c= 8.6375(4)	68.13	6.17	25.70
	α	*	59.09	20.44	20.46

Table 9: Equilibrium samples at 400°C; * Structure not determined

Three three-phase-fields were found. The first one is between Al, Ge and a new phase with the approximate composition Al₅₈Ge₂₂Ti₂₀, which will be called α in this work. All available information about α will be discussed in chapter 5.2.1. There are some small deviations between the different samples regarding the exact composition and the lattice parameter of the corners of this phase field, which can be seen in Table 9. However, sample 27, 28 and 32 were prepared not by long annealing at one temperature but by slow cooling from 550°C to 400°C and by a subsequent short annealing in order to obtain single crystals for α . Therefore there is the assumption that those three samples, although they show the right phases, did not have enough time at the chosen temperature to reach the exact composition and the correspondent lattice parameters. The other samples in this phase field are also in quite good agreement with the binary phase diagrams and are therefore used for the construction of the phase field.

The phase field Al₃Ti- γ - α contains another new ternary - here called γ - phase with the approximate composition Al₉₋₂₁Ge₅₈₋₄₆Ti₃₃, which again will be discussed later in chapter 5.2.3. The shift in the lattice parameter of γ , which was observed in sample 7, 8 and 31, is in correlation with its change in composition. This can be explained by the different thermal history of these samples.

Al-Al₃Ti- α is the last three-phase-field observed in this isothermal section. It shows consistent lattice parameter and atomic percentages but since the measurement of aluminium in sample 46 did not show realistic values of weight percentage, it was not

used for the construction of Figure 24. Al_3Ti shows a remarkable solubility of germanium. This will be further discussed in chapter 5.1.2, since the solubility was not determined at 400°C .

5.1.2. 520°C

The composition of all prepared samples annealed at 520°C is drawn in Figure 25, as well as the resulting phase fields. The results from those samples which were found to be in equilibrium are presented in Table 10.

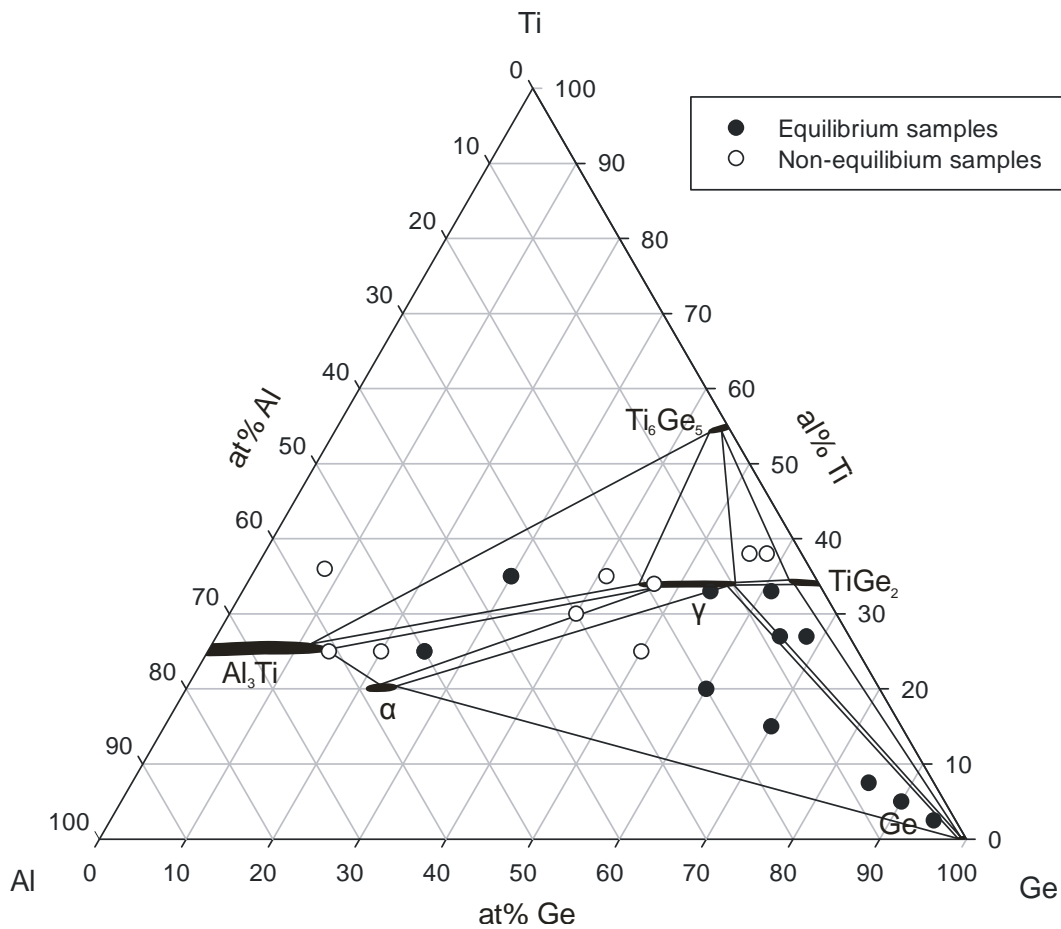


Figure 25: partial isothermal section and prepared samples at 520°C

Equilibrium samples in three-phase-field Ge- γ - α					
Sample	XRD		SEM (at%)		
Composition	Phase	Lattice parameter (Å)	Al	Ge	Ti
Sample 40 $\text{Al}_{2.5}\text{Ge}_{95}\text{Ti}_{2.5}$	Ge	a= 5.65738(1)	0.00	100.00	0.00
	γ	a= 3.6862(3) c= 28.248(5)	15.06	52.22	32.73
	α	refinement not possible	54.77	24.19	21.04
Sample 41 $\text{Al}_5\text{Ge}_{90}\text{Ti}_5$	Ge	a= 5.65808(1)	0.00	100.00	0.00
	γ	a= 3.6862(1) c= 28.261(2)	10.23	57.24	32.53
	α	refinement not possible	55.08	24.39	20.53
Sample 42 $\text{Al}_{7.5}\text{Ge}_{85}\text{Ti}_{7.5}$	Ge	a= 5.65901(1)	0.00	100.00	0.00
	γ	a= 3.68526(8) c= 28.275(1)	11.70	54.84	33.46
	α	refinement not possible	55.23	23.98	20.79
Sample 43 $\text{Al}_{15}\text{Ge}_{70}\text{Ti}_{15}$	Ge	a= 5.65916(1)	1.61	98.39	0.00
	γ	a= 3.68448(5) c= 28.2812(7)	13.13	52.89	33.98
	α	refinement not possible	55.39	23.95	20.67
Sample 44 $\text{Al}_{20}\text{Ge}_{60}\text{Ti}_{20}$	Ge	a= 5.660349(9)	0.00	100.00	0.00
	γ	a= 3.68380(2) c= 28.3098(3)	10.22	55.73	34.05
	α	refinement not possible	55.32	23.77	20.91
Equilibrium samples in three-phase-field Al_3Ti - γ - α					
Sample	XRD		SEM (at%)		
Composition	Phase	Lattice parameter (Å)	Al	Ge	Ti
Sample 75 $\text{Al}_{50}\text{Ge}_{25}\text{Ti}_{25}$	Al_3Ti	a= 3.82090(4) c= 8.6666(1)	61.74	12.68	25.58
	γ	a= 3.69622(5) c= 28.0432(9)	17.62	48.58	33.81
	α	refinement not possible	57.52	21.96	20.51

Equilibrium samples in three-phase-field Ge-TiGe ₂ - γ					
Sample	XRD		SEM (at%)		
Composition	Phase	Lattice parameter (Å)	Al	Ge	Ti
Sample 53 Al ₈ Ge ₆₅ Ti ₂₇	Ge	a= 5.66004(2)	1.58	98.42	0.00
	TiGe ₂	a= 8.6137(3) b= 5.0341(2) c= 8.8112(3)	3.44	63.06	33.50
	γ	a= 3.68370(2) c= 28.3254(2)	10.44	56.01	33.55
Sample 69 Al ₅ Ge ₆₈ Ti ₂₇	Ge	a= 5.65725(2)	1.39	98.22	0.39
	TiGe ₂	a= 8.6078(1) b= 5.03076(6) c= 8.8000(2)	2.26	63.41	34.33
	γ	a= 3.68144(4) c= 28.3095(6)	9.27	56.60	34.14
Non-Equilibrium samples in three-phase-field TiGe ₂ -Ti ₆ Ge ₅ - γ					
Sample	XRD		SEM (at%)		
Composition	Phase	Lattice parameter (Å)	Al	Ge	Ti
Sample 71 Al ₆ Ge ₅₆ Ti ₃₈	TiGe ₂	a= 8.615(2) b= 5.031(2) c= 8.804(2)	4.16	61.46	34.37
	Ti ₆ Ge ₅	a= 16.9234(6) b= 7.9441(3) c= 5.2317(2)	1.34	44.30	54.36
	γ	a= 3.68445(2) c= 28.3223(4)	10.27	55.67	34.06
	Ge	a= 5.65977(5)	2.90	96.38	0.73

Sample 72 $\text{Al}_4\text{Ge}_{58}\text{Ti}_{38}$	TiGe_2	a= 8.6152(1) b= 5.0353(1) c= 8.8004(2)	2.21	63.16	34.63
	Ti_6Ge_5	a= 16.9239(3) b= 7.9444(2) c= 5.23113(9)	0.75	44.56	54.69
	γ	a= 3.68396(3) c= 28.3227(5)	8.85	56.86	34.30
	Ge	a= 5.65937(4)	1.73	97.66	0.61
Equilibrium samples in three-phase-field $\text{Al}_3\text{Ti}-\text{Ti}_6\text{Ge}_5-\gamma$					
Sample	XRD		SEM (at%)		
Composition	Phase	Lattice parameter (\AA)	Al	Ge	Ti
Sample 74 $\text{Al}_{35}\text{Ge}_{30}\text{Ti}_{35}$	Al_3Ti	a= 3.82472(6) c= 8.6571(2)	63.33	11.01	25.66
	Ti_6Ge_5	a= 16.9323(5) b= 7.9470(2) c= 5.2336(1)	2.51	43.31	54.18
	γ	a= 3.70481(6) c= 27.883(1)	20.78	45.26	33.96
Two-phase field samples					
Sample	XRD		SEM (at%)		
Composition	Phase	Lattice parameter(\AA)	Al	Ge	Ti
Sample 48 $\text{Al}_6\text{Ge}_{61}\text{Ti}_{33}$	TiGe_2	a= 8.61150(7) b= 5.03409(4) c= 8.81223(8)	3.85	62.40	33.76
	γ	a= 3.6833(3) c= 28.322(4)	10.02	56.14	33.84
Sample 49 $\text{Al}_{13}\text{Ge}_{54}\text{Ti}_{33}$	Ge	a= 5.65895(9)	1.87	95.96	2.17
	γ	a= 3.68464(2) c= 28.3067(2)	13.47	52.78	33.75

Table 10: Equilibrium samples at 520°C

In the three-phase-field α - γ -Ge the samples show a consistent behaviour except for the distribution of the Al:Ge ratio in the γ phase, which exceeds the error of the SEM device of approximately 1%. This occurred most likely due to a different composition of γ after arc melting, which, afterwards, did not reach equilibrium during annealing because diffusion is quite low at this temperature.

The phase fields $\text{Al}_3\text{Ti-Ti}_6\text{Ge}_5$ - γ , Ge-TiGe_2 - γ , $\text{Al}_3\text{Ti-}\gamma$ - α either consist of just one equilibrium-sample or show quite consistent behaviour and therefore no further discussion is needed for those.

Also, in this isothermal section Al_3Ti shows a high solubility for germanium. In theory this can be explained by substitution of aluminium by germanium on aluminium positions since they show similar covalent radius and chemical behaviour. This could be confirmed by Rietveld refinement. In Figure 26 there is the calculated pattern of Al_3Ti once with some amount of germanium on both aluminium positions (blue line) and once without germanium (red line) in comparison with the measured pattern of sample 74. Refinements of the Ge-site occupation are in acceptable agreement with the composition results from SEM measurements. The refined composition in comparison with the composition measured with SEM can be found in Table 11. Also the ratio of the shown peaks indicates the trend to higher electron densities necessary at the aluminium positions. It was not possible to draw a significant graph showing the relation between the change of composition and the lattice parameter for this phase because not enough samples with varying composition were produced.

	Al	Ge	Ti
XRD	58.96	16.07	24.97
SEM	63.33	11.01	25.66

Table 11: Comparison of refined XRD data and data measured by SEM of Al_3Ti in Sample 74

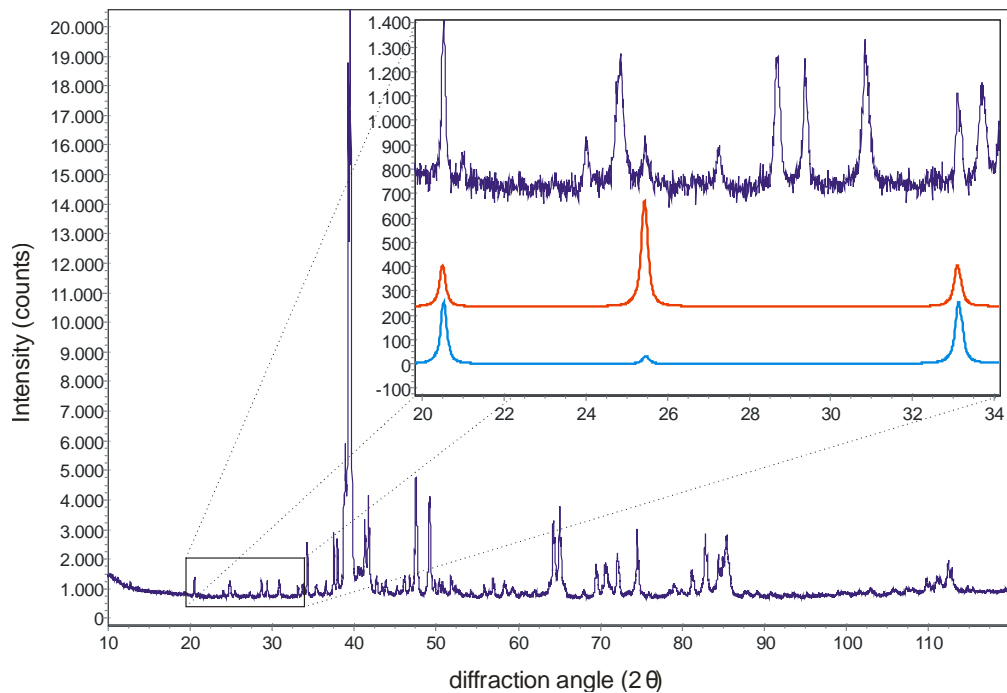


Figure 26: XRD of sample 74, calculated Al_3Ti with refined Ge:Al ratio positions (blue) and without (red)

In the phase field $\text{TiGe}_2\text{-Ti}_6\text{Ge}_5\text{-}\gamma$ there are just two non-equilibrium samples showing all expected phases together with a small amount of pure germanium. Since all surrounding phase fields are already described free of doubt, this phase field has to exist based on simple geometry. Therefore the germanium in these samples is considered to be a residue of the non equilibrium conditions after arc melting which could not be removed completely. These circumstances, in connection with the fact that no new phase was found in this region, make this phase field to the most probable solution. The resulting phase field fits perfectly in the remaining gap in this region and the measured composition of all three corners yield reasonable results. Therefore these samples are used to construct this three-phase-field even though they are not in equilibrium.

The SEM measurements of the two-phase field samples containing a big amount of γ was very difficult due to the brittleness of γ hindering the polishing process. In Addition the other phases were present in such little amounts that the minimal area necessary for a measurement was barely reached. The measurement is considered to be not very reliable and it is therefore neglected.

It was necessary to adjust the Ge-corners of the phase fields Ge- α - γ and Ge-TiGe₂- γ because the phase fields overlapped slightly, which is obviously forbidden. The error was in the range of about 1at.% and is therefore most likely due to inaccuracy of the SEM measurement. In the Ge- α - γ phase field Ge showed in several measurements no solubility at all, while in the Ge-TiGe₂- γ phase field Ge solved about the amount of aluminium and titanium expected from the binary phase diagrams. Since no solubility at all is a quite unlikely case considering all other informations, the aluminium and titanium content in Ge in the Ge- α - γ phase field was increased so no more overlapping occurred.

5.1.3. 1000°C

The samples at 1000°C worked best of all chosen temperatures. Again all equilibrium and non-equilibrium samples as well as the resulting phase equilibria are drawn in Figure 27.

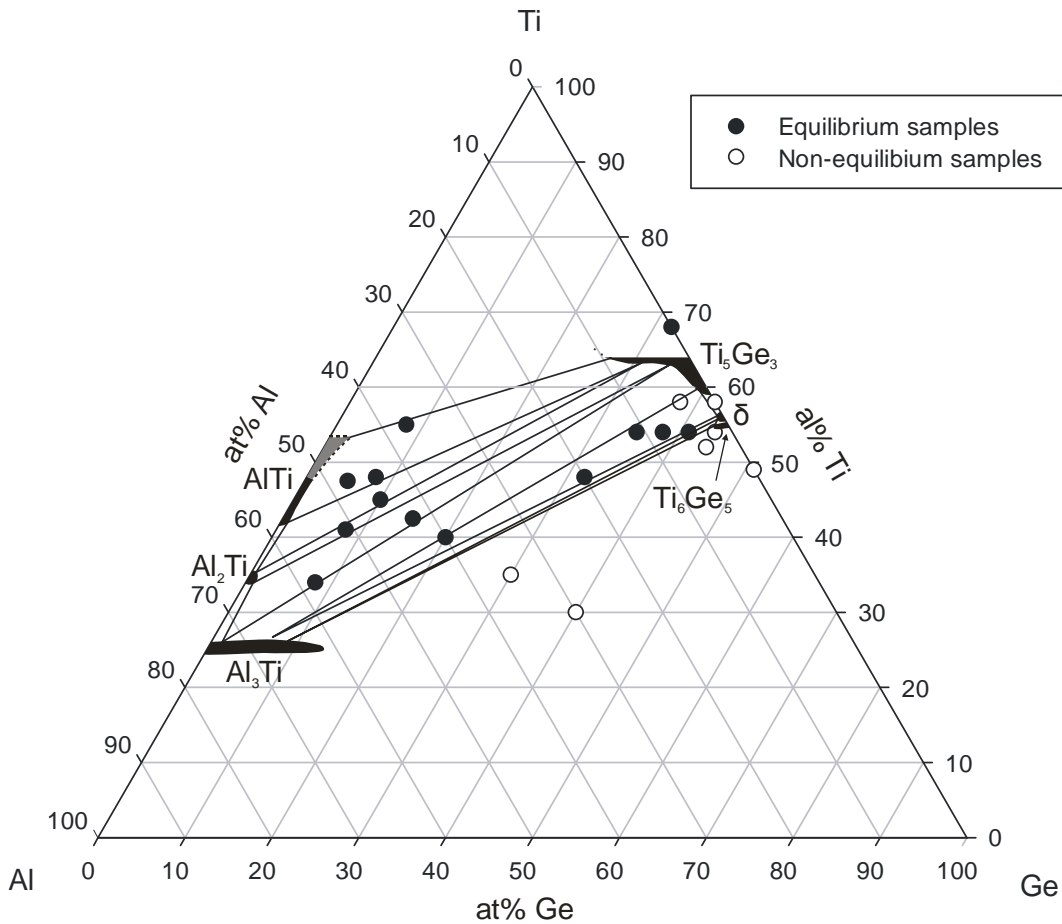


Figure 27: Partial isothermal section and prepared samples at 1000°C

Equilibrium samples in three-phase-field AlTi-Al ₂ Ti-Ti ₅ Ge ₃					
Sample	XRD		SEM (at%)		
Composition	Phase	Lattice parameter (Å)	Al	Ge	Ti
Sample 10 Al ₄₅ Ge ₁₀ Ti ₄₅	AlTi	a= 3.9897(3) c= 4.0575(4)	57.16	0.84	42.00
	Al ₂ Ti	a= 3.9730(3) c= 24.308(4)	64.16	0.54	35.30
	Ti ₅ Ge ₃	a= 7.5643(1) c= 5.2302(1)	5.78	30.96	63.26

Equilibrium samples in three-phase-field Al ₃ Ti-Al ₂ Ti-Ti ₅ Ge ₃					
Sample	XRD		SEM (at%)		
Composition	Phase	Lattice parameter (Å)	Al	Ge	Ti
Sample 11 Al _{42.5} Ge ₁₅ Ti _{42.5}	Al ₃ Ti	a= 3.85124(9) c= 8.6036(4)	72.44	1.43	26.13
	Al ₂ Ti	a= 3.9695(1) c= 24.306(2)	65.17	1.00	33.83
	Ti ₅ Ge ₃	a= 7.55925(5) c= 5.22891(6)	3.14	34.25	62.62
Sample 18 Al ₅₈ G ₁₈ Ti ₃₄	Al ₃ Ti	a= 3.85111(4) c= 8.6058(1)	72.98	1.09	25.93
	Al ₂ Ti	a= 3.9697(1) c= 24.304(2)	65.22	0.83	33.96
	Ti ₅ Ge ₃	a= 7.5524(1) c= 5.2330(2)	2.24	34.41	63.35
Equilibrium samples in three-phase-field Al ₃ Ti- Ti ₅ Ge ₃ -δ					
Sample	XRD		SEM (at%)		
Composition	Phase	Lattice parameter (Å)	Al	Ge	Ti
Sample 55 Al ₅ Ge ₄₁ Ti ₅₄	Al ₃ Ti	a= 3.8397(4) c= 8.630(1)	65.16	7.09	27.74
	Ti ₅ Ge ₃	a= 7.6488(1) c= 5.3087(1)	1.00	38.69	60.31
	Δ	a= 6.66227(7) b= 12.8482(1) c= 6.76832(8)	0.59	43.15	56.25
Sample 56 Al ₈ Ge ₃₈ Ti ₅₄	Al ₃ Ti	a= 3.8390(3) c= 8.6305(8)	66.30	7.37	26.33
	Ti ₅ Ge ₃	a= 7.65428(7) c= 5.31151(7)	1.00	39.26	59.75
	δ	a= 6.6640(1) b= 12.8501(2) c= 6.7698(1)	0.52	43.28	56.19

Sample 70 $\text{Al}_{20}\text{Ge}_{32}\text{Ti}_{48}$	Al_3Ti	a= 3.8370(1) c= 8.6277(4)	68.20	5.77	26.03
	Ti_5Ge_3	a= 7.65124(9) c= 5.31061(9)	1.17	39.51	59.32
	δ	a= 6.6612(2) b= 12.8447(4) c= 6.7665(2)	0.69	43.17	56.14
Two-phase field sample					
Sample	XRD		SEM (at%)		
Composition	Phase	Lattice parameter (Å)	Al	Ge	Ti
Sample 68 $\text{Al}_0\text{Ge}_{32}\text{Ti}_{68}$	Ti_5Ge_3	a= 7.55562(4) c= 5.22312(4)	0	36.76	63.24
	Ti (Mg-type)	a= 2.9310(5) c= 4.669(1)	0	4.47	95.53
Sample 9 $\text{Al}_{47.5}\text{Ge}_5\text{Ti}_{47.5}$	Ti_5Ge_3	a= 7.5710(3) c= 5.2331(5)	11.32	27.16	61.52
	AlTi	a= 3.98812(8) c= 4.0807(1)	54.21	0.58	45.22
Sample 15 $\text{Al}_{37}\text{Ge}_8\text{Ti}_{55}$	Ti_5Ge_3	a= 7.5887(2) c= 5.2388(2)	9.09	27.06	63.86
	AlTi	a= 3.9897(4) c= 4.0626(6)	44.34	2.34	53.32
Sample 16 $\text{Al}_{44}\text{Ge}_8\text{Ti}_{48}$	Ti_5Ge_3	a= 7.5756(1) c= 5.2352(2)	7.29	29.45	63.26
	AlTi	a= 3.9869(1) c= 4.0769(2)	55.45	0.74	43.81
Sample 12 $\text{Al}_{44}\text{Ge}_8\text{Ti}_{48}$	Ti_5Ge_3	a= 7.6294(1) c= 5.2981(2)	1.27	38.62	60.11
	Al_3Ti	a= 3.83728(6) c= 8.6214(2)	69.18	5.21	25.61

Sample 57 Al ₁₁ Ge ₃₅ Ti ₅₄	Ti ₅ Ge ₃	a= 7.6398(1) c= 5.3001(1)	1.07	39.28	59.64
	Al ₃ Ti	a= 3.8352(3) c= 8.658(2)	69.34	5.54	25.12
Sample 17 Al ₅₁ Ge ₈ Ti ₄₁	Ti ₅ Ge ₃	a= 7.56568(8) c= 5.2312(1)	4.71	31.99	63.30
	Al ₂ Ti	a= 3.97453(5) c= 24.3173(5)	63.19	0.96	35.85
Binary non-equilibrium sample					
Sample	XRD		SEM (at%)		
Composition	Phase	Lattice parameter (Å)	Al	Ge	Ti
Sample 67 Al ₀ Ge ₄₂ Ti ₅₈	Ti ₆ Ge ₅	a= 16.916(2) b= 7.9377(7) c= 5.2263(6)	not found in SEM		
	Ti ₅ Ge ₃	a= 7.6518(2) c= 5.3090(1)	0	40.09	59.91
	δ	a= 6.6614(2) b= 12.8492(3) c= 6.7680(2)	0	43.85	56.15

Table 12: Samples at 1000°C

In the titanium richer part two three-phase fields were found between Ti₅Ge₃, Al₂Ti in combination with either Al₃Ti or AlTi. Al₃Ti shows again a noteworthy solubility, while there is just minor solubility for germanium in AlTi and Al₂Ti. Ti₅Ge₃ also shows remarkable solubility of aluminium but only in the titanium rich part of the phase. The change of the lattice parameter with changing composition for Ti₅Ge₃ is drawn in Figure 28. Because of the shape of the single phase field not all produced compositions of this phase have the same titanium content. Linear behaviour of volume, however, is just expected if only the ratio of two elements changes. The aluminium poor part is simultaneously the titanium poor part (grey marks). These data are just given for completeness but no systematic relationship is expected there. On the other hand in the aluminium rich part the titanium content doesn't change significantly and there the anticipated linear behaviour is more or less confirmed. The binary samples 67 and 68 fit well to the linear behaviour for high and low titanium content. However, sample 67

with low titanium content is not drawn in Figure 28 because it is not in equilibrium but its data are listed in Table 12 for comparison.

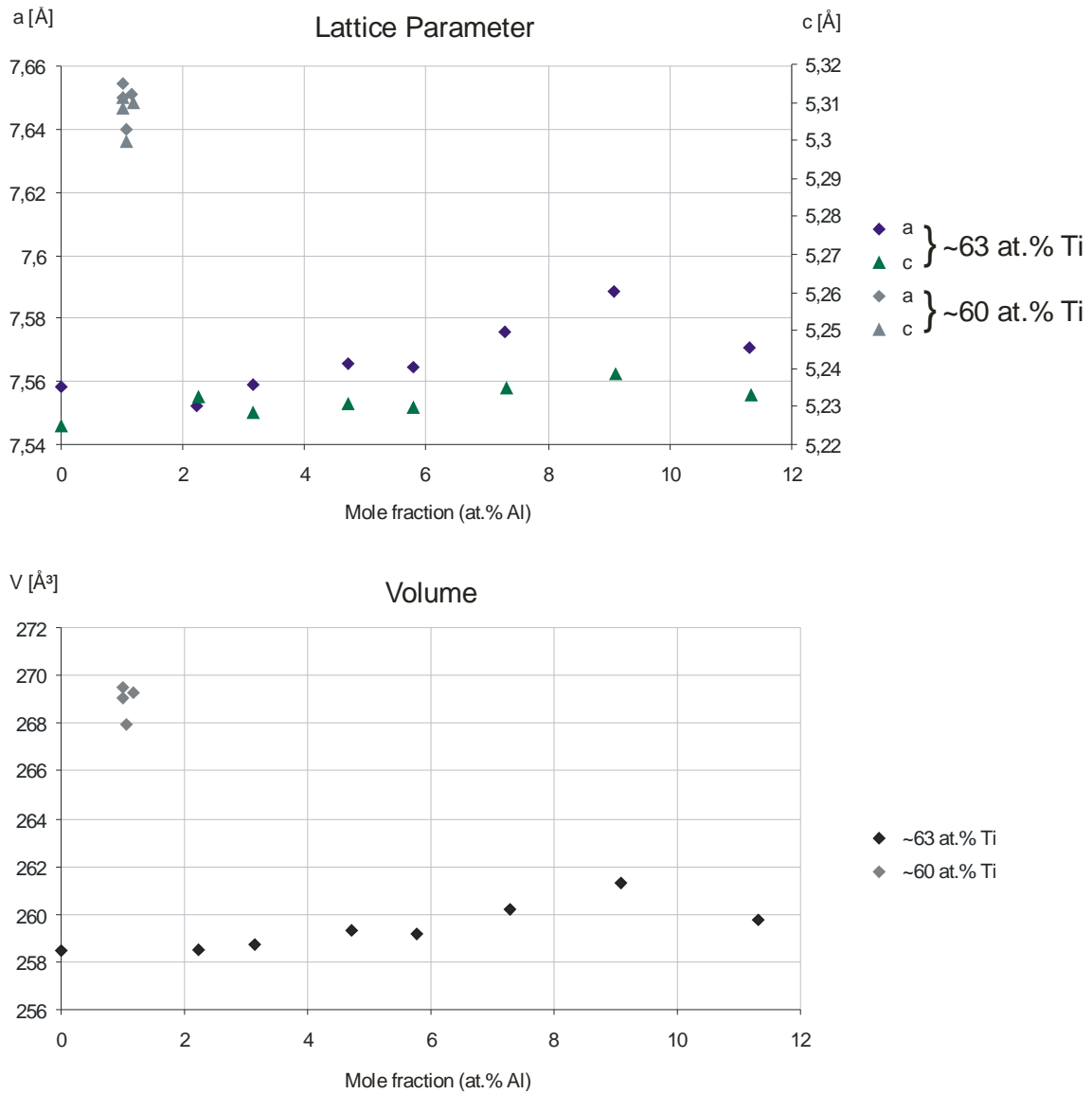


Figure 28: Change of lattice parameters and volume for Ti_5Ge_3 with the composition

In the titanium poorer part a new phase was found next to Ti_6Ge_5 , here called δ . All structural details will be discussed in chapter 5.2.4. Several samples were found to be in the three-phase field between Ti_5Ge_3 , Al_3Ti and δ .

5.2. Structure of new compounds

5.2.1. The α -phase

A powder XRD of almost pure α with the approximate composition of $\text{Al}_{58}\text{Ge}_{22}\text{Ti}_{20}$ could be produced using Sample 29 (Figure 29). The blue line in this illustration is the measured diffractogram, the red is the calculated for Al, Ge and γ and the black is the difference between those two. Since all other present structures are known, the black diffractogram matches with the diffractogram of α . Although small amounts of contamination were present, they could be discarded for the evaluation of the crystal structure of α since their structure is known. The remaining peaks were indexed in order to search for fitting crystal structures. But it was not possible to find a satisfying structure with this approach. The next step for the investigation was the attempt to produce single crystals by slow cooling of samples which were expected to be in the primary crystallisation region of α before the liquidus projection was investigated (Sample 61 and 62). This, however, led to not very satisfying results and no further attempts were done. Therefore the structure of α is not known up to now.

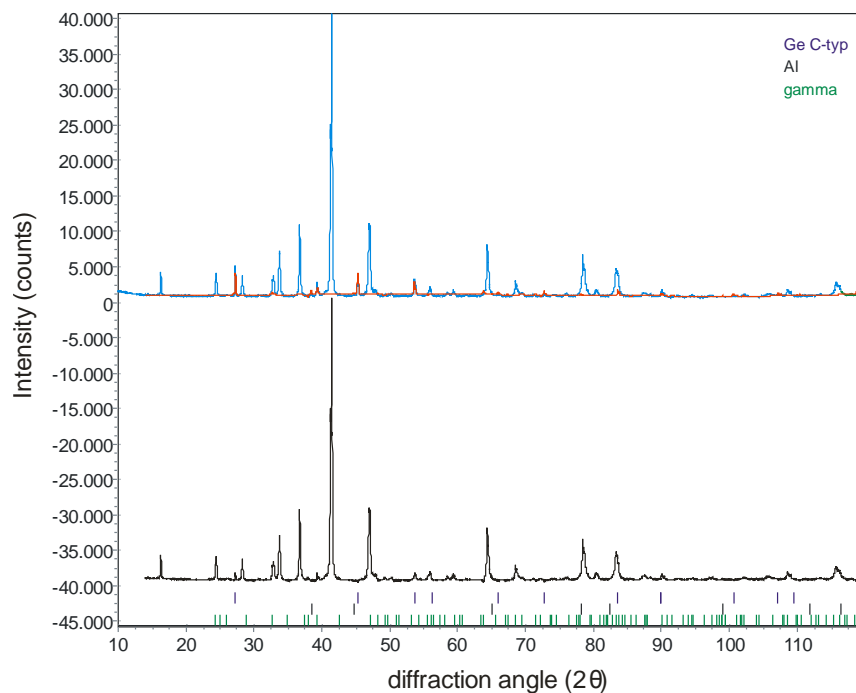


Figure 29: Powder XRD of Sample 29

5.2.2. The β -phase

In several non-equilibrium samples a compound with the composition $\text{Al}_{52}\text{Ge}_{34}\text{Ti}_{15}$ was found. However, this phase couldn't be produced pure despite multiple attempts at different temperatures. It was only found in samples which were partial liquid during annealing, covering other grains. For example in Figure 30, showing Sample 2, one can see grains of Ge (white), Al_3Ti (dark grey), β (bright grey) and Al (black).

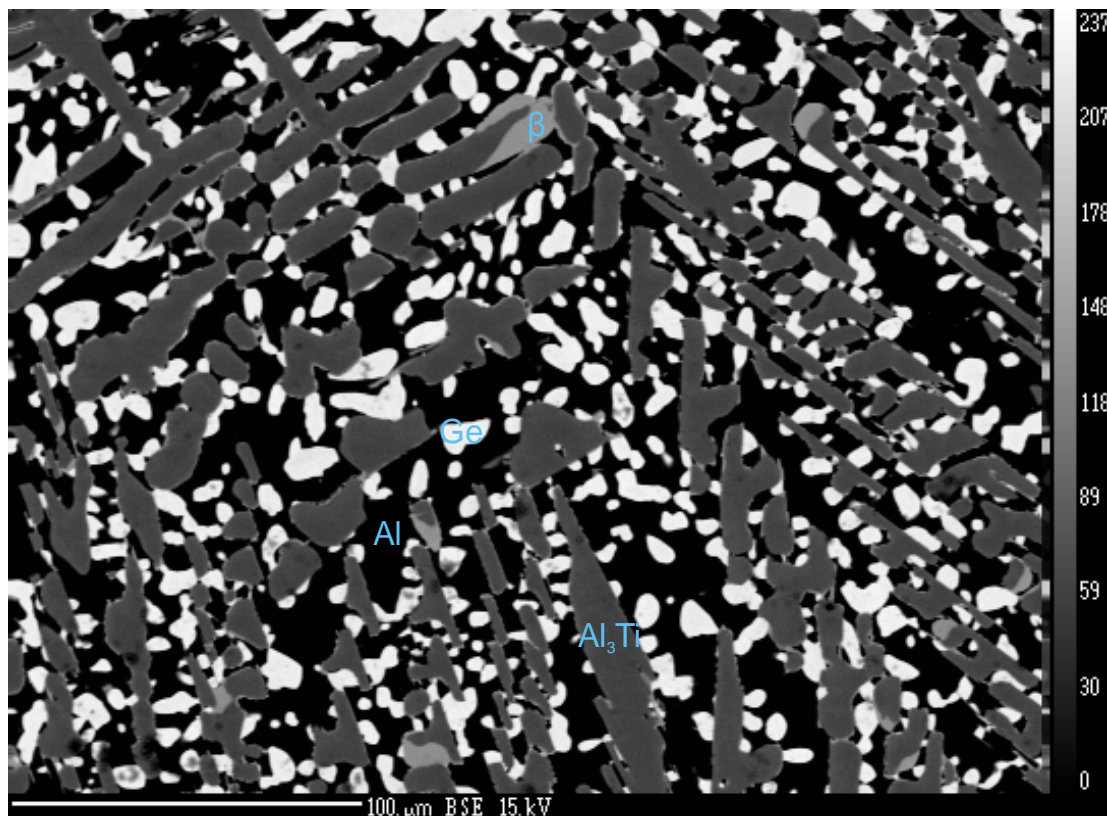


Figure 30: BSE picture of Sample 2

In this sample – as well as in the other samples containing β – at least four phases were present during annealing. In this case the temperature during annealing (400°C) was too low for the eutectic to become liquid. According to thermodynamics only three phases can be simultaneously present in a ternary system unless the temperature is exactly at a specific reaction temperature, which is highly unlikely. The existence of a fourth phase, β , indicates the presence of a fourth element, which may stabilize β . One possible explanation is that small amounts of oxygen were released from the quartz ampoule by reaction with titanium. Thus, the most likely explanation is that β is an impurity-stabilized phase and not an equilibrium phase in this ternary system.

The structure of β could not be identified due to the small amounts present in the samples. Since already preparation of pure β failed, preparation of single crystals was not an option.

5.2.3. The γ -phase

The structure of γ with the approximate composition of $\text{Al}_{11-24}\text{Ge}_{56-43}\text{Ti}_{33}$ at 520°C was investigated by powder XRD and subsequent Rietveld refinement. Sample 49 was used since it contained primarily γ . It was already known that also (Ge) was present in this sample. Therefore (Ge) was refined first to avoid undesired correlation between already explained peaks and to optimize several parameters for the refinement. The remaining peaks then were indexed to search for a possible cell. The lattice parameters of multiple cell proposals then were used to search for structures with similar dimensions, symmetry and chemical properties of the single atoms in the inorganic crystal structure database (ICSD). Several of these results were used as possible starting models. One of the results was based on $\text{Al}_4\text{Si}_5\text{Zr}_3$ [38], [39] showing remarkable agreement with the position of the peaks, distribution of peak intensities and also the composition in comparison with SEM results. It counts therefore as confirmed that γ is isostructural with $\text{Al}_4\text{Si}_5\text{Zr}_3$. All relevant data for the structure of γ refined from Sample 49 are listed in Table 13.

Spacegroup	I4 ₁ /amd							
Pearson symbol	tI24							
Structure type	Al ₄ Si ₅ Zr ₃							
Cell Volume	384.307(4) Å ³							
Crystal Density	5.99(4) g/cm ³							
Lattice parameter								
a	3.68464(2)Å							
c	28.3067(2)Å							
Site	Np	x	y	z	Occ.: Al	Occ.: Ge	Occ.: Ti	B
Al	4	0	0	0	0.82(2)	0.18(2)	0	0.71(9)
Ge1	4	0	0	0.5	0.01(1)	0.99(1)	0	0.65(5)
Ge2	8	0	0	0.34298(5)	0.03(2)	0.97(2)	0	1.34(5)
Ti	8	0	0	0.17483(7)	0	0	1	0.55(6)

Table 13: Structural data of γ

γ shows no variability in the titanium content (33.3at.%). Aluminium and germanium, on the other hand, are variable between 11 and 24 at.% aluminium. This leads to the assumption that titanium is only on one atomic position and it neither substitutes the other elements on the other positions nor is substituted itself in relevant amounts. Aluminium and germanium each prefer specific sites, but mixed occupations are clearly observable. The diffractogram of Sample 49 is given in Figure 31 together with the calculated pattern of the present phases. Several drawings of this structure can be found in Figure 32.

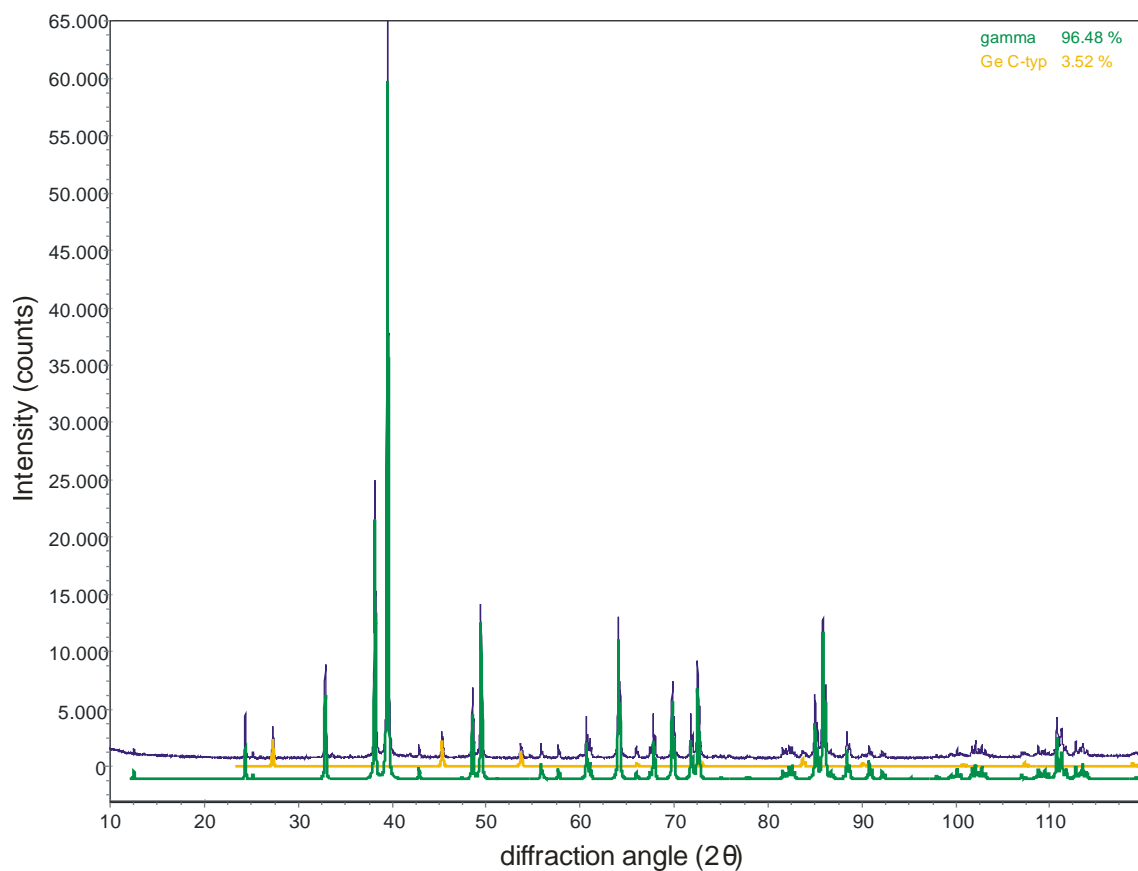


Figure 31: Powder XRD of sample 49

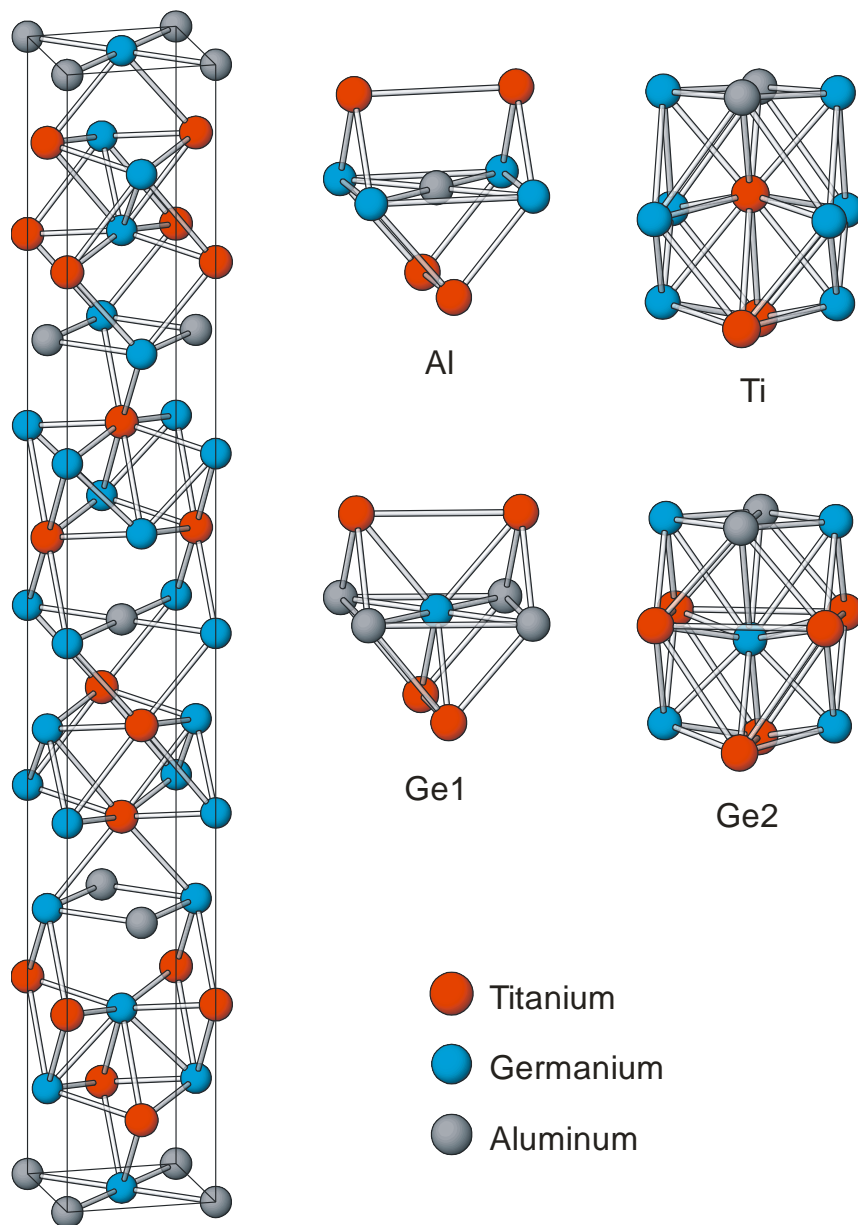


Figure 32: Crystal structure and coordination polyhedra of γ

Although this structure model worked well to describe the patterns in the aluminium poor part of this phase, in the aluminium rich part some problems occurred. First of all, the lattice parameters show a bend between 14 and 15 at.% aluminium, as drawn in Figure 33. Together with this bend, the XRD pattern changes slightly. Some new peaks appear. Therefore, the structure obviously changes at this point. However, it was not possible to clarify the character of the structural transition. The formation of a superstructure is a possible explanation for this behaviour but further investigation is necessary to settle this.

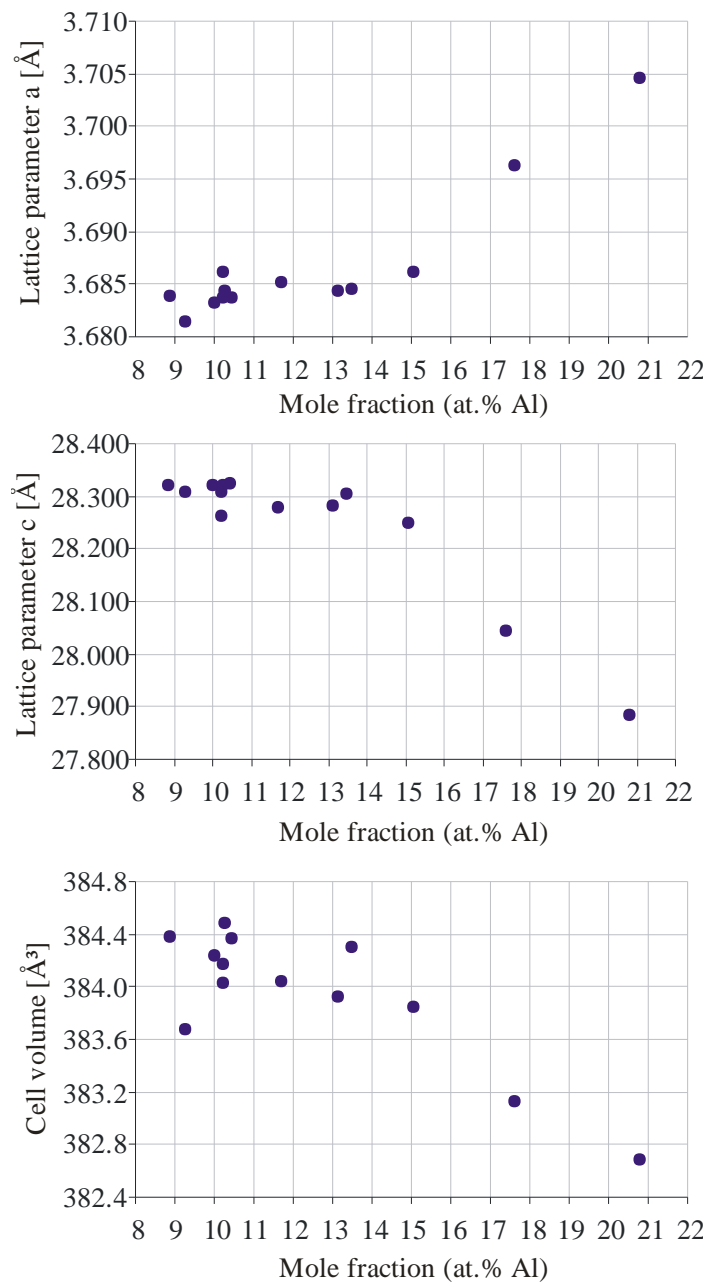


Figure 33: Lattice parameter (refined from powder XRD) development of γ with changing composition (measured by SEM); data acquired from multi-phase samples

5.2.4. The δ -phase

The δ -phase, with the approximate composition $\text{Ge}_{44}\text{Ti}_{56}$, was observed in several ternary samples in equilibrium with Al_3Ti , Ti_5Ge_3 and Ti_6Ge_5 . It was found to contain only very small amounts of Al ($\sim 0.5\text{at.}\%$), which suggested that it might be a binary rather than a ternary phase. However, such a conclusion cannot be drawn from ternary samples, so a re-investigation of the binary phase diagram was performed to confirm, that δ is in fact a binary phase. Details on these experiments are given in chapter 5.4.

The structure of δ was once again investigated using powder XRD measurement, Rietveld refinement and the same procedure as described in 5.2.3. A very convincing solution could be found with a structure based on Ge_4Sm_5 [40]. The pattern of the peaks as well as the stoichiometry of Ge_4Sm_5 fits very well to the new phase once samarium is replaced with titanium. All relevant data for this phase refined from sample 56 are listed in Table 14 and several drawings are in Figure 34.

Spacegroup	<i>Pnma</i>					
Pearson symbol	<i>oP36</i>					
Structure type	Ge_4Sm_5					
Cell Volume	579.72(2) \AA^3					
Crystal Density	6.0707(2) g/cm^3					
Lattice parameter						
a	6.6640(1) \AA					
b	12.8501(2) \AA					
c	6.7698(1) \AA					
Site	Np	x	y	z	Occ.	B
Ge1	4	0.9525(8)	0.25	0.1092(6)	1	0.95(9)
Ge2	4	0.1846(8)	0.25	0.6541(7)	1	1.5(1)
Ti1	4	0.333(1)	0.25	0.999(1)	1	1.4(1)
Ge3	8	0.1952(5)	0.9607(2)	0.5307(5)	1	1.9(1)
Ti2	8	0.1542(8)	0.1279(4)	0.3346(7)	1	2.1(1)
Ti3	8	0.9919(9)	0.0930(3)	0.8180(7)	1	1.35(6)

Table 14: Structural data of δ

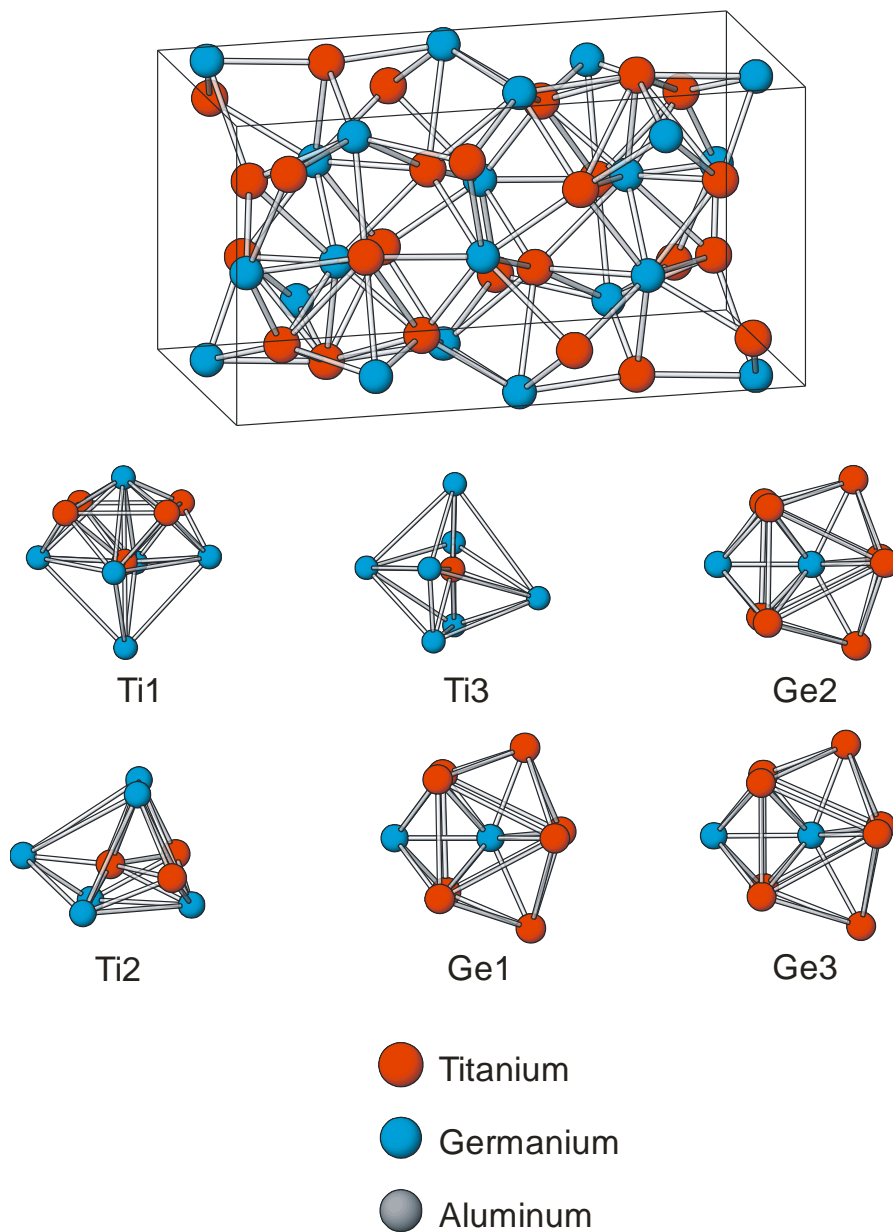


Figure 34: Crystal structure and coordination polyhedra of δ

The powder diffractogram of sample 56, which contains δ , is given in Figure 35. In this sample the composition based on the structural model yields a titanium content of 55.6 at.% in δ , while in SEM 56.2 at.% were measured. Therefore also the composition fits very well together.

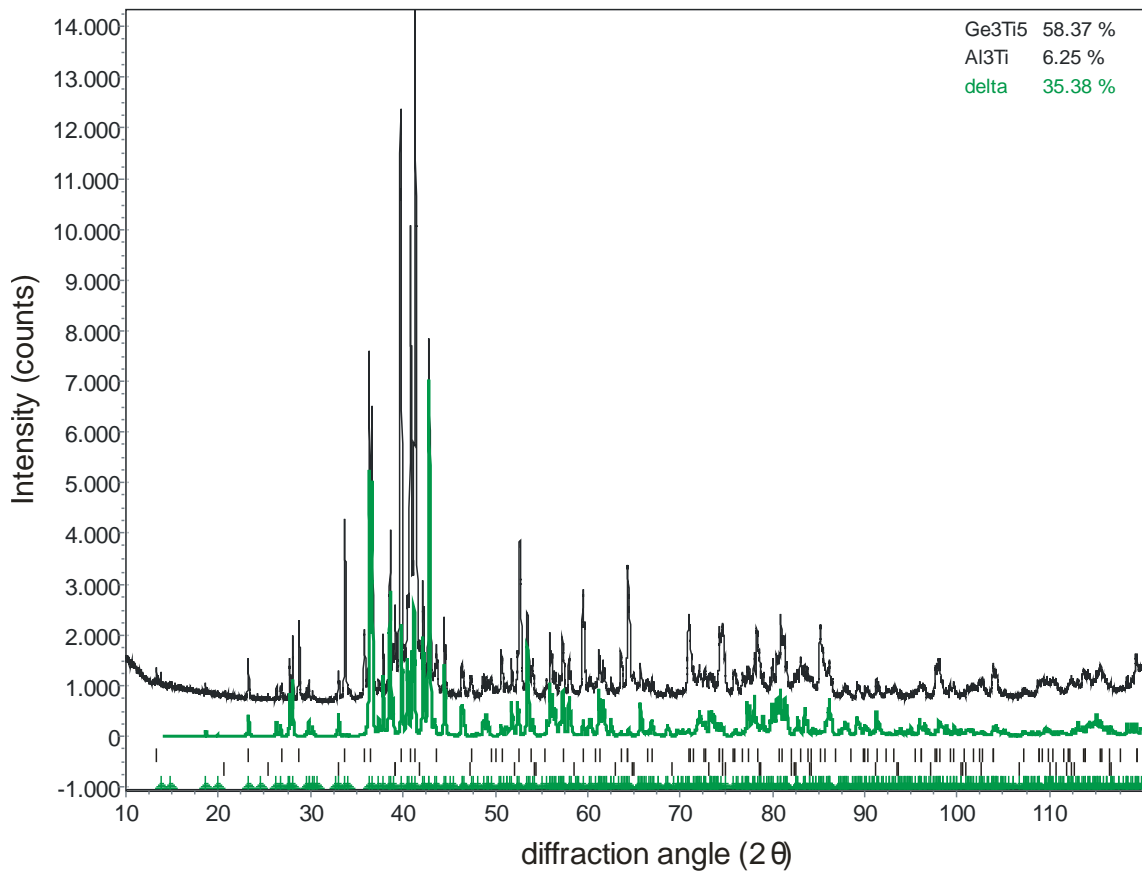


Figure 35: Powder XRD of sample 56

5.3. Reaction scheme, isopleths and liquidus projection

DTA measurements in combination with SEM and XRD results were used in order to construct simultaneously a partial reaction scheme, a partial liquidus projection and isopleths to be consistent with each other. All relevant DTA data can be found in Table 15, Table 16 and Table 17.

5. Results and discussion

Sample	Reactions below 900°C						
4	424				539	550	
5	422				534		
7					529		808
8					527		803 860
9							
10							
11							
12							
15							
16							
17							
18							
27	423			507			
28	423			521			
31					529		807
32	423			494			
40					528		918
41					530		805 901
42					530		804 882
43					531		802 842
44					531		
46		480					
48							
49							
53							798 820
55							
56							
57							
66							
69							796 895
70							
73		481	539				
74							
75						544	
78							

E1: L -> Al+Ge+ α

T1: L+Al₃Ti -> Al+ α

n.i.r.: L+Al₃Ti+Al -> L+Al₃Ti

n.i.r.: L+ α -> L+ α +Al₃Ti and/or L+ α +Al₃Ti -> L+Al₃Ti

T2: L+ γ -> Ge+ α

P1: Al₃Ti+ γ +L -> α

T3: L+TiGe₂ -> Ge+ γ

n.i.r.: L+Ge+TiGe₂ -> L+Ge or L+Ge+TiGe₂
-> L+TiGe₂

Table 15: DTA data below 900°C

Sample	Reactions between 900°C and 1210°C						
4	924						
5		961					
7				1036			
8							
9							
10							1214
11							
12							
15							
16							
17							1210
18							
27							
28							
31							
32							
40							
41							
42							
43				1040			
44			992				
46							
48			987				
49			993				
53				1014			
55						1203	
56						1211	
57							
66					1110		
69							
70						1207	
73							
74	912						
75	920						
78		929					

T4: $\text{Ti}_6\text{Ge}_5 + \text{L} \rightarrow \text{Al}_3\text{Ti} + \gamma$
E: $\text{L} \rightarrow \text{Ge} + \text{TiGe}_2$
n.i.r.: $\text{L} + \gamma \rightarrow \text{L} + \gamma + \text{Ge}_6\text{Ge}_5$ and/or $\text{L} + \gamma + \text{Ge}_6\text{Ge}_5 \rightarrow \text{L} + \text{Ti}_6\text{Ge}_5$
P2: $\text{TiGe}_2 + \text{Ti}_6\text{Ge}_5 + \text{L} \rightarrow \gamma$
n.i.r.: $\text{L} + \text{TiGe}_2 \rightarrow \text{L} + \text{TiGe}_2 + \text{Ti}_6\text{Ge}_5$ and/or $\text{L} + \text{TiGe}_2 + \text{Ti}_6\text{Ge}_5 \rightarrow \text{L} + \text{Ti}_6\text{Ge}_5$
P: $\text{Ti}_6\text{Ge}_5 + \text{L} \rightarrow \text{TiGe}_2$
T5: $\text{Ti}_6\text{Ge}_5 + \text{Ti}_5\text{Ge}_3 \rightarrow \text{Al}_3\text{Ti} + \delta$
T6: $\text{AlTi} + \text{Ti}_5\text{Ge}_3 \rightarrow \text{Al}_3\text{Ti} + \text{Al}_2\text{Ti}$

Table 16: DTA data between 900°C and 1210°C

5. Results and discussion

Sample	Reactions above 1200°C							measured	
4							1075	*	up to 1450
5							1143	*	up to 1450
7							1066	1045	up to 1450
8							1036	1071	up to 1450
9							1410	1428	up to 1450
10							1408	1417	up to 1450
11				1356	1365		1374	1385	up to 1450
12			1332				1343	1354	up to 1450
15						1427	*	*	up to 1450
16						1418	*	*	up to 1450
17						1400	*	*	up to 1450
18				1357	1366		*	*	up to 1450
27							958	*	up to 1450
28							925	*	up to 1600
31							991	1046	up to 1200
32							997	1017	up to 1200
40							911	930	up to 1000
41							966	1016	up to 1400
42							1003	1049	up to 1400
43							1146	*	up to 1400
44							1183	1216	up to 1400
46							1279	1292	up to 1450
48							*	*	up to 1550
49							*	*	up to 1550
53							994	1086	up to 1350
55	1215						*	*	up to 1600
56	1221						*	*	up to 1600
57		1283					*	*	up to 1600
66							*	*	up to 1150
69							895	915	up to 1150
70	1214						1226	1254	up to 1450
73							1267	1254	up to 1300
74	1210						1244	1298	up to 1500
75	1217						1191	1227	up to 1450
78							1043	1064	up to 1200
T7: Ti5Ge3+L -> Ti6Ge5+ Al3Ti									
T8: AlTi+L -> Ti5Ge3+Al3Ti									
Liquidus on cooling									
Liquidus on heating									

Table 17: DTA data above 1200°C and liquidus values at all temperatures; * Liquidus temperature too high or no peak visible in the measurement

Since the melting temperature rises rather steep with increasing titanium content only the titanium poor part up to approximately 30at.% titanium could be investigated with the available equipment. The resulting Scheil diagram is drawn in Figure 36 and Figure 37.

This scheme is only valid for the titanium poor part as well as for temperatures up to 1300°C since the samples only were investigated in this region of the phase diagram. This reaction scheme is the most likely solution based on the present data.

However, there are still some uncertainties. There was no evidence for the reaction between AlTi, Al₂Ti and Ti₅Ge₃ forming a maximum, whether it is of the peritectic or the eutectic type. In the scheme is just one of those two possibilities presented in order to obtain a complete concept.

Another uncertainty is the formation of δ . Since the existence of δ wasn't known until now it is very likely, that Ti₆Ge₅ is stable at higher temperatures than δ . Combined with the fact that both phases are present at 1000°C, a peritectoid type solid state reaction is proposed for the formation of Ti₅Ge₄. This is under the assumption that Ti₆Ge₅ is thermally more stable than δ , but no investigation of the primary crystallization or high temperature XRD was performed to confirm this. DTA measurements also didn't show any reaction up to 1500°C, but this isn't all too unlikely for such a solid state reaction. The reaction also may take place at higher temperature but these temperatures were not accessible with the used equipment.

It is also important to note, that the transition between 1d-APS and AlTi is not clarified in the binary and therefore the reaction scheme for the ternary in this region also remains uncertain. For the sake of clarity "AlTi" is used for both phases in the reaction scheme.

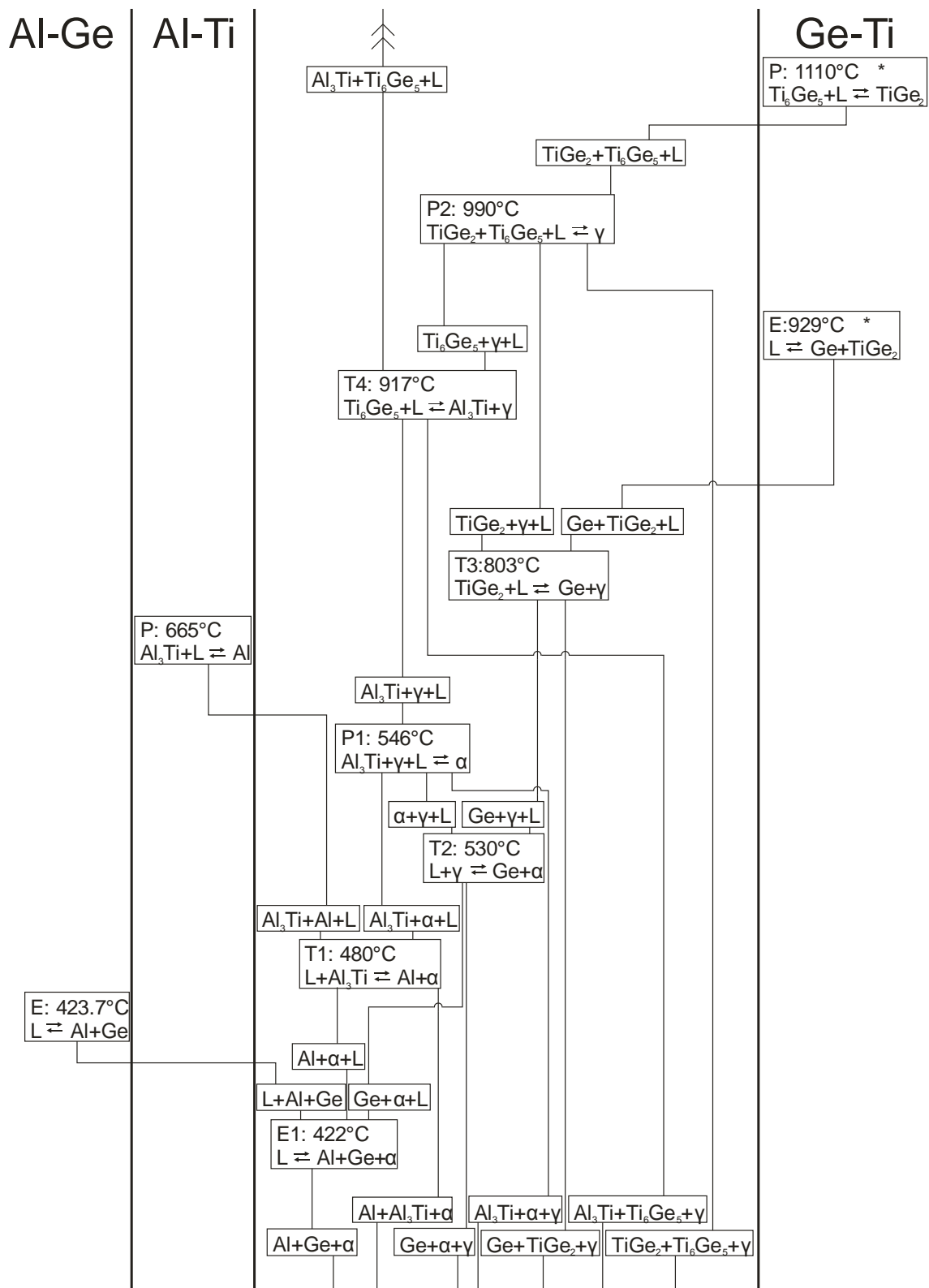


Figure 36: Reaction scheme for the titanium poor part roughly below 1000°C
 * These temperatures were not taken from literature but were re-evaluated in this work

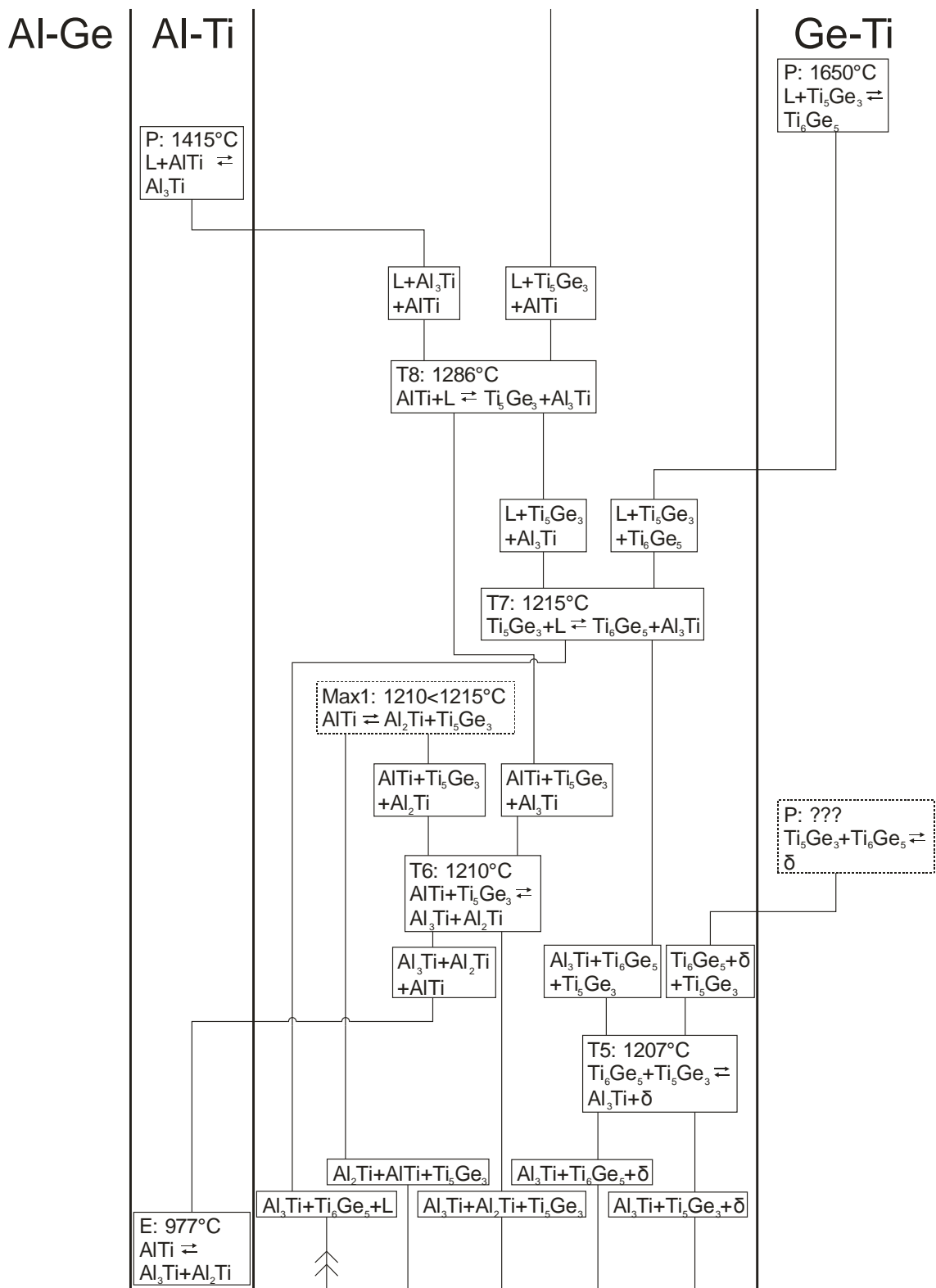


Figure 37: Reaction scheme for the titanium poor part roughly above 1000°C

The estimated compositions of the different phases during the reactions can be found in Table 18.

5. Results and discussion

Reaction	Temperature	Phase	Estimated composition (at.%)		
			Al	Ge	Ti
E1: $L \leftrightarrow Al+Ge+\alpha$	422°C	α	58	22	20
		L	71.5	28.3	1
		Al	98	1	0.5
		Ge	1.5	98	0.5
T1: $L+Al_3Ti \leftrightarrow Al+\alpha$	480°C	L	76.8	23	0.2
		Al_3Ti	65.5	10.5	24
		Al	99	0.5	0.5
		α	58	22	20
T2: $L+\gamma \leftrightarrow Ge+\alpha$	530°C	L	61	38	1
		γ	18	49	33
		Ge	1	98	1
		α	57	23	20
P1: $Al_3Ti+\gamma+L \leftrightarrow \alpha$	546°C	Al_3Ti	60.5	15	24.5
		γ	18	48.7	33.3
		L	61.5	36.5	2
		α	57.5	22.5	20
T3: $TiGe_2+L \leftrightarrow Ge+\gamma$	803°C	$TiGe_2$	2.5	65	32.5
		L	71	28	1
		Ge	0.5	98.5	1
		γ	12.5	55	32.5
T4: $Ti_6Ge_5+L \leftrightarrow Al_3Ti+\gamma$	917°C	Ti_6Ge_5	2	45	53
		L	60	34	6
		Al_3Ti	63	11	26
		γ	17	50	33
P2: $TiGe_2+Ti_6Ge_5+L \leftrightarrow \gamma$	990°C	$TiGe_2$	2	65	33
		Ti_6Ge_5	1	46	53
		L	30	63	7
		γ	12.5	54.5	33

Reaction	Temperature	Phase	Estimated composition (at.%)		
			Al	Ge	Ti
T5: $Ti_6Ge_5 + Ti_5Ge_3 \leftrightarrow Al_3Ti + \delta$	1207°C	Ti_6Ge_5	2	45	53
		Ti_5Ge_3	1.5	37.5	61
		Al_3Ti	68	6	26
		δ	0.5	43.5	56
T6: $AlTi + Ti_5Ge_3 \leftrightarrow Al_3Ti + Al_2Ti$	1210°C	$AlTi$	65	1	34
		Ti_5Ge_3	7	30.5	62.5
		Al_3Ti	68	6	26
		Al_2Ti	65.5	0.5	34
Max1: $AlTi \leftrightarrow Al_2Ti + Ti_5Ge_3$	1210<1215°C	$AlTi$	64.3	1	33.7
		Al_2Ti	65.8	0.2	34
		Ti_5Ge_3	5	32	63
T7: $Ti_5Ge_3 + L \leftrightarrow Ti_6Ge_5 + Al_3Ti$	1215°C	Ti_5Ge_3	2	35	63
		L	62	22	16
		Ti_6Ge_5	2	45	53
		Al_3Ti	67	8	25
T8: $AlTi + L \leftrightarrow Ti_5Ge_3 + Al_3Ti$	1286°C	$AlTi$	70	1	29
		L	63	17	20
		Ti_5Ge_3	1	38.5	60.5
		Al_3Ti	69.5	5.5	25

Table 18: Composition during invariant reactions

Two isopleths were drawn. One with a constant titanium content of 10 at.% (Figure 38) and a second with constant Al:Ti ratio of 1:1 (Figure 39). These isopleths were constructed using all available data and not only those within the isopleth itself.

Ternary DTA data indicated that the reaction temperature of $L \rightarrow Ge + TiGe_2$ should be very likely higher than in the literature. Another sample already showed that the reaction temperature of a different reaction in the same literature source was too low. Therefore another sample was produced to investigate this temperature once again with the result that it is higher than previously published. Further details can be found in chapter 5.4.

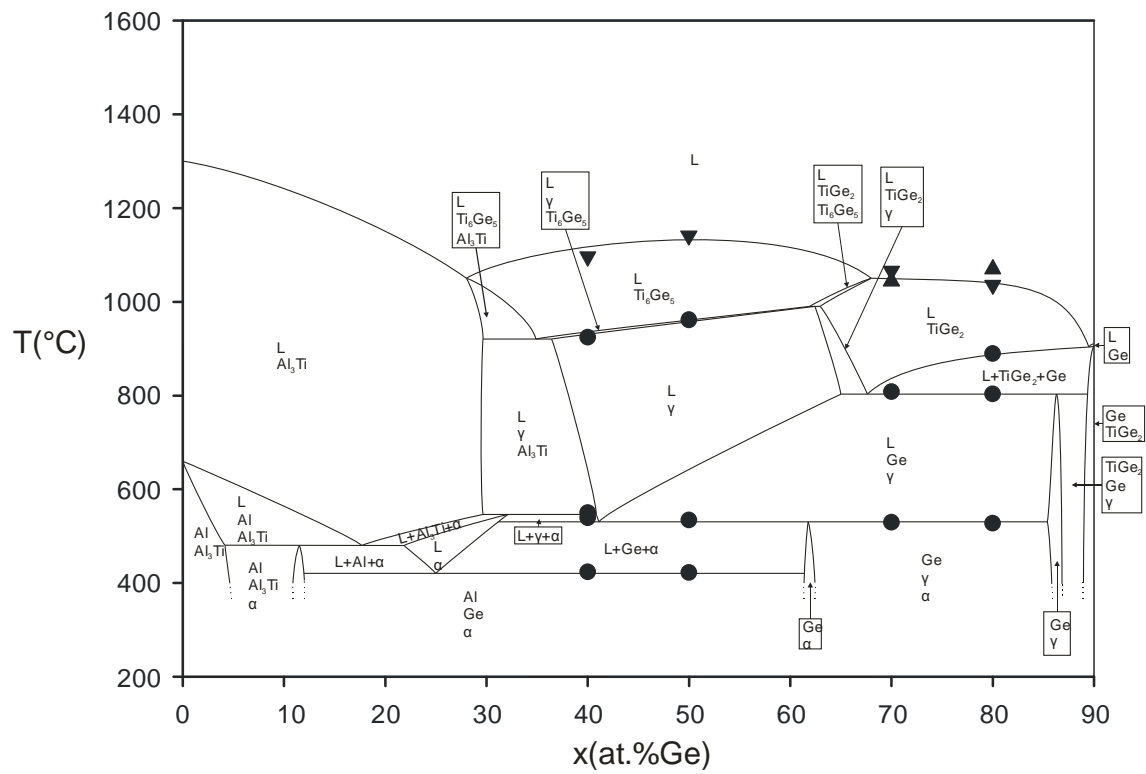


Figure 38: Isopleth with 10 at.% Ti

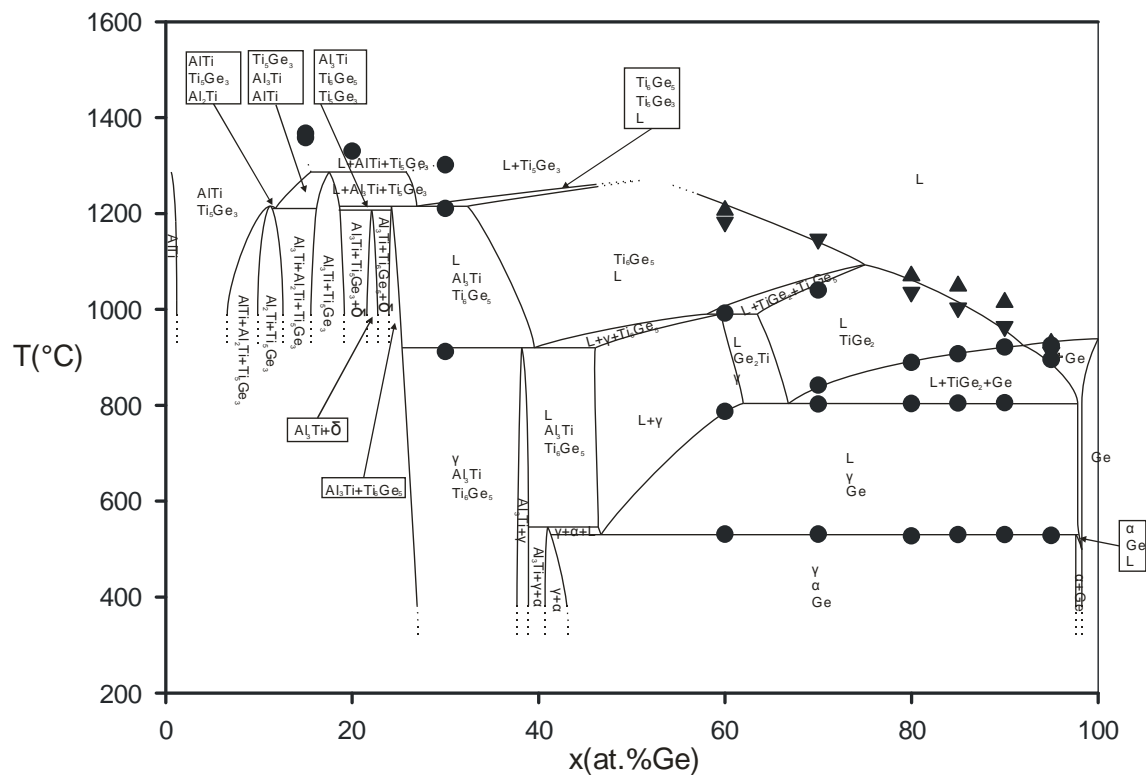


Figure 39: Isopleth with 1:1 Al:Ti ratio

The resulting partial liquidus projection using all available DTA data is presented in Figure 40. The dotted lines representing every full 100°C are constructed using the binary phase diagrams and ternary samples. The phases which show primary crystallization at certain compositions are noted on the correspond areas.

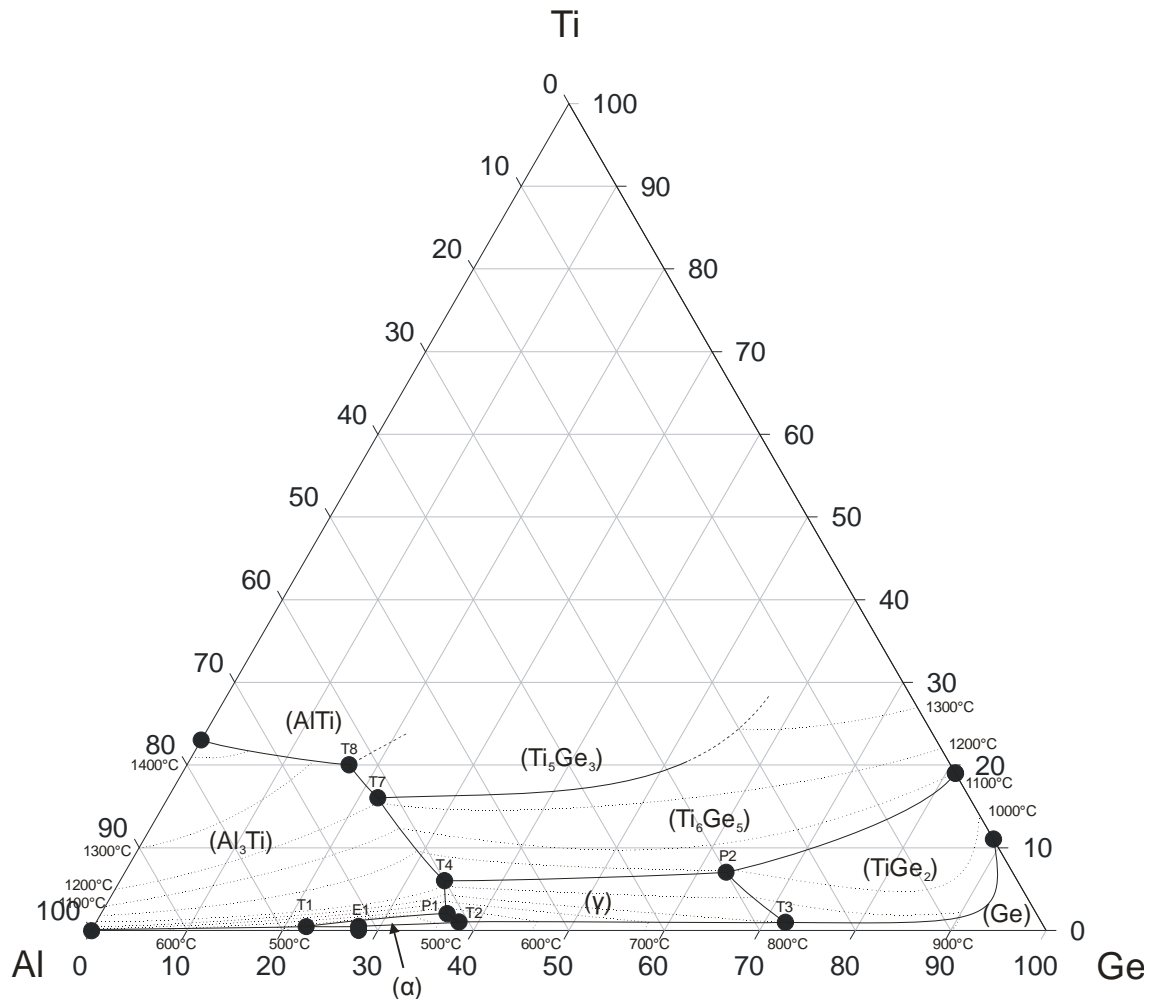


Figure 40: Liquidus projection

5.4. Discussion of the binary Ge-Ti system

Some discrepancies between the phase diagram published by Rudometkina [25] and this work were found. First of all and probably most important a new phase with the approximate composition $\text{Ge}_{44}\text{Ti}_{56}$, here called δ , appeared not only in ternary but also in binary samples. This structure was most likely overlooked because it is in the rather small gap between Ti_5Ge_3 and Ti_6Ge_5 . No sample was investigated in this gap by Rudometkina. In this work δ couldn't be produced pure which is most likely because the thermal very stable surrounding phases are formed during cooling out of the liquid and afterwards during annealing the time wasn't sufficient with one month at 1000°C to reach equilibrium. The highest content of δ in a sample according to XRD measurements was about 50%. Data about this sample can be found in Table 19, Table 14 and Figure 41. Stabilization of this phase by impurities cannot be excluded rigorously, but there is no evidence for it.

Sample	XRD		SEM (at%)		
Composition	Phase	Lattice parameter (\AA)	Al	Ge	Ti
Sample 79 $\text{Al}_0\text{Ge}_{42.5}\text{Ti}_{57.5}$	Ti_6Ge_5	a= 16.9127(7) b= 7.9344(3) c= 5.2298(2)	no SEM measured		
	Ti_5Ge_3	a= 7.5173(2) c= 5.2209(2)			
	δ	a= 6.66046(6) b= 12.8465(1) c= 6.76653(7)			

Table 19: XRD and SEM data of sample 79

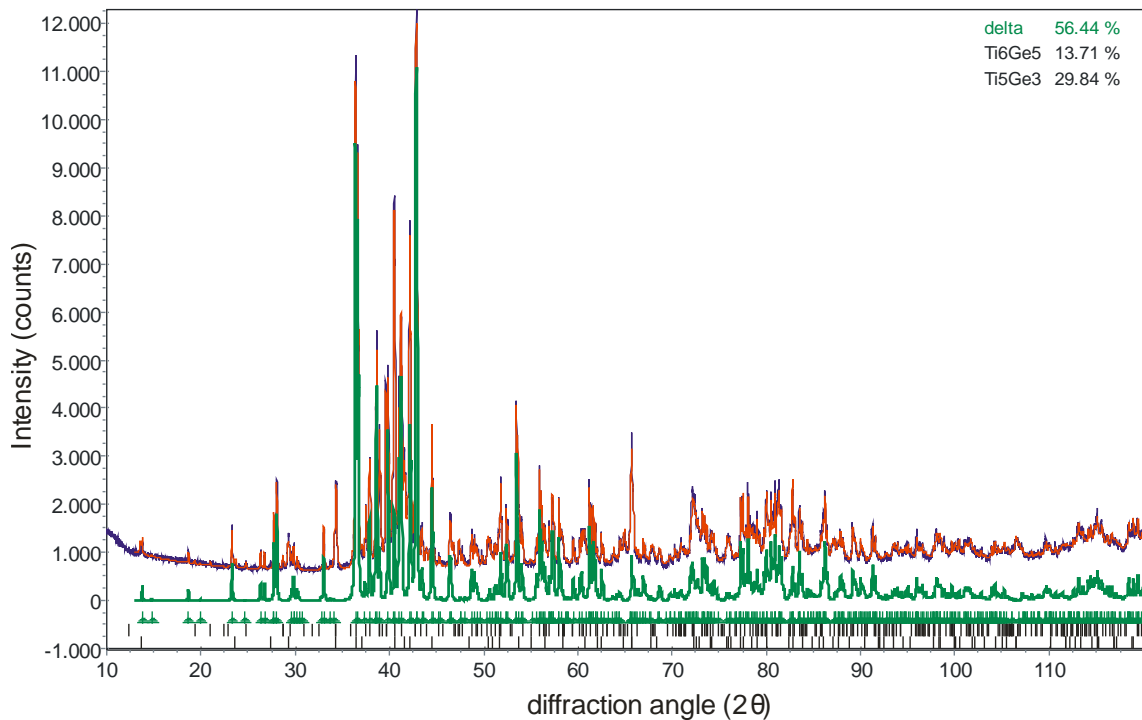


Figure 41: XRD measurement of Sample 79

Another difference between this work and the original phase diagram is the temperature for the peritectic reaction $\text{Ti}_6\text{Ge}_5 + \text{L} \leftrightarrow \text{TiGe}_2$. In this work this reaction was found to be at 1110°C and therefore 35°C higher than previously published. One sample was produced in this region but although it was tempered in the $\text{Ti}_6\text{Ge}_5 + \text{TiGe}_2$ phase field, it showed minor amounts of Ti_5Ge_3 in addition to the expected phases. A DTA measurement of this sample is shown in Figure 42 and other data about this sample in Table 20. The presence of small amounts of Ti_5Ge_3 should not affect the decomposition of TiGe_2 . Since this expected reaction includes liquid, it is quite unlikely that the corresponding effect is too small to be seen, which would also put into question what kind of peak was measured here. The more likely solution is, that the temperature was not as good determined and that it occurs at about 1110°C instead of 1075°C . However since only one non-equilibrium sample was investigated, further investigations are crucial to confirm or disprove this result.

Sample	XRD		SEM (at%)		
	Phase	Lattice parameter (Å)	Al	Ge	Ti
Sample 66 $\text{Al}_0\text{Ge}_{51}\text{Ti}_{49}$	Ti_6Ge_5	a= 16.9205(2) b= 7.94076(8) c= 5.23000(5)	0	45.10	54.90
	Ti_5Ge_3	a= 7.5104(2) c= 5.2348(3)	not found in SEM		
	TiGe_2	a= 8.6106(1) b= 5.03124(7) c= 8.7888(1)	0	65.71	34.29

Table 20: XRD and SEM data of sample 66

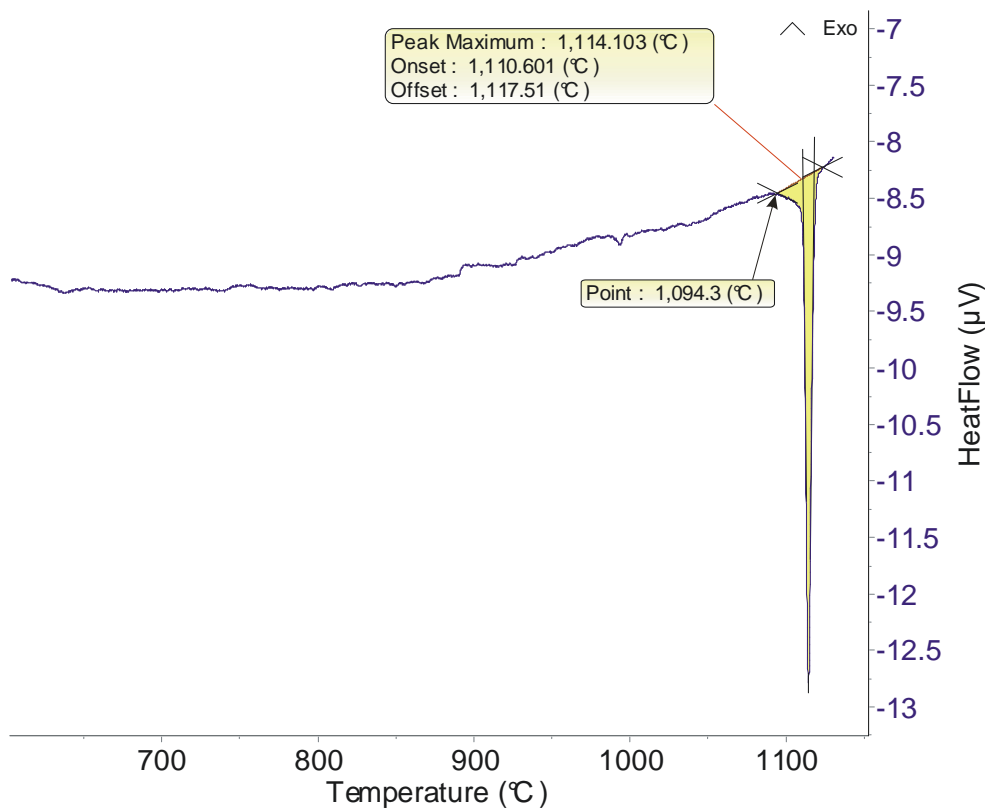


Figure 42: DTA measurement of Sample 66

During construction of the isopleths, a similar problem was observed for the reaction $\text{L} \rightleftharpoons \text{Ge} + \text{TiGe}_2$. The temperature for this reaction was published with 900°C but in this work we measured a temperature of 929°C with the binary sample 78 (Table 21) which was, based on the binary phase diagram, on the germanium rich side of the eutectic. Even more surprising was the liquidus temperature with 1043°C during cooling and

1067°C during heating on average, since from the binary phase diagram it should be in between the eutectic temperature and the melting point of pure germanium (938.3°C). The most probable explanation for this behaviour is that the eutectic composition actually is germanium-richer and this sample is located on the TiGe_2 side of the eutectic where such liquidus temperatures are expected. However, these conclusions just were drawn based on a single sample, so another examination of this area of the phase diagram is necessary.

Sample	XRD		SEM (at%)		
	Phase	Lattice parameter (Å)	Al	Ge	Ti
Sample 78 $\text{Al}_0\text{Ge}_{90}\text{Ti}_{10}$	Ge	a= 5.65632(2)	no SEM measured		
	TiGe_2	a= 8.6179(2) b= 5.0371(2) c= 8.7957(3)			

Table 21: XRD and SEM data of sample 78

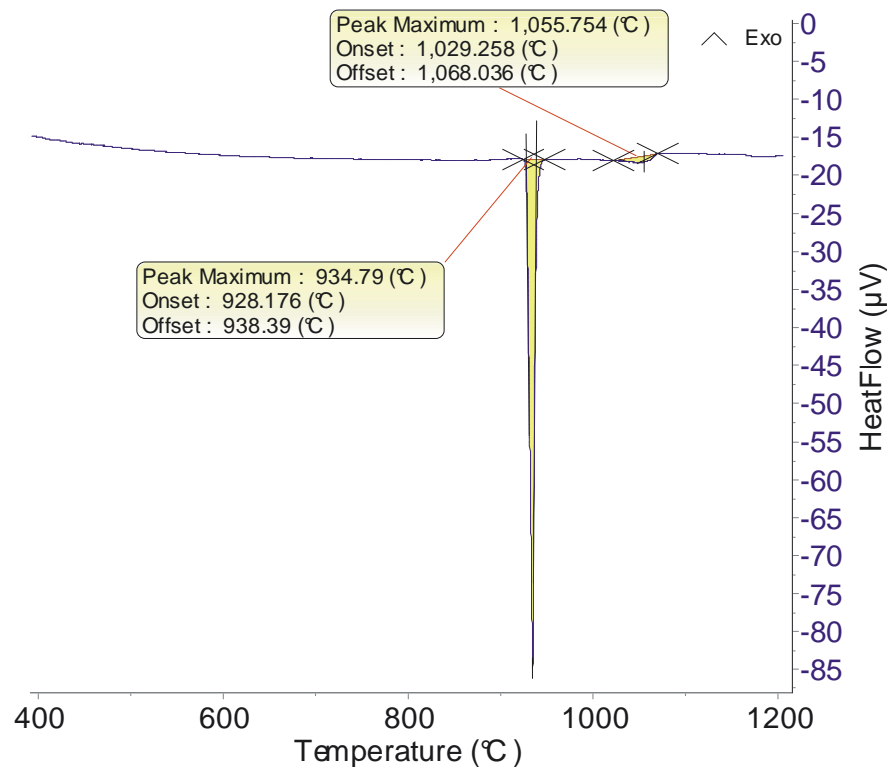


Figure 43: DTA measurement of Sample 78

6. Diffusion brazing and wetting

As already mentioned aluminium titanium alloys are rather expensive in production and processing especially because of their oxygen affinity and their high melting point which leads to the necessity for inert atmosphere and high energy consumption overall. Therefore an efficient joining technique is needed. Diffusion brazing, or also called transient liquid phase bonding (TLPB), is such an elegant method capable to join two pieces without high thermal or physical stress. Thereby a low melting solder is used.

6.1. Theoretical background [7]

The procedure of this technique is drawn in Figure 44. The first step is thereby the initial situation showing a gap between two pieces. In step 2 a small amount of low melting filler metal is positioned filling the gap. The solder is molten then for a short time and solidified again to obtain a good coverage on both surfaces (Step 3).

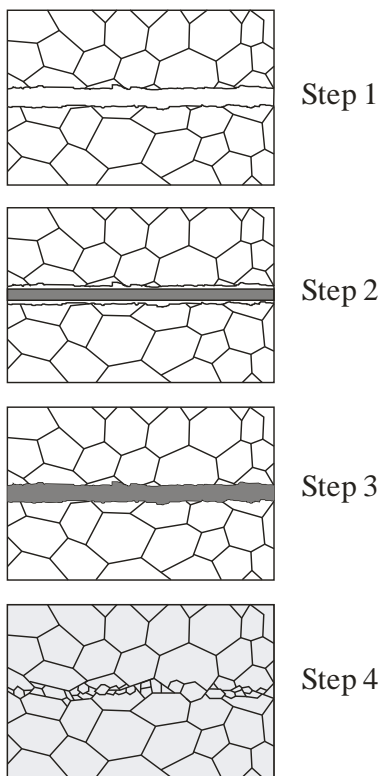


Figure 44: Different steps of diffusion brazing

Afterwards a longer heat treatment is applied for diffusion to take place. The atoms of the filler metal diffuse into the bulk material and the other way round until the bulk as well as the joint share approximately the same composition, the same crystal structure and therefore similar physicochemical properties, which is illustrated in step 4. Thereby the used filler material is distributed over a wide range, so it doesn't contribute significantly to the properties.

The requirements to the solder are therefore a low melting point to avoid thermal stress to the work piece and good wetting properties to avoid gaps in the joint. Also, the composition should be as close as possible to the bulk material to decrease diffusion time. It is also desirable that no high melting brittle phases are produced during the process, which hardly can be removed by diffusion due to their thermal stability.

6.2. Experimental section

The melting point and similarity of the solder to the bulk is already evident out of the phase diagram but no conclusions about the wettability of the liquid on the substrate or the formed phases during brazing can be drawn. Therefore wetting and brazing experiments were performed to be able to make a statement about their behaviour in this context.

In this work Al-Ge-Ti solder materials were selected based on the presented phase diagram. Aluminium and titanium are used because the final bulk material consist out of it, so their presence decrease the necessary time for diffusion, while germanium was chosen because it forms a quite deep melting eutectic together with aluminium to decrease the melting point of the solder. Therefore the idea was to still be able to add a certain amount of titanium in order to have a similar composition to the bulk while being in a temperature range which can be easily handled. The temperature treatment was performed in a vacuum furnace at 10^{-6} mbar.

For wetting and brazing experiments the bulk material was produced by arc furnace melting of the pure elements in a ratio to create Al_3Ti , AlTi and AlTi_3 . These were cut with a diamond saw in roughly 2mm thin slices, grinded with decreasing grain size and finally polished. The material was cleaned in an ultrasonic bath with acetone per analysis and afterwards degassed for one hour in the vacuum furnace.

Two different alloys were used as solder material each prepared on two different ways. The first alloy was $\text{Al}_{70}\text{Ge}_{26}\text{Ti}_4$ because the melting point of this alloy was at approximately 1000°C which was desirable because of procedural reasons. The second alloy was simply the eutectic mixture of aluminium and germanium which was the initial idea for the project in the first place.

The first method of soldering was to powder those two alloys and mix them with a binder. The binder is used to improve the brushability. During the heating program, an isothermal period at 150°C for one hour was added to remove the solvent used in the binder and another isothermal period at 400°C for another hour to decompose the binder residue-free, which simultaneously reduces metal oxides in the solder. Oxides may be present simply because of the high surface area of the powder. The second method was

to cut those two alloys in foil-like slices and used them as solder. No binder was used in this case but due to the smaller surface area also the amount of oxides was expected to be negligible.

With those precursors two similar types of experiments were performed. In wetting experiments the solder material was placed on top of a piece of bulk material, while for brazing experiments it was placed in between two pieces of bulk material. After the initial decomposition step of the binder, if necessary, these arrangements were exposed to a temperature program for the actual experiment between 440 and 1070°C for 5 to 10 minutes depending on the solder. The exact specific treatment of the samples can be found in Table 22.

Bulk \ Solder	TiAl – solder - TiAl	Ti ₃ Al – solder - Ti ₃ Al	TiAl – solder - Ti
	Wetting and brazing		Only Brazing
Eutectic mixture	440°C (10min), foil	440°C (10min), foil	440°C (10min), foil
	600°C (10min), foil	600°C (10min), foil	600°C (10min), foil
Al _{69.5} Ge _{24.5} Ti ₆	1050 (5 min), powder	1050 (5 min), powder	
	1070 (10min), foil	1070 (10min), foil	

Table 22: Performed wetting and brazing experiments

Similar to the previous experiments these samples were cut, embedded, polished and investigated with SEM and EPMA (electron probe micro analysis).

6.3. Results and discussion

Experiments performed at 440°C using the eutectic mixture as solder showed independent of the bulk material the same behaviour. The solder wetted the substrate quite well but almost no reaction between the surface of the bulk and the solder took place. The link between the single pieces therefore was very weak. Exemplary one experiment is shown in Figure 45, the others tempered at 440°C look comparable. This leads to the conclusion that even though the solder melts at 423.7°C, a higher

temperature, a longer heat treatment, the application of pressure or a combination of the mentioned options is necessary to gain a satisfying result.

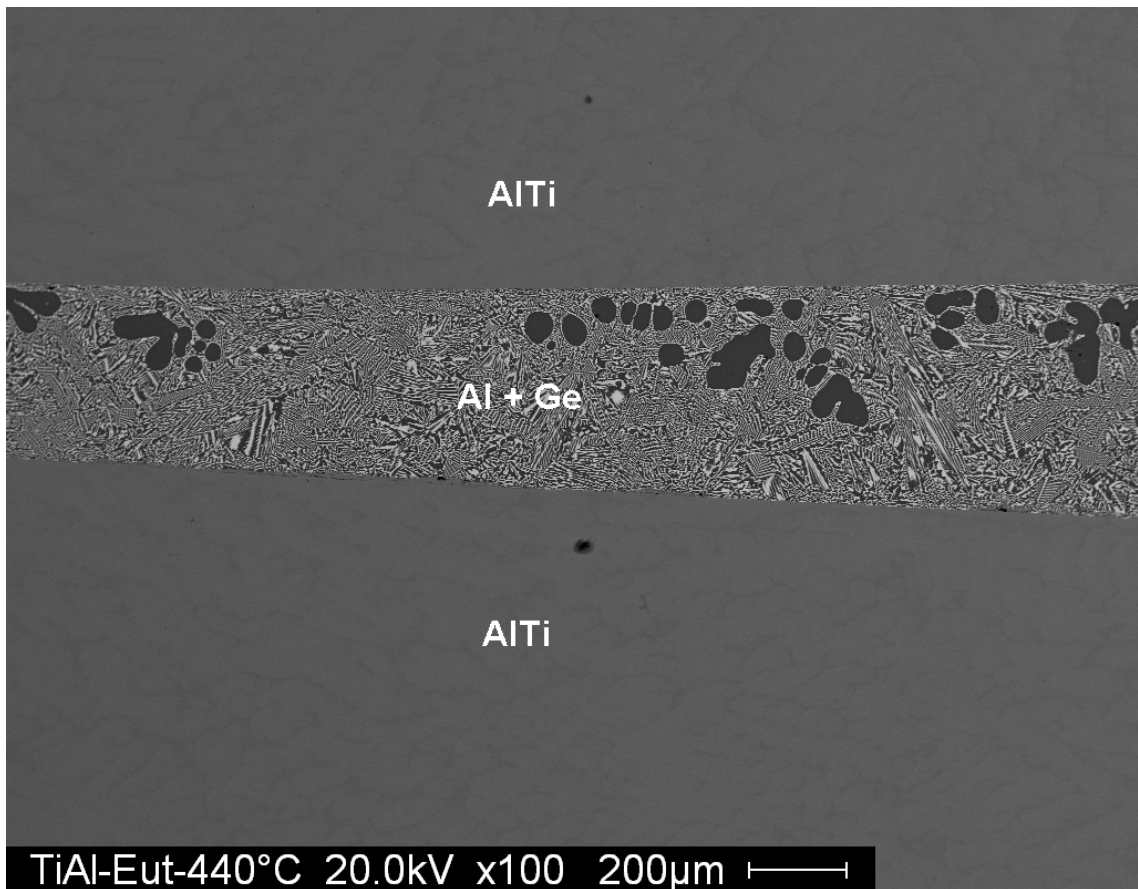


Figure 45: Brazing of AlTi – eutectic mixture – AlTi at 440°C

We decided to increase the reaction temperature to 600°C but maintained the other parameter. At this temperature reactions between the bulk and the solder occurred and the phases α and Al_3Ti were formed but only at specific points of the interface with the AlTi and AlTi_3 bulk material. In between those reaction zones voids appeared. By additional application of pressure it may be possible to avoid the formation of these holes but this isn't investigated yet. The reaction of the eutectic mixture with pure titanium bulk material, on the other hand, proceeds without formation of any voids and yield already without pressure very pleasing outcome. (Figure 46 and Figure 47)

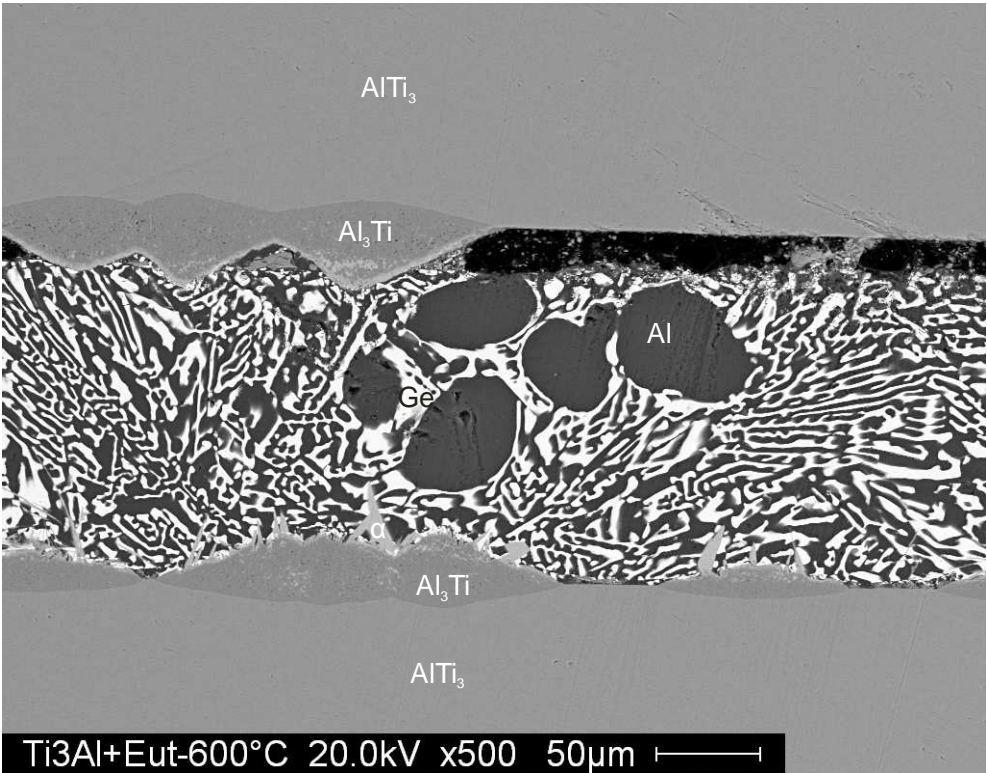


Figure 46: Brazing experiment of $AlTi_3$ - eutectic mixture – $AlTi_3$ at 600°C

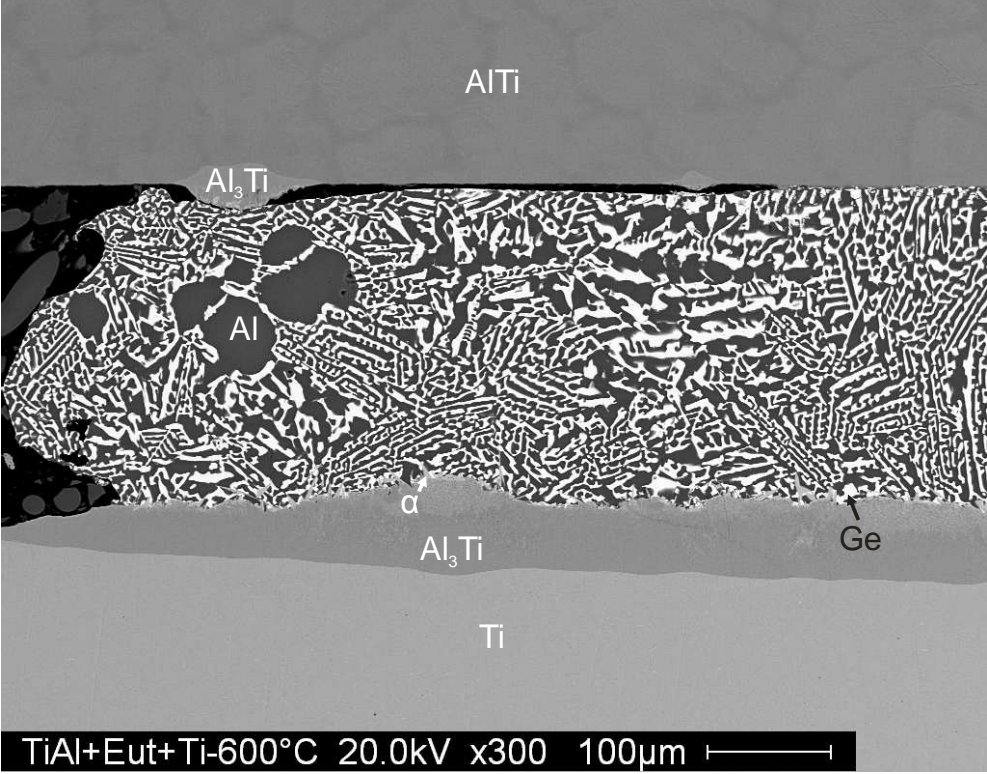


Figure 47: Brazing experiment of $AlTi$ – eutectic mixture – Ti at 600°C

For the second solder with a melting point at around 1000°C the processing temperature had to be increased. The samples tempered at 1050°C showed very good wetting and reactivity with the bulk but easily broke apart at the joint because of the formation of the brittle Al_3Ti phase. Since the differences between AlTi and AlTi_3 as bulk material are minor only one is shown in Figure 48. They also showed several cracks and voids within the solder eased again by the brittleness of Al_3Ti . The samples at 1070°C show similar behaviour in comparison to the 1050°C samples confirming that solder applied as a mixture of powder and binder works just as good as foil-like slices (Figure 49). They do, however, show a stronger reaction with the bulk but this is most likely due to the higher temperature which is applied also for a longer time. Because of the stronger reaction the voids are more pronounced. Therefore for this solder 1050°C for 5 minutes are sufficient. For further improvement of the joint thinner slices and the application of pressure should be the next steps to minimize the voids.

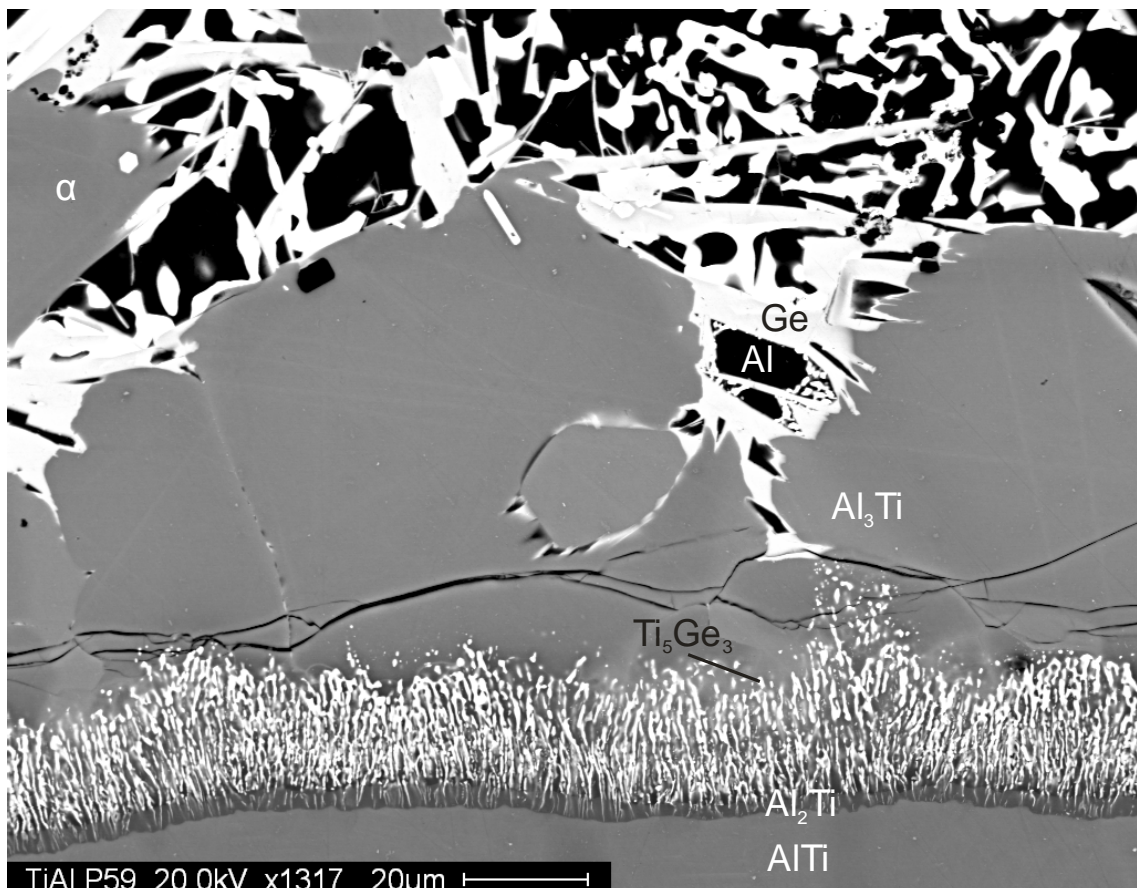


Figure 48: Wetting experiment of $\text{AlTi} - \text{Al}_{69.5}\text{Ge}_{24.5}\text{Ti}_6$ at 1050°C

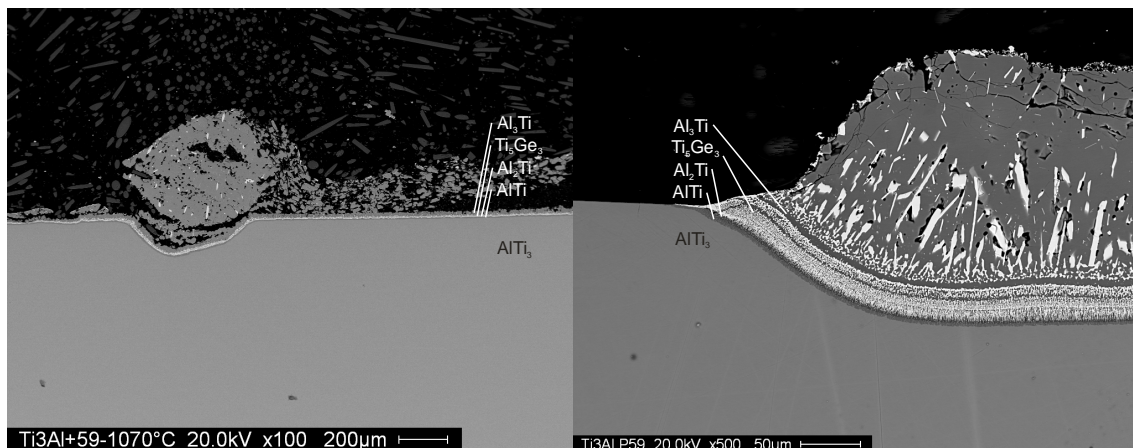


Figure 49: Wetting experiment of AlTi_3 - $\text{Al}_{69.5}\text{Ge}_{24.5}\text{Ti}_6$ at 1070°C (left) and 1050°C (right)

It is also very pleasing that the measured layers of the joint are in good agreement with the already investigated phase diagram, since this experiment is comparable to a diffusion couple experiment. In such arrangement phases which share a border have to have a common two-phase-field at the chosen temperature. This is true considering that the eutectic mixture as well as the grains of α inside are liquid at the chosen temperature and according to the reaction scheme in equilibrium with Al_3Ti .

Independent from the used solder and temperature program in any case Al_3Ti is formed in significant amounts. This is a considerable drawback for the final application since it is a quite high melting and brittle phase making it necessary to get rid of it for a proper joint which on the other hand will be a quite time consuming task because of the high melting point.

Although there are some drawbacks it still may be possible to create a working method. Therefore further tests are necessary to improve the wettability of the eutectic mixture on AlTi and AlTi_3 , to investigate the influence of the presence of the Al_3Ti phase on the following heat treatment and the impact of the application of pressure on various aspects of the process.

7. Appendices

7.1. List of figures

Figure 1: Calculated Al-Ge phase diagram by McAlister and Murray [9] and experimental data by different authors; the legend was adopted to fit to this work.....	3
Figure 2: Calculated Al-Ge phase diagram by Srikanth et al [10] and experimental data by different authors; the legend was adopted to fit to this work.....	4
Figure 3: Al-Ti phase diagram by Murray [19]	6
Figure 4: Al-Ti phase diagram after second update by Okamoto [12], [13]	7
Figure 5: Assessed phase diagram by Schuster et al [24].....	8
Figure 6: Ge-Ti phase diagram by Rudometkina et al [17]	10
Figure 7: Examples for: isothermal section: red; isopleth: green; ternary phase diagram at constant pressure: black	13
Figure 8: Binary example phase diagram for lever rule and invariant and non-invariant reactions	14
Figure 9: Binary examples for Gibb's (phase rule.....	15
Figure 10: Binary example for Landau and Palatnik rule.....	16
Figure 11: Interactions between electron beam and solid matter	17
Figure 12: Possible transitions for the K, L and M shell [23]	19
Figure 13: Diffraction of X-rays, Bragg Equation.....	20
Figure 14: Focusing circle	22
Figure 15: Bragg-Brentano pseudo focusing circle	23

Figure 16: Example for DTA signal.....	25
Figure 17: Prepared samples	30
Figure 18: Arc furnace MAM1 Johanna Otto [34]	31
Figure 19: Scanning electron microscope Zeiss Supra 55 VP [35].....	34
Figure 20: X-ray powder diffractometer Bruker D8 Discover Series 2 [36].....	35
Figure 21: differential thermal analyzer Setaram SETSYS Evolution TGA & DTA 2400 [37]	36
Figure 22: Schematic DTA setup	36
Figure 23: DTA heating program.....	37
Figure 24: partial isothermal section at 400°C and prepared samples	38
Figure 25: partial isothermal section and prepared samples at 520°C	41
Figure 26: XRD of sample 74, calculated Al_3Ti with refined Ge:Al ratio positions (blue) and without (red)	46
Figure 27: Partial isothermal section and prepared samples at 1000°C.....	48
Figure 28: Change of lattice parameters and volume for Ti_5Ge_3 with the composition ..	52
Figure 29: Powder XRD of Sample 29	53
Figure 30: BSE picture of Sample 2.....	54
Figure 31: Powder XRD of sample 49	56
Figure 32: Crystal structure and coordination polyhedra of γ	57
Figure 33: Lattice parameter (refined from powder XRD) development of γ with changing composition (measured by SEM); data acquired from multi-phase samples ..	58
Figure 34: Crystal structure and coordination polyhedra of δ	60

Figure 35: Powder XRD of sample 56.....	61
Figure 36: Reaction scheme for the titanium poor part roughly below 1000°C * These temperatures were not taken from literature but were re-evaluated in this work	66
Figure 37: Reaction scheme for the titanium poor part roughly above 1000°C.....	67
Figure 38: Isopleth with 10 at.% Ti	70
Figure 39: Isopleth with 1:1 Al:Ti ratio.....	70
Figure 40: Liquidus projection	71
Figure 41: XRD measurement of Sample 79.....	73
Figure 42: DTA measurement of Sample 66	74
Figure 43: DTA measurement of Sample 78	75
Figure 44: Different steps of diffusion brazing	76
Figure 45: Brazing of AlTi – eutectic mixture – AlTi at 440°C.....	79
Figure 46: Brazing experiment of AlTi ₃ - eutectic mixture – AlTi ₃ at 600°C.....	80
Figure 47: Brazing experiment of AlTi – eutectic mixture – Ti at 600°C.....	80
Figure 48: Wetting experiment of AlTi - Al _{69.5} Ge _{24.5} Ti ₆ at 1050°C.....	81
Figure 49: Wetting experiment of AlTi ₃ - Al _{69.5} Ge _{24.5} Ti ₆ at 1070°C (left) and 1050°C (right)	82

7.2. List of tables

Table 1: Crystal structure for the binary Al-Ge phase diagram [11], [10]	5
Table 2: Phase equilibria for the binary Al-Ge phase diagram [11], [10]	5
Table 3: binary Al-Ti phases [24].....	8

Table 4: binary Al-Ti reactions [24]	9
Table 5: binary Ge-Ti phases [19].....	11
Table 6: binary Ge-Ti reactions [19].....	11
Table 7: Composition and temperature program of all prepared samples. Equilibrium samples: bold.....	29
Table 8: EPMA setup	35
Table 9: Equilibrium samples at 400°C; * Structure not determined	40
Table 10: Equilibrium samples at 520°C	44
Table 11: Comparison of refined XRD data and data measured by SEM of Al ₃ Ti in Sample 74.....	45
Table 12: Samples at 1000°C.....	51
Table 13: Structural data of γ	55
Table 14: Structural data of δ	59
Table 15: DTA data below 900°C.....	62
Table 16: DTA data between 900°C and 1210°C	63
Table 17: DTA data above 1200°C; * Liquidus temperature too high or no peak visible in the measurement.....	64
Table 18: Composition during invariant reactions	69
Table 19: XRD and SEM data of sample 79	72
Table 20: XRD and SEM data of sample 66	74
Table 21: XRD and SEM data of sample 78	75
Table 22: Performed wetting and brazing experiments	78

8. References

1. Duwez, P. and J.L. Taylor, *Crystal structure of TiAl*. Journal of Metals, 1952. **4**(Trans.): p. 70-1.
2. Goldak, A.J. and J.G. Parr, *The structure of Ti₃Al*. Transactions of the American Institute of Mining, Metallurgical and Petroleum Engineers, 1961. **221**: p. 639-40.
3. Lipsitt, H.A., *Titanium aluminides - an overview*. Materials Research Society Symposium Proceedings, 1985. **39**(High-Temp. Ordered Intermet. Alloys): p. 351-64.
4. Loria, E.A., *Gamma titanium aluminides as prospective structural materials*. Intermetallics, 2000. **8**(9-11): p. 1339-1345.
5. Karfoul, M.K., *Diffusion processes at the interface of titanium/aluminum diffusion welded pair in ambient air atmosphere*. DVS-Berichte. **263**(Hart- und Hochtemperaturloeten und Diffusionsschweissen): p. 308-313.
6. Simoes, S., F. Viana, V. Ventzke, M. Kocak, A.S. Ramos, M.T. Vieira, and M.F. Vieira, *Joining of TiAl alloys using Ni/Al multilayers*. Microscopy and Microanalysis, 2009. **15**(Suppl. 3): p. 73-74.
7. Jacobson, D.M. and G. Humpston, *Principles of Brazing*. 2005: ASM International.
8. Srikanth, S., D. Sanyal, and P. Ramachandrarao, *A re-evaluation of the Al-Ge system*. CALPHAD Computer Coupling of Phase Diagrams and Thermochemistry, 1996. **20**(3): p. 321-332.
9. McAlister, A.J. and J.L. Murray, *The aluminum-germanium system*. Bulletin of Alloy Phase Diagrams, 1984. **5**(4): p. 341-7, 409-10.
10. Kroll, W., *The diagram germanium-aluminum*. Metall und Erz, 1926. **23**: p. 682-4.
11. Stohr, H. and W. Klemm, *Binary systems with germanium. I. Germanium-aluminum, germanium-tin and germanium-silicon*. Zeitschrift fuer Anorganische und Allgemeine Chemie, 1939. **241**: p. 305-23.
12. Clark, J.B. and W.F.T. Pistorius, *Aluminum-germanium eutectic temperature to 40 kilobars*. Journal of the Less-Common Metals, 1974. **34**(2): p. 233-6.
13. Glazov, V.M., T.e.-J. Chien, and C.-y. Liu, *Solubility of the binary and ternary systems of germanium with aluminum and antimony*. Zhurnal Neorganicheskoi Khimii, 1962. **7**: p. 576-81.

14. Wilder, T.C., *An electromotive-force study of the thermodynamic properties of the liquid Al-Ge system and the germanium-rich Al-Ge liquidus*. Transactions of the Metallurgical Society of AIME, 1966. **236**(1): p. 88-94.
15. Eslami, H., J. De Franceschi, M. Gambino, and J.P. Bros, *An electromotive force study of the activity of aluminum in aluminum-gallium, aluminum-germanium and aluminum-gallium-germanium systems*. Zeitschrift fuer Naturforschung, Teil A Astrophysik, Physik und Physikalische Chemie, 1979. **34A**(7): p. 810-17.
16. Eslami, H., Y.M. Muggianu, M. Gambino, and J.P. Bros, *Enthalpies of formation of liquid aluminum-germanium, gallium-germanium, and aluminum-gallium-germanium between 713 and 1230 K*. Journal of the Less-Common Metals, 1979. **64**(1): p. 31-44.
17. Caywood, J.M., *Measurement of the solubility of germanium in aluminum utilizing MeV helium(+) ion backscattering*. Metallurgical Transactions, 1973. **4**(3): p. 735-43.
18. Minamino, Y., T. Yamane, H. Araki, T. Adachi, Y.S. Kang, Y. Miyamoto, and T. Okamoto, *Isobaric sections of the aluminum phase field in the aluminum-germanium phase diagram at high pressures up to 2.6 GPa*. Journal of Materials Science, 1991. **26**(20): p. 5623-30.
19. Murray, J.L., *Calculation of the titanium-aluminum phase diagram*. Metallurgical Transactions A Physical Metallurgy and Materials Science, 1988. **19A**(2): p. 243-7.
20. Okamoto, H., *Al-Ti (aluminum-titanium)*. Journal of Phase Equilibria, 1993. **14**(1): p. 120-121.
21. Okamoto, H., *Al-Ti (aluminum-titanium)*. Journal of Phase Equilibria, 2000. **21**(3): p. 311.
22. Kattner, U.R., J.C. Lin, and Y.A. Chang, *Thermodynamic assessment and calculation of the titanium-aluminum system*. Metallurgical Transactions A Physical Metallurgy and Materials Science, 1992. **23A**(8): p. 2081-90.
23. Kainuma, R., M. Palm, and G. Inden, *Solid-phase equilibria in the Ti-rich part of the Ti-Al system*. Intermetallics, 1994. **2**(4): p. 321-32.
24. Schuster, J.C. and M. Palm, *Reassessment of the binary aluminum-titanium phase diagram*. Journal of Phase Equilibria and Diffusion, 2006. **27**(3): p. 255-277.
25. Rudometkina, M.V., Y.D. Seropegin, A.V. Griбанov, and L.S. Gusei, *Phase equilibria in the titanium-niobium-germanium system at 1170 K*. Journal of the Less-Common Metals, 1989. **147**(2): p. 239-47.
26. Wirringa, J. and M. Binnewies, *Chemical vapor transport of intermetallic systems. Part 8. Chemical transport of titanium germanides*. Zeitschrift fuer Anorganische und Allgemeine Chemie, 2000. **626**(4): p. 996-998.

27. Villars, P., *Handbook of ternary alloy phase diagrams*. 1995, Metals Park, OH: ASM International.
28. Nartova, T.T. and T.V. Mogutova, *Effect of germanium on phase equilibriums of titanium-aluminum alloys*. 1981: p. 144-8.
29. Ipser, H., *VO Phasendiagramme - in der Materialchemie*. 2010, University of Vienna.
30. Goldstein, J.I., *Scanning electron microscopy and x-ray microanalysis*. 2. ed. 1992, New York, NY: Plenum Press. XVIII, 820 S.
31. Cullity, B.D., *Elements of X-ray diffraction*. 2. ed. ed. 1978, Reading, Mass. [u.a.]: Addison-Wesley. XII, 555 S.
32. Richter, K., *VO Experimentelle Methoden zur Bestimmung von Phasendiagrammen*. 2011, University of Vienna.
33. Hemminger, W.F. and H.K. Cammenga, *Methoden der Thermischen Analyse*. 1989: Springer-Verlag.
34. <http://www.edmund-buehler.de/bilder/OTTO8.JPG>. 6. June 2011.
35. <http://nanozentrum.univie.ac.at/typo3temp/pics/c48e0c5583.jpg>. 6. June 2011.
36. http://www.bruker-axs.com/uploads/pics/Rund_9d8e85e824_high_01.jpg. 6. June 2011.
37. http://img.directindustry.de/images_di/photo-g/simultanes-thermoanalysegerat-tga-dta-tga-dsc-419407.jpg. 6. June 2011.
38. Schubert, K., K. Frank, R. Gohle, A. Maldonado, H.G. Meissner, A. Raman, and W. Rossteutscher, *Structural data on metallic phases. VIII*. *Naturwissenschaften*, 1963. **50**(No. 2): p. 41.
39. Raman, A. and K. Schubert, *The constitution of some alloy series related to TiAl₃. I. Investigations in some T₄-Zn-Al, T₄-Zn-Ga, and T₄-Ga-Ge systems*. *Zeitschrift fuer Metallkunde*, 1965. **56**(1): p. 40-3.
40. Smith, G.S., Q. Johnson, and A.G. Tharp, *Crystal structure of Sm₅Ge₄*. *Acta Crystallographica*, 1967. **22**(2): p. 269-72.

9. Curriculum Vitae

Personal Information	Name	Roland Wolfgang Bittner, B.Sc.
	Family status	Single
	Nationality	Austrian
	Date of birth	21. April 1986
	Place of birth	Salzburg, Austria
	Religion	Catholic
	Contact Information	Address
Telephone		+43/699/12369885
Email		rolandbittner@gmx.at
Education		14.2.2011 – 14.3.2011 Research stay at the EMPA in Dübendorf for brazing experiments in the course of the master thesis
	Since 2010 Master thesis at the Institute for Inorganic Chemistry/Materials Chemistry at the University of Vienna	
	28.4.2009 Finished with the degree Bachelor of Science	
	Since 2005 Chemistry study at the University of Vienna	
	2004 –2005 Military Service with training as a paramedic	
	14.6.2004 Finished the secondary school with the “Matura”	
	1996-2004 Secondary school: Erzbischöfliches Privatgymnasium Borromäum	
Skills	German	mother tongue
	English	fluent
	French	basic
	Latin	basic
		Driving licence class B
		Good computer literacy especially with Microsoft Office and basic knowledge of Adobe Flash

10. Abstract

The phase diagram Al-Ge-Ti is of potential interest for joining applications for titanium-aluminides which are important alloys for high temperature components. Aluminium and Germanium form a deep eutectic at 423.7°C which could be used for soldering of titanium-aluminides in the transient liquid bonding process. A thorough knowledge of ternary phase equilibria is required for the realization of interface reactions during bonding and the search for possible ternary Al-Ge-Ti alloys that could be employed as solders. However, up to now the Al-Ge-Ti phase diagram was not studied.

In this work the phase equilibria of Al-Ge-Ti have been investigated using scanning electron microscopy (SEM), powder x-ray diffractometry (XRD) and differential thermal analysis (DTA) measurements in order to obtain partial isothermal sections at 400°C, 520°C and 1000°C. Different annealing temperatures in different parts of the system were necessary because of the strongly varying melting points (between 423.7°C and 1980°C). In this work the titanium poor part up to 50 at.% titanium was investigated. Two ternary and one new binary compounds were found to exist, two of which could be structurally characterized ($\text{Al}_{0.10-0.24}\text{Ge}_{0.42-0.56}\text{Ti}_{0.33}$, $\text{Al}_4\text{Si}_5\text{Zr}_3$ -typ, $I4_1/amd$, $tI24$) ($\text{Ge}_{44}\text{Ti}_{56}$, Ge_4Sm_5 -typ, $Pnma$, $oP36$). DTA data were used to construct a ternary reaction scheme (Scheil) up to approximately 1300°C. Also, preliminary brazing experiments were performed in order to test the wetting behaviour and interface reactions. For these experiments the eutectic mixture of aluminium and germanium on one hand and the same mixture with additional titanium (6 at.%) on the other hand were used as solder, while AlTi, Al_3Ti and Ti were used as bulk material. In the course of this work also some of the temperatures of the binary phase diagram Ge-Ti were measured again, indicating higher temperatures than previously published.

11. Zusammenfassung

Titan-Aluminium Legierungen spielen eine wichtige Rolle für zahlreiche technische Anwendungen. Aufgrund der hohen Schmelzpunkte und Sauerstoffempfindlichkeit sind Fügeverfahren wie Schweißen aber nur bedingt anwendbar. Ein elegantes Fügeverfahren, bei dem diese Eigenschaften eine untergeordnete Rolle spielen, ist das Diffusionslöten. Dabei wird ein niedrig schmelzendes Lot zwischen zwei Werkstücken kurzzeitig aufgeschmolzen und durch eine anschließende Wärmebehandlung mittels Diffusion über den gesamten Verbund verteilt. Ziel dieser Arbeit war ein auf Aluminium und Germanium basierendes Lot, da diese beiden Elemente bei 28,4at.% Germanium ein sehr tiefes Eutektikum bei 423,7°C bilden und gleichzeitig eines der beiden Elemente der Zielverbindung so ebenfalls im Lot vorhanden ist. Um dieses Verfahren erfolgreich anwenden zu können, ist aber ein fundiertes Wissen über das Phasendiagramm der beteiligten Elemente notwendig, das bisher nicht adäquat untersucht wurde.

Zur Untersuchung des Phasendiagramms wurden SEM (scanning electron microscopy), Pulver XRD (X-ray diffractometry) und DTA (differential thermal analysis) Messungen eingesetzt, um drei partielle isotherme Schnitte bei 400°C, 520°C und 1000°C im titanarmen Teil bis maximal 50 at.% Titan zu konstruieren. Die unterschiedlichen Temperaturen in den verschiedenen Teilen des Phasendiagramms waren notwendig, um trotz der stark variierenden Schmelzpunkte der einzelnen Phasen (zwischen 423,7°C und 1980°C) das thermodynamische Gleichgewicht zu erreichen. Im Zuge der Arbeit wurden zwei ternäre sowie eine neue binäre Verbindung im Ge-Ti System gefunden. Zwei dieser Verbindungen konnten bereits strukturell aufgeklärt werden ($\text{Al}_{0,10-0,24}\text{Ge}_{0,42-0,56}\text{Ti}_{0,33}$, $\text{Al}_4\text{Si}_5\text{Zr}_3$ -Typ, $I4_1/amd$, $tI24$) ($\text{Ge}_{44}\text{Ti}_{56}$, Ge_4Sm_5 -Typ, $Pnma$, $oP36$). Mit Hilfe der DTA Daten konnte ein ternäres Reaktionsschema bis 1300°C erstellt werden (Scheil Diagramm). Weiters wurden erste Lötversuche durchgeführt, bei denen die reine eutektische Mischung des Al-Ge Systems, sowie die eutektische Mischung mit einem Zusatz von 6 at.% Titan als Lot verwendet wurden. Als Substrat wurde AlTi, Al_3Ti und Titan verwendet. Im Zuge der Arbeit wurden außerdem einige Temperaturen des binären Ge-Ti Phasendiagramms neu bestimmt. Die Messungen ergaben dabei etwas höhere Temperaturen als in früheren Publikationen.